126730

NHTSA-98-3588-105

MSU COMBUSTION RESEARCH LABORATORY (CRL)
REPORT NO. 10-31-99

DEPARTMENT OF MECHANICAL ENGINEERING
MICHIGAN STATE UNIVERSITY

Final Report

GM CAR-FIRE PROJECT AT MICHIGAN STATE UNIVERSITY

Theoretical and Experimental Study of Thermal Barriers Separating Automobile Engine and Passenger Compartments

Grant No. 71-2755 (MSU), MSU Reference: APP #69668
GM Project No. PLBV00238
Dates of Project: 4/1/97 – 3/31/98
Budget: $50,000

Supervisor: Dr. Douglas W. Kononen
General Motors Research and Development Center
30500 Mound Road, Building 1-3
Mail Code 480-103-001
Warren, MI 48090-9055

Research Conducted by: Indrek S. Wichman, James V. Beck, A. Bukola Oladipo, Robert L. McMasters IV, Erica Little

Research Conducted in: Department of Mechanical Engineering
Combustion Research Laboratory (CRL)
Michigan State University
East Lansing, MI 48824-1226

Corresponding Author: I.S. Wichman
Tel: (517) 353-9180
Fax: (517) 353-1750
email: wichman@egr.msu.edu

TABLE OF CONTENTS

10

CHAPTER 1

INTRODUCTION

1.0 STATEMENT OF RESEARCH

The purpose of this project is to examine the effectiveness of various combinations of insulations in the prevention of heat transfer from the engine to the passenger compartment through the bulkhead. We wish to experimentally determine the reduction of heat transfer that can be obtained with various layered insulations that may or may not be attached to the bulkhead.

Our study of the performance of the thermal barrier separating engine and passenger compartments will be in collaboration with the Vehicle Fire Safety Research Program at General Motors Research and Development Center. Commercially available materials currently in use will be tested at General Motors. These materials will be mounted on a test stand and then be subjected to a radiant heat source on one side (the "front"). The following measurements relating to the performance of the thermal barrier will be made during these GM tests: (1) surface temperatures of the barrier and metal bulkhead; (2) radiant and convective heat fluxes to the heated surface of the barrier; (3) radiant, convective, and conductive heat fluxes from the non-heated ("passenger side") surface of the barrier to the ambient surrounding ("passenger compartment"). These measurements will be made for steady-state and non-steady-state heating.

1.1 GENERAL PROBLEM BACKGROUND DISCUSSION

The problem of heat transfer from the outside into the passenger compartment is complicated and depends upon many physical quantities. Among these are:

1. Point of origin or source of heat transfer,
2. Vehicle orientation during heat transfer,
3. Number and location of compartment openings relative to point of origin or source of heat transfer. This includes HVAC air intake, heater and A/C feed-throughs, steering column.

We shall examine in this one-year study the effectiveness of the "bulkhead" in preventing heat transmission to the "passenger compartment." The geometry of the "bulkhead" is generally complex and three-dimensional. Many coverings of the "bulkhead" are available, depending mostly upon the "market segment" of the automobile. Some "bulkheads" have no insulation attached, and amount to only a physical metal barrier separating "engine" and "passenger" compartments. Other automobile "bulkheads" may have a "sound blanket" on the engine side and a "dash blanket" on the "passenger" side, covered by the interior carpet. Both the "sound blanket" and the "dash blanket" may consist

of multiple layers of materials including materials like carpet. In addition, the entire "bulkhead" may be considered as a single barrier whose overall behavior can be changed by altering one or more of the constituent layers.

Possible ways to examine the heat transfer between the "engine" and "passenger" compartments include:

1. Full-scale testing by burning whole crash-tested cars.
2. Full-scale numerical modeling using computational fluid dynamics (CFD): The transient, three-dimensional equations of fluid dynamics are coupled to the energy and species equations, which are simultaneously solved using numerical methods. The coupling between the equations makes unambiguous solutions extremely difficult to obtain. Such a study would be valuable if the conditions of the simulation are well understood.
3. Development of models: It is understood that the convective and radiant transfer of heat in realistic conditions occurs over large spatial regions, of the order of a cubic meter. Hence, two- and three-dimensional effects are important in reality. Heat conduction through the "bulkhead", by contrast, can be locally one-dimensional, because the "bulkhead" is relatively thin and temperature gradients normal to the barrier can be smaller than those in the plane of the "bulkhead". Consequently, one-dimensional models can be used to describe the heat transfer from the "engine" to the "passenger" compartment.

We believe that reliable information on the effectiveness of thermal barriers separating hypothetical automotive "engine" and "passenger" compartments can be obtained through a one-dimensional analysis.

This information will require temperature measurements and possibly heat flux measurements. These measurements will be carried out at MSU in conjunction with the model experiments being conducted by GM. Our numerical analysis, which will utilize the temperature measurements coupled with the solution of the energy equations, amounts to an *inverse problem of heat transfer.*

1.2 RESEARCH OBJECTIVES

The goal of this project is to describe heat transmission through a model intact automobile "bulkhead." This research will have limited relevancy to post-crash heat transmission through a vehicle bulkhead that has lost structural integrity in a crash. Even if heat transmission through an intact bulkhead could be effectively reduced by material application, other pathways for heat

transmission may exist, such as HVAC, electrical and mechanical systems pass-throughs.

We ask specific questions in order to connect our research to the practical evaluation of thermal barriers in automobiles. These questions will be answerable through our research at MSU.

1. Which material property can reduce the transient heat flux across the layered material constituting the thermal barrier?
2. Can certain types of materials alter the rate of heat transfer?
3. Can we produce models that provide agreement between calculated results and our experimental measurements? Can we optimize the agreement?

1.3 SUMMARY AND DELIVERABLES

We intend to examine the "bulkhead" separating "engine" and "passenger" compartments, to learn how to enhance the effectiveness of hypothetical automotive thermal barriers. We shall do this by conducting experiments and developing numerical models that simulate the experimental measurements. These models can possibly be later used to computationally design new materials and thermal barriers. This aspect will not be covered in this one-year project. The thermal property experiments will be conducted in the MSU Thermal Property Measurement Laboratory. The numerical model for parameter estimation will also be developed at MSU. The goal will not be the measurement of the thermal properties of the individual constituent *per se*, but rather a thermal characterization of the barriers. The novel aspect of our research is that it combines experimental and analytical/numerical methods to produce a "product" – the model – which predicts the behavior of the layer, or "bulkhead" assembly.

Our deliverables are the following:

1. Analytical/numerical model with constant properties and transient heating. Provides indication of influences of property changes on rates of heat transfer through layer. Indicates which parameters and groups of parameters are most important.
2. Numerical model with variable properties, transient heating. Included in this model will be separate results for each of the materials (layered "bulkhead" assemblies). Techniques of parameter estimation and inverse methods will be used to develop the model.
3. Residual database of experimental results for each of the bulkhead assemblies.

1.4 NOMENCLATURE

Because of the length of this report, all symbols used are defined in alphabetical order. There is occasional overlap between symbols in the report. Where such overlap occurs it is immediately noted.

ENGLISH SYMBOLS

A_i Area of surface 'i' (see Appendix) (m^2)
Bi Biot number, $Bi = hL/k$ (*unitless*)
c_p Specific hat at constant pressure (gas) ($J/kg\text{-}K$)
F_{ab} View factor from surface 'a' to surface 'b' (*unitless*)
Gr Grashof number, $Gr = gx^3\beta\Delta T/\nu^2$ (*unitless*)
h Convective heat transfer coefficient ($W/m^2\text{-}K$)
k Thermal conductivity ($W/m\text{-}K$)
l Scrim layer thickness (Chapter 2). Standoff distance (Appendix) (m)
L_i Thickness of layer 'i' in the thermal barrier (m)
N Number of temperature measurements at a point (*unitless*)
Nu Nusselt number, $Nu = hx/k$ (*unitless*)
$p(i)$ Mollification factor weighting (see Sec. 3.3.3) (*unitless*)
Pr Prandtl number, $Pr = \nu/\alpha$ (*unitless*)
q Heat flux (W/m^2)
Q Heating power (W)
r Thermal responsivity, $r^2 = k\rho c$ ($W^2\text{-}s/m^4\text{-}K^2$)
t Time (s)
t^+ Nondimensional characteristic thermal diffusion time (Chapter 2), $t^+ = \alpha t/L^2$ (*unitless*)
t^* Characteristic thermal diffusion layer heating time, $t^* = L^2/\alpha$ (s)
T_f Flame temperature (see Equation (2.1)) (K)
T_v Solid material gasification or 'vaporization' temperature (Equation (2.1) (K)
T_∞ Ambient temperature (K)
T_i Inverse conduction theoretical temperature solution (K)
u_f Flame spread rate (see Equation (2.1)) (m/s)
u_g Gas flow speed (see Equation (2.1)) (m/s)
x Direction perpendicular to thermal barrier surface ($x=0$ at front face, $x=L$ at rear face) (m)
X Sensitivity coefficient matrix (K)
X_i Individual sensitivity coefficient (K)
X^T Transpose of matrix X (if $X = X_{ij}$ then $X^T = X_{ji}$) (K)
y Direction along (or in the plane of) thermal barrier (m)
Y_i Experimentally measured temperatures (K)
z Same definition as y above (m)

GREEK SYMBOLS

α Thermal diffusivity, $\alpha=k/\rho c$ (m^2/s cm^2/s)

α,β,γ Constants in correlations for c,k in Chapter 2
δ Mollification parameter (see Sec. 3.3.3)
η Temperature vector for regularization analysis (see Sec. 3.3.3)
ρ Density (kg/m^3)
ν Kinematic viscosity (m^2/s or cm^2/s)
σ Standard deviation (*unitless*)

SUBSCRIPTS

c Contact conductance layer
g Gas
gf Glass fiber mat
gffs Glass fiber mat with facing scrim layers
i Insulation layer
s Steel layer (also 'solid' in Equation (2.1))
x In *x*-direction
y In *y*-direction
z In *z*-direction
1,2 Separate thermal barrier layers (*2* is usually steel)

ACRONYMS

ASTM American Society for Testing and Materials
DSC Differential Scanning Calorimeter
GM General Motors
GM1.EXE Windows-based parameter-estimation code developed at MSU
MSU Michigan State University
PROP1D, PROP1DR Computer programs written by Prof. J. V. Beck
SM Secondary Material (see Figure 2.2)
TC Thermocouple
TIM TC Installation Material (see Chapter 2)

CHAPTER 2

PARAMETER ESTIMATION OF THERMOPHYSICAL PROPERTIES IN THERMAL BARRIER MATERIALS

2.0 INTRODUCTION

In this part of the project we examine the thermal properties of the separate materials constituting the "bulkhead." These materials consist of insulation, such as carpet material, glass fiber, kaowool ceramic fiber and elastomeric (rubbery) material, and metal plate material onto which these insulating materials are mounted (usually by mechanical means, such as plastic fasteners). In our research, no mechanical fasteners were employed.

It will be demonstrated that the determination of the thermal properties of the separate materials is a difficult undertaking because the insulating materials are fibrous, porous and light. Therefore, properties may vary with packing density and degree of adhesion. For these reasons the experiments described herein were difficult to perform especially for higher temperatures. In the latter case placement of thermocouples became very difficult.

The trends, however, suggest that over the limited range of temperatures examined, certain individual materials possess thermal properties that can reduce heat transmission rates during the initial transient heating stage. We observe, however, that when steady-state heating is attained, all materials allow the passage of an identical amount of heat.

2.1 BACKGROUND

It is well known that the combustion of solid materials involves several processes, such as heat transfer to the unburned fuel, solid pyrolysis, and ignition, whose rates depend on the thermal properties of the material under study. For example, DeRis (1969) showed that the rate of flame spread over a thermally thick sample of condensed-phase (solid, not liquid) combustible material is given by

$$u_f = u_g \frac{k_g \rho_g c_{pg}}{k_s \rho_s c_s} \left[\frac{T_f - T_v}{T_v - T_\infty} \right]^2 . \tag{2.1}$$

This formula demonstrates the influence of the thermal properties, k_s and $\rho_s c_s$, of the solid fuel on the flame spread rate, u_f. Here k_s is the solid material thermal conductivity, ρ_s is the solid material density, and c_s is the solid material heat capacity. The quantity $\rho_s c_s$ is the material volumetric heat capacity (units energy/volume-K). See the Nomenclature in Sec. 1.4 for definitions of the remaining symbols. In this research we frequently use the combination ρc as a thermal property because it

appears in this form in the conservation equations of heat transfer, see, e.g., Equation (2.3).

In describing an effective thermal barrier for slowing the rate of heat transfer to the "passenger" compartment, it is important to accurately establish the thermal properties of the individual insulation materials. This can be done by coupling a careful examination of material thermal measurements to a numerical solution of the heat transfer through the multi-layered wall.

Several insulation materials supplied by the General Motors Research and Development Center were used in this study. They include the following: glass fiber bonded with phenol formaldehyde; elastomeric (rubbery) compound of undetermined composition; MgO; Kaowool ceramic fiber; carpet material. The objective is first to accurately determine the thermal conductivity, k and the volumetric heat capacity, ρc of these materials, and second to use this information to conduct numerical simulations aimed at understanding the role of each material when used as part of the thermal barrier.

The numerical simulations reported in this work were all conducted using the numerical codes PROP1D and PROP1DR developed by Professor J. V. Beck of Michigan State University. The details of the codes are described later in this chapter.

2.2 PHYSICAL ARRANGEMENT OF AUTOMOBILE THERMAL BARRIER LAYERS

A possible arrangement of the thermal barrier layers in a hypothetical "bulkhead" assembly is shown in Figure 2.1. The "bulkhead layer" is the metal wall that separates the "engine compartment" from the "passenger cabin." The "dash" and "sound" blankets are placed next to the "bulkhead" layer on the "passenger" and the "engine" side, respectively. The "dash" and "sound" blankets can be layered materials, consisting of several separate materials. The "sound" blanket may consist of a thin layer of elastomer sandwiched between two layers of glass fiber mats whose thickness ranges from 2 to 7 times that of the elastomer. The materials examined here can be used as part of the "sound" blanket, and may thus perform the dual roles of thermal insulation and external noise attenuation. Not all vehicles employ "dash" blankets and insulation materials ("sound" blankets) on both sides of the metal substrate (the "bulkhead"). Also, not all "bulkheads" are made of steel. Still yet, vehicle manufacturers do not all use the terms "dash" blanket, "sound" blanket or "bulkhead" for such assemblies.

2.3 EXPERIMENTS

Two sets of experiments are relevant in the pursuit of the objectives of this study. The first,

which were performed at General Motors Research and Development Center by GM personnel, involved transient temperature measurements on a mock bulkhead and sound blanket assembly. Some of the numerical simulations reported in this article are based on selected GM data. The second set, which formed the bulk of the experimental tests employed in this study, was performed at Michigan State University (MSU). They involved measurements of transient temperature response of the thermal barrier materials to heat flux inputs in order to determine the thermal properties $k_s\ \rho_s c_s$ of the various materials.

2.3.1 GM Experimental Setup

Since some of the numerical computations reported in this article are based on the GM data, this section describes the GM experimental set-up. This description is also applicable to the work presented in Chapter 3. A $90\,\text{cm} \times 90\,\text{cm} \times 0.085\,\text{cm}$ flat black carbon steel panel mounted with thermocouples and heat flux gages is employed as the "bulkhead". The thermal barrier material to be studied is mounted on the "engine-ward" face; the "passenger-compartment" side is bare. In other words, there is no "sound" blanket. Heat flux supplied from quartz halogen lamps located at controlled distances from the "bulkhead" assembly impinges on the test material. There are no fissures or gaps in this hypothetical "bulkhead" apparatus. A "bulkhead" with gaps might simulate a "bulkhead" that had been torn in a crash, for example, or openings may exist for cables and other passages. There is a provision for varying the assembly angle, relative to the heater, in order to simulate a non-vertical "bulkhead." For the vertical configuration, the impinging heat flux is nearly one-dimensional in an approximately 15cm × 15cm area near the center of the plate. After establishing the desired radiant emission from the lamps, the heat flux through the barrier and the temperature profiles are measured with gauges and thermocouples, respectively. The latter were unshielded.

2.3.2 MSU Experimental Setup and Procedure

Two identical test samples are cut from each material of interest for the thermal property test. The length and width dimensions of the samples are 7.62cm by 5.08cm (3" by 2"), respectively with the thickness maintained as received (see Table 2.1). A custom-made, planar heater of equal length and width dimensions as the sample and 0.19cm (0.075") thick is placed between the two identical samples, as shown in Figure 2.2. The sample surface in contact with the heater (Figure 2.2, $x=a$) is denoted "front" while the opposite one across the sample thickness ($x=b$) is denoted "back." With

this arrangement, heat flow into the test samples is along the x direction and the surface area over which the heat is applied is 7.62 x 5.08 = 38.7cm^2. The thermal properties obtained from the tests in this arrangement are the components in the direction of major heat flow through the material assembly layer.

It is possible to question the validity of the assumption of one-dimensional heat flow assumption across the thickness of the materials considering the dimensions of our test samples. For instance, one may assert that having 10cm × 10cm × 0.1cm will more closely approximate one-dimensionality since the length (y) and the width (z) scale can be considered to be large in comparison to the thickness (100:1). The dimensions, 7.62cm × 5.08cm × 2cm (using the Kaowool material as an example), on the other hand, produces a width-to-thickness ratio of only 2.5. However, since the length and width of the electric heater used are the same as those of the test samples, the heater surface matches the entire heated surface of the test sample. With this arrangement, the heat flow will be approximately one-dimensional provided (1) the relevant components of the test material thermal properties and (2) the heating power from the electric heater are uniformly distributed in the heating plane. For the MSU setup, shown in Figure 2.2, the first condition implies that, for any x,

$$\frac{\partial k_x}{\partial y} = \frac{\partial k_x}{\partial z} = 0. \tag{2.2}$$

This condition is approximately satisfied because the materials being tested are homogeneous in composition. The second condition is also partially satisfied because the MSU electric heaters used have a high wire density (number of wire loops per unit surface area) and the wires are arranged as uniformly as possible over the cross-section.

A secondary material (SM) is placed in contact with the sample at the back surface. This SM can either be an insulating material or a highly conducting material, depending on the material whose thermal properties are being measured. It was shown by Oladipo et al. (1999) that when the thermal conductivity of the test material is low (less than about ten times that of a typical insulation material, for instance), the use of a highly conducting material, e.g. an aluminum block as the SM produces more accurate and self-consistent estimates of the thermal properties being measured. Since the materials that are being tested here are insulation materials it is necessary to employ a SM having a much higher thermal conductivity such as aluminum. The detailed reasoning for such requirements

is readily found in the literature of parameter estimation in heat transfer, see, e.g., Beck and Osman (1988).

Type E, gauge 40 (0.008cm diameter) thermocouples are attached to the test samples to record the temperature history. A total of six thermocouples are used per sample, four at the front surface, two at the back. To reduce the influence of imperfect thermal contact, a thin layer of Dow Corning 340 Silicone Grease is introduced between adjacent surfaces as shown in the figure.

We describe briefly the attachment of the TCs, which was a lengthy and difficult process. In the MSU experiments a small piece of elastomer (the third material in Table 2.1) was used as the TC installation material (TIM). The elastomer piece was heated and melted using soldering equipment to hold the TC joint on the test material. Upon heating during actual testing the TIM starts to melt at temperatures exceeding approximately 350K, as indicated by a phase transformation that yields constant temperatures with subsequent heating. This is why the temperature range of the MSU tests for the conductivity tests peaked at 345K. The TC was not reading only TIM temperatures because the test sample was treated as a two-layer material. The *heater + TIM + Si grease* formed one layer and the test materials and the back *Al* block formed the other layer. Additional details on the experiments, and the reasoning on which they are based, can be found in the PhD thesis of Oladipo (1998). The assembly consisting of heater and materials and TCs was then placed inside a controlled oven in order to perform the tests at various levels of initial temperature.

The temperature response of the material layers of Figure 2.2 is governed by the transient, one dimensional, heat conduction equation,

$$\frac{\partial}{\partial x}\left(k\frac{\partial T}{\partial x}\right)=\rho c\frac{\partial T}{\partial t}, \tag{2.3}$$

applied to each individual layer. The conductive heat transfer through the layers is coupled by the interface conditions

$$k_s\left.\frac{\partial T_s}{\partial x}\right|_{L_s^-}=k_{s+1}\left.\frac{\partial T_{s+1}}{\partial x}\right|_{L_s^+},\quad T\big|_{L_s^-}=T\big|_{L_s^+} \tag{2.4}$$

for adjacent layers s and $s+1$. A variable heat flux boundary condition is applied at the "front" surface ($x=a$) and a zero heat flux condition, or a temperature boundary condition, is applied at the "back" surface ($x=b$), depending on whether the insulation, or the aluminum block, is used as the SM, see Figure 2.2. The temperature distributions, T_i, obtained from the inverse numerical solution

of these equations are employed with the experimentally measured temperatures, Y_i and the experimental heating power, Q, to estimate the test material effective thermal properties k and ρc. The procedure involves the minimization of the sum-of-squares function

$$\sum_{i=1}^{N}\left[(Y_i - T_i)^2\right] \tag{2.5}$$

with respect to parameters k and ρc. Here N is the total number of temperature data points at a particular TC location. This experimental set-up has been validated and used satisfactorily to measure the thermal properties of various materials including wood fiber/thermoplastic composites, Oladipo et al. (1999); aluminum and carbon-carbon composites, Dowding et al. (1996); and thermosetting carbon/epoxy composites, Scott and Beck (1992). Readers interested in further details of the thermal property estimation procedure or general solution methods for inverse heat conduction problems may consult the work of Beck and Osman (1981), Beck and Arnold (1977), or Beck et al. (1985).

The successful estimation of k and ρc will depend on the sensitivity of the measured and computed temperatures to k and ρc. In other words, the experiment will be well-designed and capable of accurately estimating the material thermal properties when the sensitivity coefficients, $k\partial T / \partial k$ and $(\rho c)\partial T / \partial(\rho c)$, are of significant order of magnitude relative to the temperature rise attained during the test ΔT. The qualifier "significant" means a *measurable non-negligible fraction.* If, for example, $\Delta T^{-1} k\partial T/\partial k$ is of order 10^{-6}, the sensitivity of the temperature change to changes of k would be negligible. When $\Delta T^{-1} k\partial T/\partial k$ is of order unity, or even of order 10^{-1}, changes of k clearly influence the temperature distribution (and vice-versa). In order that parameters k and ρc can both be determined from this procedure, the sensitivity coefficients $k\partial T/\partial k$ and $\rho c\partial T/\partial(\rho c)$ cannot be auto-correlated with respect to each other. In other words, the sensitivities must be independent of one another. Also, the residuals $(Y_i - T_i)$ must be small in comparison to the temperature rise and of random distribution. A typical indication of a good estimation procedure is that the sequential estimated values of the parameters be constant in the latter part of the test after possible initial fluctuations. If the first two conditions do not hold, it may not be possible to estimate the two properties uniquely but only a ratio of the two. In such a case it will be necessary to employ other methods to determine one of the test material properties (either k or ρc).

Typical transient temperature profiles measured during the experimental tests are shown in Figure 2.3. The test duration was chosen so that the dimensionless time, t^+, defined as the ratio of the actual measured time to the characteristic thermal diffusion time, $t^+=t/(L^2/\alpha)=\alpha t/L^2$, was approximately 4.0. This value ensures that while there is ample time for the thermal energy flux to penetrate the samples, the heat transfer process does not become quasi-steady where the expression "quasi-steady" means "very nearly independent of time." The designation of a physical process as "quasi-steady" is a common one in the literature of science and engineering because truly steady processes are few.

Plots of sensitivity coefficients from tests conducted on the glass fiber mat are shown in Figure 2.4. It can be seen from these plots that the experiment is insensitive to the heat capacity of the materials. With ΔT approximately equal to 10 °C for both tests, the maximum value of $(\rho c)\partial T / \partial(\rho c)$ is only about 2% of the temperature rise, which is considered small. On the other hand, the sensitivity coefficient with respect to the thermal conductivity attained values as high as 25%. For this reason, only the thermal conductivity of the thermal barrier materials could be accurately established from the experimental methods described previously.

In order to determine the volumetric heat capacity of the materials, the differential scanning calorimeter (DSC) was used. The DSC measures the amount of heat absorbed or released as a sample undergoes controlled heating in a known, regulated (e.g., air or nitrogen) atmosphere. Reversible heat events, related to the heat capacity of the sample, and non-reversible events, related to non-reversible physical and chemical changes the sample might undergo, are both measured. This information is used to compute the specific heat capacity of the material.

2.4 RESULTS AND DISCUSSION

The plots of the specific heat capacity of the thermal barrier materials as measured with the DSC method are shown in Figure 2.5. These plots show that the specific heat capacities of all the materials rise with temperature. The addition of a polyester layer to the glass fiber mat increases the specific heat capacity. Finally, the results show identical heat capacity of the elastomer and the glass fiber mat with facing polyester scrim layers on both sides. Hence, a compound material layer consisting of elastomer between two layers of glass fiber mat has the same specific heat capacity as a single layer of elastomer or a glass fiber mat with polyester scrim on both sides.

The experimental data shown in Figure 2.5 correlate with temperature T (in Kelvins) via a

quadratic function: $c = \alpha T^2 + \beta T + \gamma$, where c is the specific heat capacity in J/kg K. The correlation constants α, β, and γ are shown in Table 2.1. The choice of α in the correlation for c (and later for k) is not to be confused with the thermal diffusivity, which is also described by the symbol α.

The densities of the various materials were determined as shown in Table 2.1. This allows calculation of the material volumetric heat capacities, ρc. These data are used in conjunction with the property determination tests to estimate the thermal conductivity, k.

In order to confirm that this estimation of the thermal conductivity produces accurate results, the sequential estimates from two different tests are plotted in Figure 2.6. The sequential k estimates (ordinate) leveled out after $t \approx 150$ sec, and approached constant values over the second half of the test. This is an indication that the experiment has been designed well (see Beck and Arnold (1977)). The same conclusion is supported by the normalized residuals plotted in Figure 2.7. The residuals are small, mostly lower than 1.5%, and appear to have random variation.

The variation of the thermal conductivity with temperature for the various thermal barrier materials is shown in Figure 2.8. The addition of facing polyester scrim to glass fiber mats increases the values of k and also increases the rate at which k varies with temperature. Whereas the value of k for the (bare) glass fiber mat increases by about 25% with a 50 degree rise in temperature, the corresponding increase for glass fiber mat with polyester scrims is about 90%. Therefore the ability of these two materials to conduct heat differs. The results also show that the conductivity of the elastomer is nearly independent of temperature whereas that of the ceramic fiber increases linearly with temperature. The reader should note that the values shown in Figure 2.8 for the elastomer represent the estimated thermal conductivity values after a scale-down factor of 10 has been applied. Down-scaling was done in order to show the qualitative trend of thermal conductivity with temperature for the elastomer in direct comparisons with the other materials. In quantitative terms, the elastomer has the highest values of k of all materials examined.

In the temperature range 295 K $\leq T \leq$ 345 K covered in the tests, the conductivity data shown in Figure 2.8 correlate well with temperature through the quadratic function: $k = \alpha T^2 + \beta T + \gamma$. The estimated values of the constants α, β, and γ are shown in Table 2.1.

Table 2.1: Correlation coefficients for heat capacity and thermal conductivity data (valid for: c, 295 K ≤ T ≤ 470 K; k, 295 K ≤ T ≤ 345 K)

Material ID	Density (kg/m^3)	c (J/kg K)			k (W/m K)		
		α ($J/kg\ K^3$)	β ($J/kg\ K^2$)	γ (J/kg K)	α (W/mK^3)	β (W/mK^2)	γ (W/mK)
gf	39.53	-0.0044	5.0564	-110.03	1.58E-5	-9.55E-3	1.5188
gffs	38.31	-0.0027	4.2325	89.052	3.28E-5	-0.0197	3.0292
elast	1729.1	-0.0055	6.4031	-309.43	0	3.59E-4	0.3380
kaow	96.11	-0.0049	5.2371	-276.79	0	1.16E-4	-8.67E-3

Key to material ID (material thickness in parenthesis)

gf Fiber glass mat, no facing scrim (1.96 cm)

gffs Fiber glass mat with polyester facing scrims (1.87 cm)

elast Elastomer, used between two fiber glass layers in the Cadillac sound blanket (0.14 cm)

kaow Kaowool ceramic fiber, product of K Corporation (2.0 cm)

2.5 NUMERICAL SIMULATION OF CONDUCTION HEAT TRANSFER THROUGH THE THERMAL BARRIER

The thermal properties and the experimental data from GM were utilized in the numerical code, PROP1DR, described later in this section, to investigate the influence of each material layer in the thermal barrier. As shown in Figure 2.9, the mock bulkhead assembly is modeled as a layered material of overall thickness L with known thermophysical properties. Given the heat flux, $q_A(t)$, and the temperature history, $T_A(t)$, on the "engine" side, the goal is to calculate the heat flux, $q_B(t)$, or the temperature, $T_B(t)$, on the "passenger" side.

Comparing the arrangement in Figure 2.9 with Figure 2.1, materials 1, 2, and 3 represent the "sound" blanket, the steel "bulkhead" layer, and the "dash" blanket, respectively. The experiments at GM were conducted without the "dash" blanket (see Figure 2.1) at the back of the steel wall to constitute suitable boundary conditions at that location. Specifically, convective heat transfer must be accounted for at the back wall in a complete analysis. Thus, the heat conduction analysis for the "sound" blanket was conducted separately in this study, using the interface conditions between

materials 1 and 2 of Figure 2.9 as the boundary conditions at $x=L$, where L is now L_1. One of the GM test results was used as the basis for our simulations in order to validate the numerical model and to make approximate deductions regarding the heat transfer by the various materials.

The plot of the transient thermal response of the glass fiber mat with facing scrim as obtained from the GM experiments, is shown in Figure 2.10. Thermocouples labeled X, Y, and Z are located at the front surface, the middle, and the back surface of the insulation material, respectively. Those labeled as K1, K2, and K3 are intrinsic thermocouples welded to the front surface of the steel plate, while K4 to K6 are also intrinsic on the back surface of the plate. The steady state value of the measured heat flux was 85 kW/m^2. The front scrim exposed to direct lamp heat rapidly burnt off. For this reason, it was difficult to control the thermal field. Our interest is transient data preceding ignition and subsequent burning of the material. We also see that the temperature at the front surface of the steel wall does not rise appreciably until after about 75s. Consequently, we impose a constant temperature boundary condition at the back of the insulation in our numerical computations carried out over the first 90s. For this reason, our numerical results shown in Figures 2.11-2.13 extend over only the first 90s, even though the GM results extend over an interval of 300s. Furthermore, we shall not extrapolate our results over the remaining 210 seconds of the interval.

Using the transient heat flux data as inputs and taking the average readings of K1, K2, and K3 as $T_B(t)$ (see Figure 2.10), the temperature profiles at various locations inside the insulation material are calculated using the program PROP1DR developed by Professor J. V Beck. The program employs the finite difference scheme to solve the heat conduction problem through the multi-layered barrier as posed in Eqs. (2.3) and (2.4). The thermal properties, k and ρc, of the various materials (estimated in the preceding section) are entered as inputs. The results show similar qualitative trends with the GM experimental data, see Figure 2.11. The differences between the numerical and the experimental results possibly arise from the difficulty in precisely locating the TCs in the soft, pliable materials. Also, detachment of TCs occurred from the material exposed to the incident heat flux. In addition, changes in the values of the thermal properties could have been caused by insulation burn-off during the tests.

Similar computations were performed using the data for the other materials. The results are plotted in Figure 2.12. In the figure, symbol "0" refers to the front surface exposed to the external heat flux and symbol "1/2" represents the half thickness. The results show that the largest reduction

in temperature across half-thickness of the material occurs with the Kaowool ceramic fiber because the difference between the "0" and "1/2" curves for this case is consistently the largest. It can be seen that the lowest temperatures are obtained with the elastomer even though the temperature drop across the layer is small in comparison to the other materials.

The case of a multi-layer thermal barrier wall consisting of a 0.54 cm fiber glass layer followed by a 0.44 cm layer of the elastomer and finally another 0.61 cm layer of fiberglass was investigated. The computed temperature profiles at the interface between the materials are shown in Figure 2.13. The results show that the temperature drop across the barrier is larger for this layered combination than for the individual glass fiber-based materials but lower than for the Kaowool.

2.6 SPECIAL CASES

In certain special cases the thermal variation of properties is such that transformation of the equations can produce constant coefficients. For example, the conductivity k and the volumetric heat capacity ρc may both depend upon T but the combinations $\alpha=k/\rho c$ or $r^2=k\rho c$ may be independent of temperature. Transformation can produce a readily-solvable system of equations.

We consider the former case of variable k, variable ρc and constant α. We let $u = \int_0^T \rho(s)c(s)ds$ in Equation (2.3) to find

$$\alpha_o \frac{\partial^2 u}{\partial x^2} = \frac{\partial u}{\partial t}$$

where $\alpha_o = k/\rho c$ is constant. This equation is much easier to solve than Equation (2.3).

We now consider the case where the quantity r^2 is constant. We let $u = \int_0^T (\rho c)^{-1} ds$ in Equation (2.3) and find that

$$\frac{\partial^2 u}{\partial x^2} = \left(\frac{\rho c}{r}\right)^2 \frac{\partial u}{\partial t}.$$

Here the coefficient $\rho c/r$ is still variable, but it does not appear under a derivative, as in Equation (2.3). This is a significant simplification for numerical solution.

By using the data of Table 2.1, we construct graphs of the thermal variation of $\alpha=k/\rho c$ and $r^2=k\rho c$. We see from Figures 2.14 and 2.15 that the values of α and r^2 for both elastomer and Kaowool varied much less than for the glass fiber mat with or without the "scrim". Shown in Figures 2.16 and 2.17 are the sensitivity coefficients $X = p^{-1}\partial p/\partial T$ where $p=(\alpha,r^2)$, showing that both

α and r^2 for elastomer and Kaowool are essentially insensitive to temperature.

2.7 DISCUSSION OF RESULTS FOR GLASS FIBER MAT WITH AND WITHOUT SCRIM

Figure 2.8 shows that the correlations of Table 2.1 for the glass fiber mat (gf) and the glass fiber mat with serim (gffs) produce k-values that appear to diverge as the test temperature increases. The k-value for gffs is consistently higher than the k-value for gf. At 300K, $k_{gf}=7.5\times10^{-2}$W/mK and $k_{gffs}=8.5\times10^{-2}$ W/mK, while at 345K $k_g=1\times10^{-1}$W/mK and $k_{gffs}=1.45\times10^{-1}$W/mK.. Thus, $k_{gf}/k_{gffs}=0.9$ and 0.7 at 300K and 345K respectively.

We attempt to support these results with simple calculations for steady 1-D conduction heat transfer. For a layered material of thickness L with scrims on either side (thickness ℓ) sandwiching a middle layer (thickness L-2ℓ) the solution of the steady, constant-property conduction equation gives $L/k_{gffs}=\ell/k_{scr}+(L-2\ell)/k_{gf}+\ell/k_{scr}$. Here we have defined the middle layer as the glass fiber mat (k_{gf}) and the two outer layers as the scrim (k_{scr}). The conductivity k_{gffs} is the value for the compound material with glass fiber mat and two outside scrim layers. In this steady-state problem the heat flux through each layer is identical. We rearrange the preceding formula to obtain

$$\frac{k_{gf}}{k_{gffs}}=1-\frac{2\ell}{L}\left(1-\frac{k_{gf}}{k_{scr}}\right). \tag{2.6}$$

According to this formula, $k_{gf}<k_{gffs}$ (see Figure 2.8) when $k_{gf}<k_{scr}$.

Our calculations leading to Equation (2.6) lend some support to the experimental measurements for k_{gf} and k_{gffs}. They suggest that when $k_{gf}<k_{scr}$, as shown in Figure 2.8, we also have $k_{gf}<k_{gffs}$. We did not estimate experimental values for k_{scr} and hence we did not make an actual numerical comparison in this research.

2.8 CONCLUSIONS

The results have shown that the addition of the thin polyester scrim layers to the glass fiber layer slightly increases the thermal properties, k and ρc, of the resulting multi-layered material. The polyester scrim appears to increase the rate at which the thermal conductivity rises with temperature. The thermal conductivity dictates the conductive transmission of heat through the medium. Our numerical calculations using heat flux data from GM as inputs to PROP1DR indicate that a fibrous ceramic material utilized as a single layer, or in combination with the elastomer as a multi-layered

compound material, may be an effective thermal barrier material in comparison with the other materials we examined.

A theoretical estimate is made based on a steady-state analysis of the equations of heat transfer. The estimate suggests that the data of Figure 2.8, part of which compares the fiber mats with and without scrim, shows a reasonable trend if the conductivity of the scrim is greater than the conductivity of the insulation layer in-between.

ACKNOWLEDGEMENT

The research described in this chapter was funded by General Motors pursuant to an agreement between GM and the U.S. Department of Transportation.

2.9 REFERENCES

[2.1] J. V. Beck and K.J. Arnold, *Parameter Estimation in Engineering and Science*, Wiley, 1977.

[2.2] J.V. Beck, B. Blackwell and C.R. St. Clair, *Inverse Heat Conduction: Ill-Posed Problems*, Wiley-Interscience, 1985.

[2.3] J.V. Beck and A.M. Osman, "Sequential Estimation of Temperature-Dependent Thermal Properties," *High Temperature-High Pressures*, 23:255-266, 1981.

[2.4] J.N. DeRis, "Spread of a Laminar Diffusion Flame," *Twelfth Symposium (International) on Combustion*, The Combustion Institute, Pittsburgh, 241-252, 1969

[2.5] K.J. Dowding, J.V. Beck and L. Eilens, "Method for Measuring the Orthotropic Thermal Conductivity and Volumetric Heat Capacity in a Carbon-Carbon Composite," in *Thermal Conductivity*, 23:107-118 (K. E. Wilkes, R. B. Dinwiddle, R. S. Graves eds.) Technometric, Lancaster, PA, 1996.

[2.6] A. B. Oladipo, I.S. Wichman and J.V. Beck, "Experimental Investigation of the Thermal Properties of Wood Fiber/Thermoplastic Composites," *Journal of Composite Materials*, 33(5):480-495, 1999.

[2.7] A. B. Oladipo, "Study of Thermal and Fire Behavior of Wood Fiber/Thermo-plastic Composite Materials," PhD Thesis, Michigan State University, East Lansing, MI, 1998.

[2.8] J. Santrock, Personal Communication, GM Research and Development Center, 1997.

[2..9] E.P. Scott and J.V. Beck, "Estimation of Thermal Properties in Carbon/Epoxy Composite Materials During Curing," *Journal of Composite Materials*, 26(1):20-36, 1992.

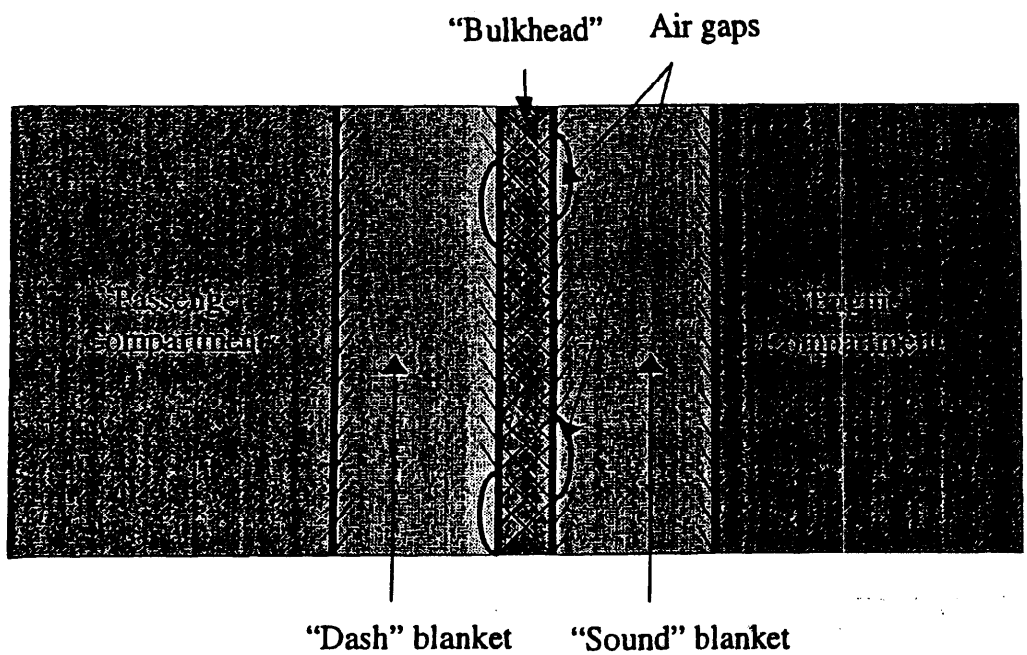

Figure 2.1: **Representation of a possible bulkhead assembly separating "engine" and "passenger" compartments, illustrating "dash" blanket, "sound" blanket and "bulkhead". Air gaps may form along the various interfaces, thereby contributing to "contact resistance.".**

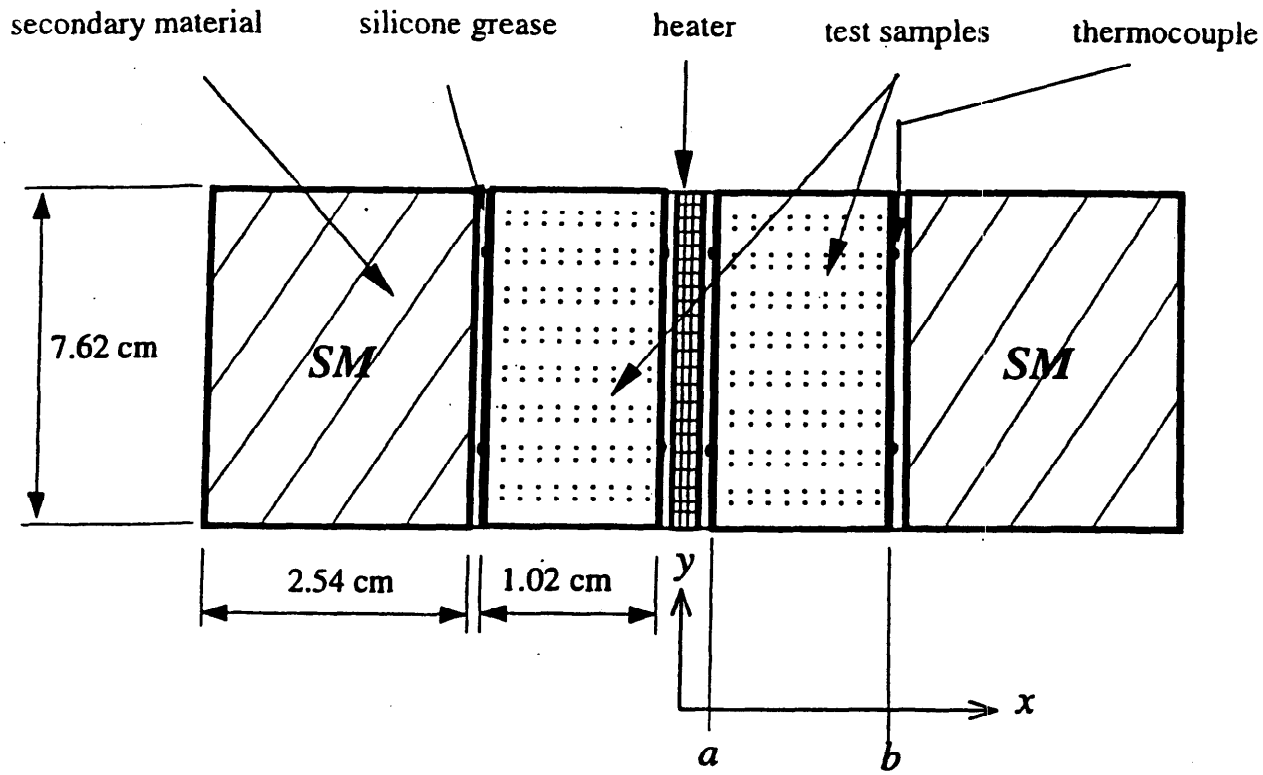

Figure 2.2: **Sample arrangement for thermal property measurement test. The components are described in Sec. 2.3.2. Note the symmetry of the arrangement with respect to the heater in the middle.**

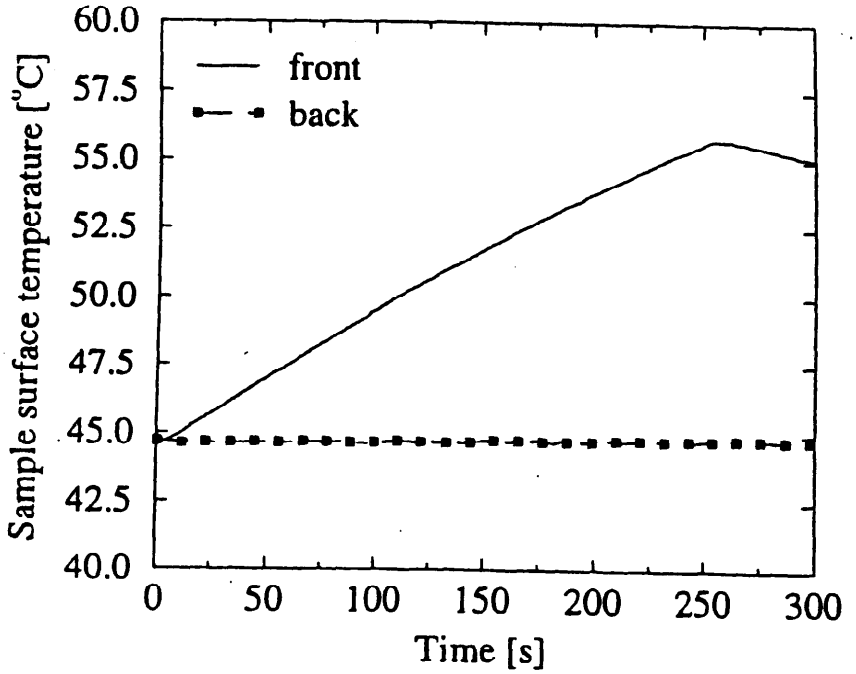

Figure 2.3: **Transient temperature profile measured during tests on fiberglass with q=285 W/m^2.**

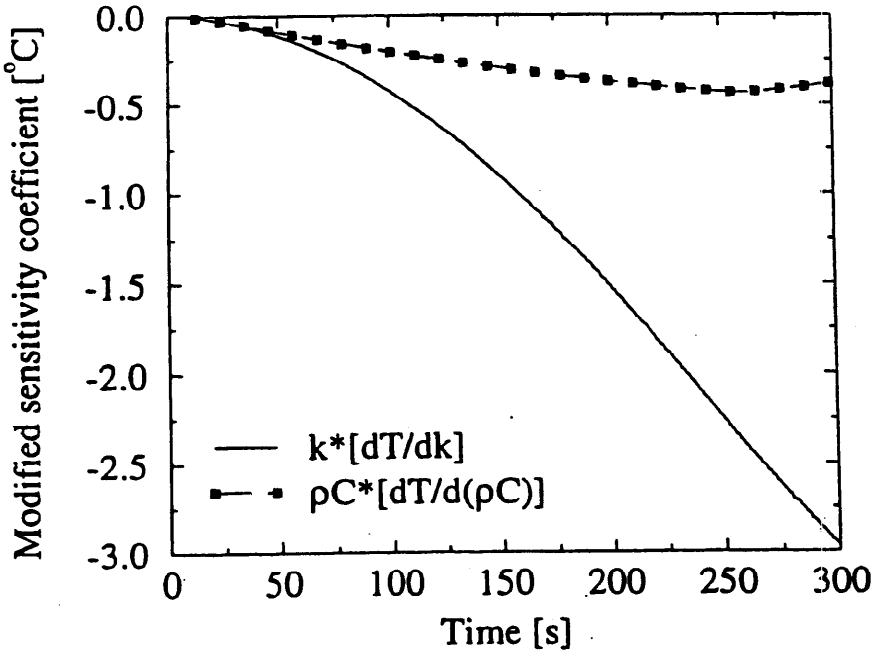

Figure 2.4: **Plot of normalized sensitivity coefficients defined in the figure. These sensitivity coefficients are uncorrelated because they possess different functional forms.**

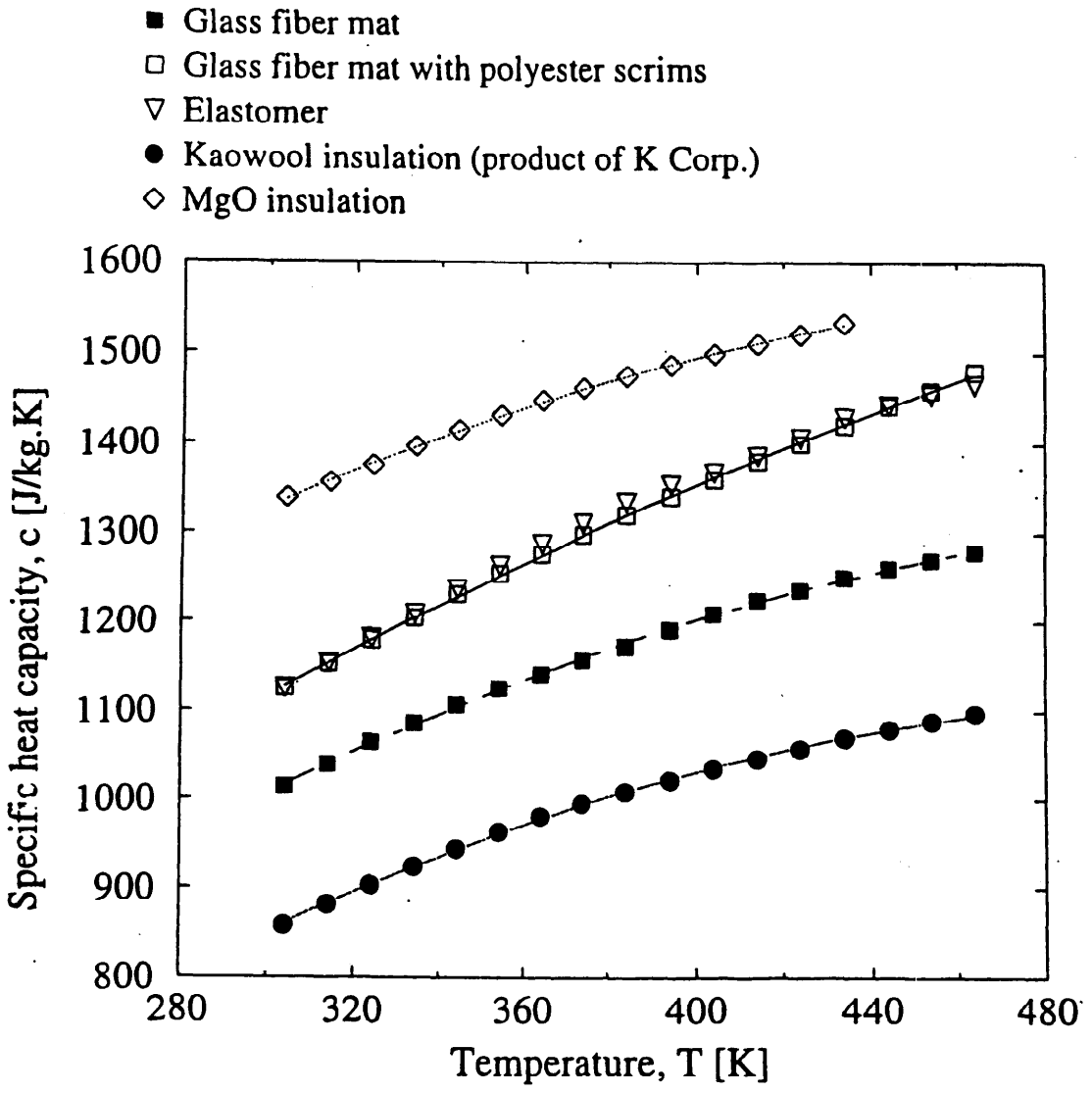

Figure 2.5: **Specific heat capacity of insulation materials as a function of the test temperature. Note the monotonic increase of the specific heat capacity as temperature rises.**

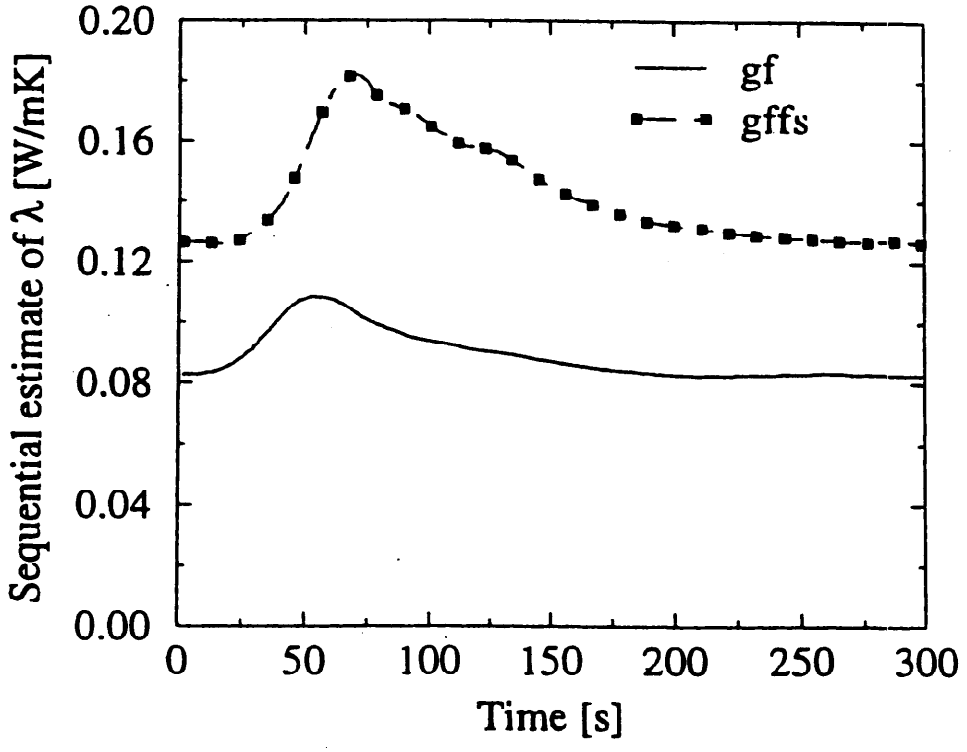

Figure 2.6: **Sequential parameter estimates of *k* for glass fiber mat (gf) and glass fiber mat with facing polyester scrim (gffs).**

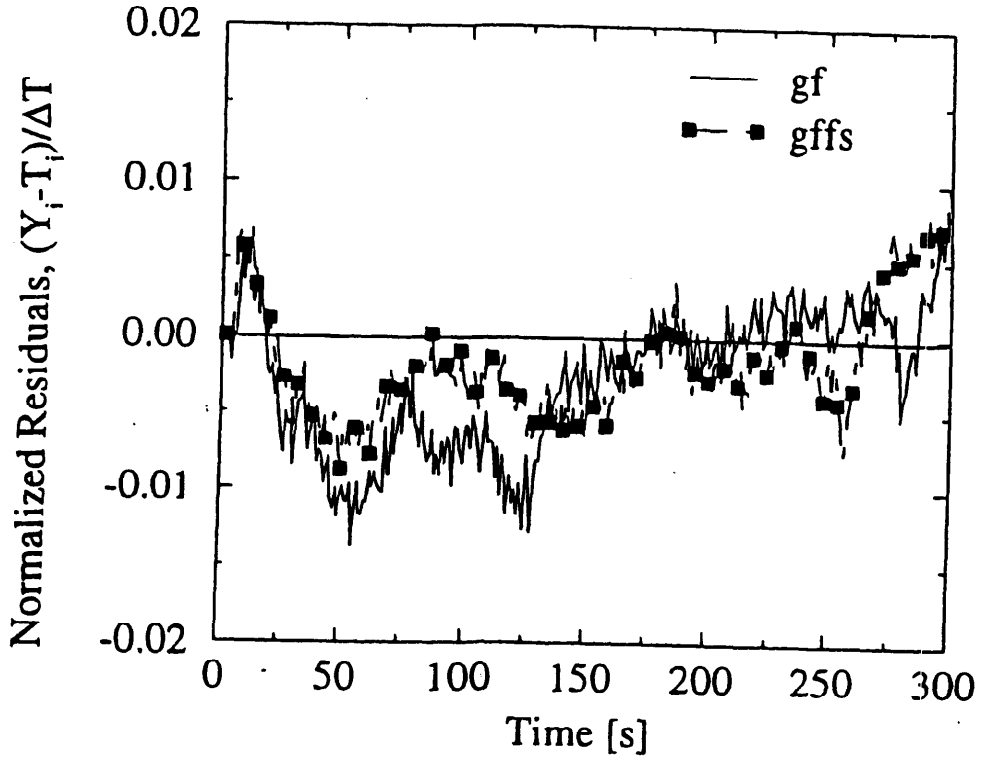

Figure 2.7: **Trend of normalized residuals for tests on thermal barriers. These appear random, as is necessary for a well designed test (Beck and Arnold (1977)).**

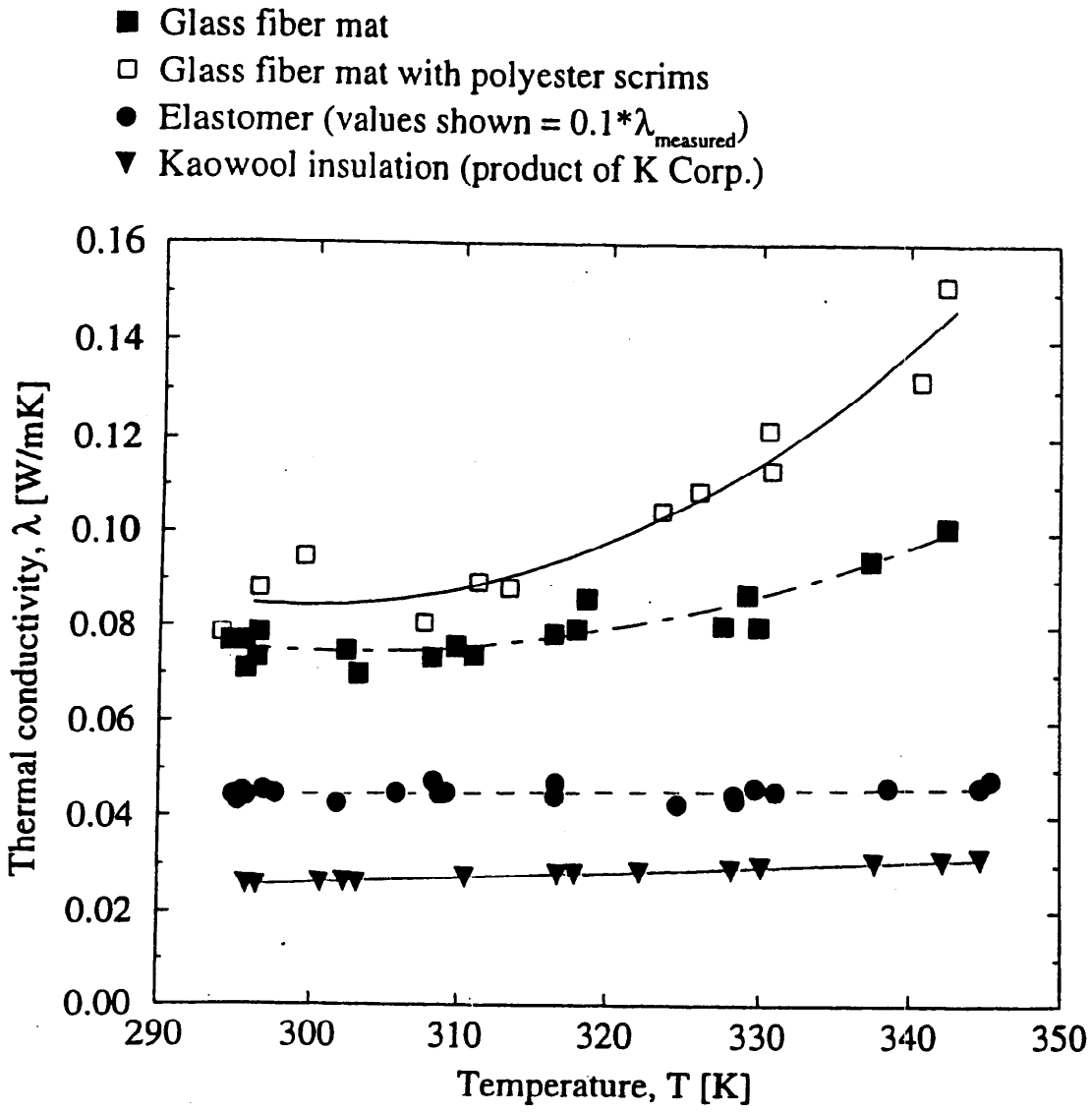

Figure 2.8: **Estimated thermal conductivity of some thermal barrier materials versus test temperature. The elastomer values are to be multiplied by 10 to obtain correct k values. The down-scaling for the elastomer was done in order to fit the comparison. Note that $k_{gf}<k_{gffs}$.**

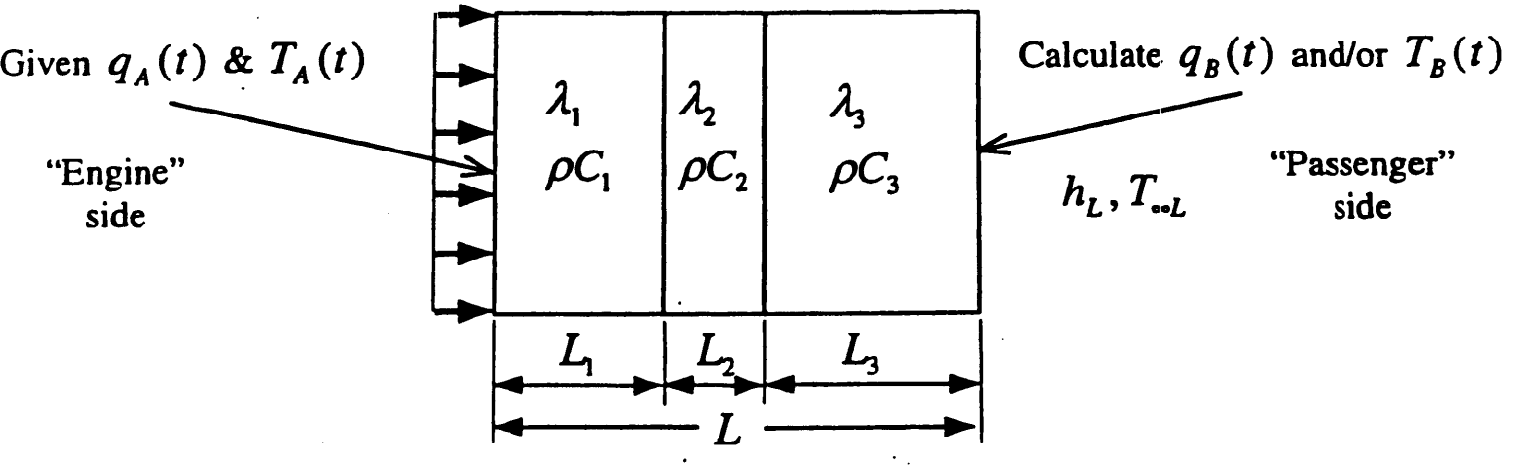

Figure 2.9: **Problem description for the model used in the numerical code PROPIDR developed at MSU by Prof. J. V. Beck.**

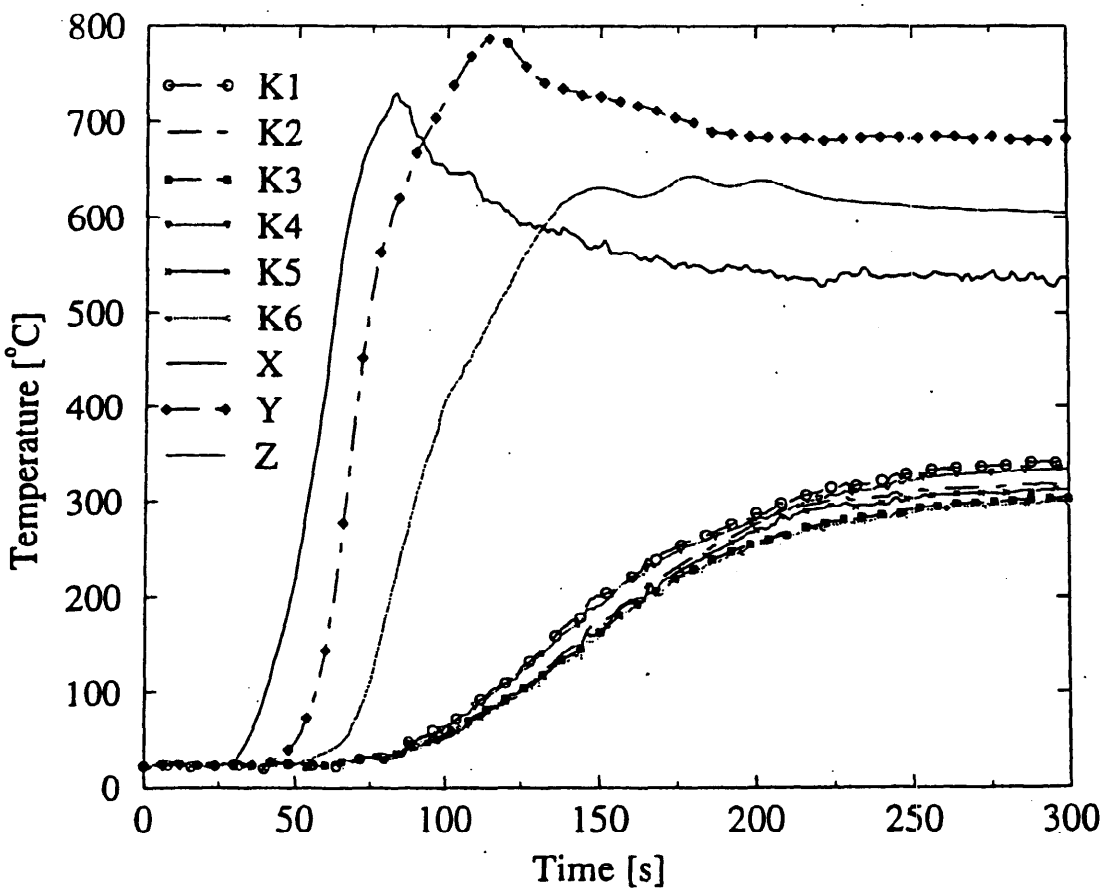

Figure 2.10: **Temperature profiles from a GM test on a glass fiber layer covered on both sides with polyester "scrim." These temperature profiles and other features of the GM experiments are examined in detail in Chapter 3.**

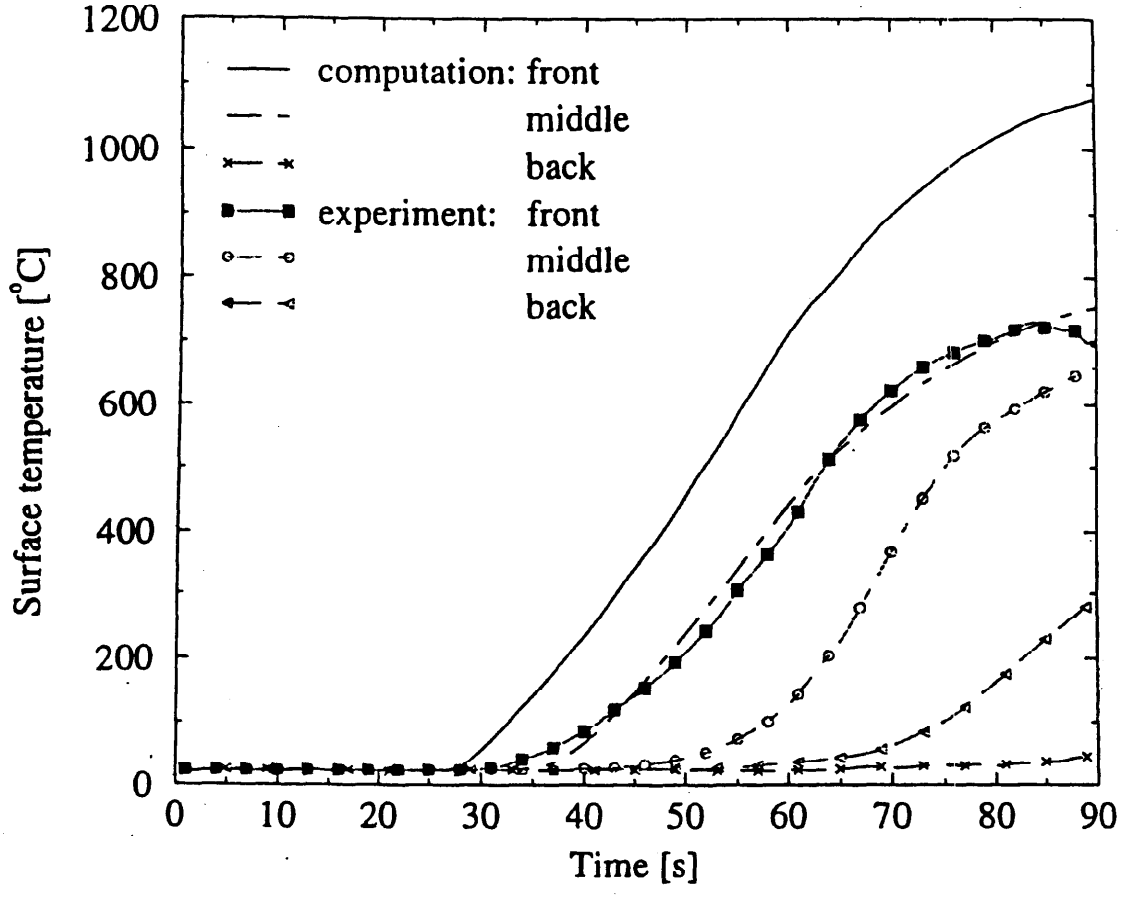

Figure 2.11: **Calculated surface temperature of fiberglass with polyester "scrim." Observe that the time internal for the computations is 90s, over which time the temperature rise of the back face is negligible. See Figure 2.10 for temperature vs. time data from thermocouples K4 to K6.**

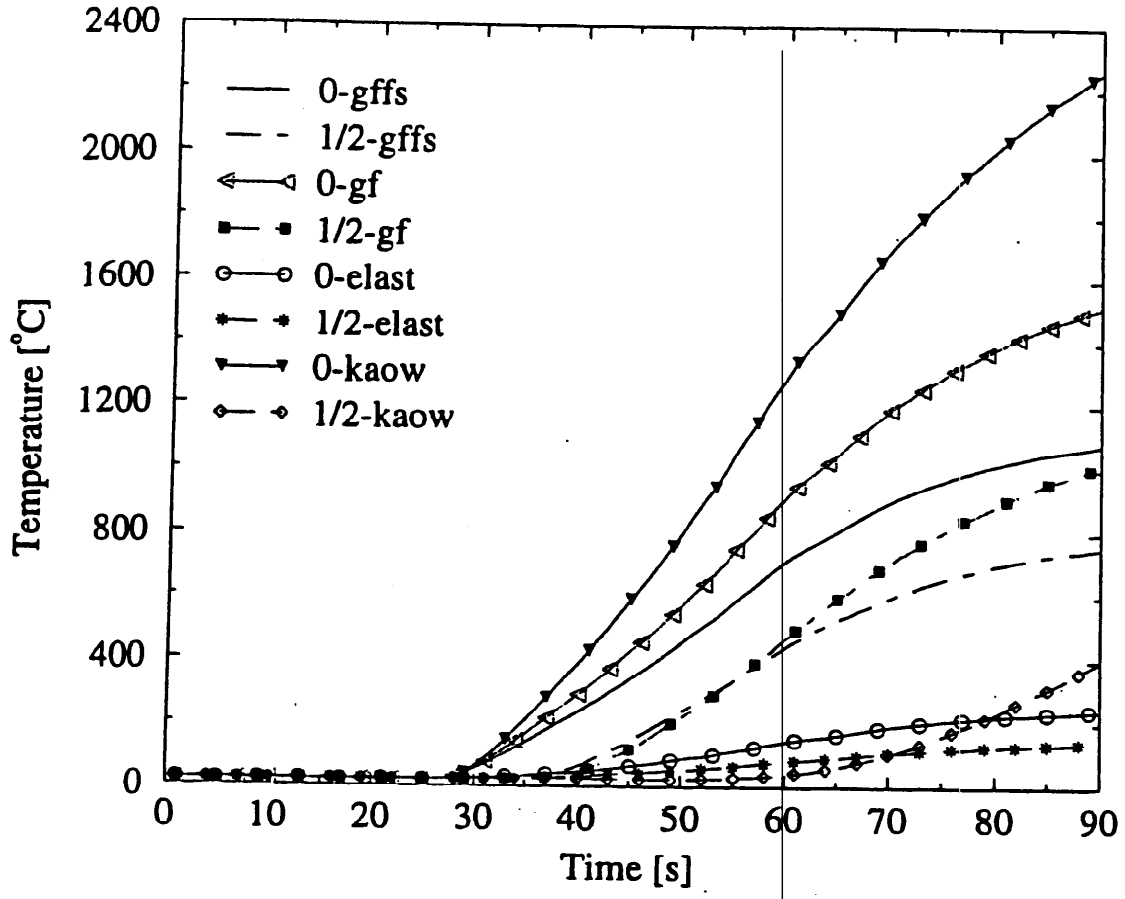

Figure 2.12: **Computed surface and mid-point temperatures for glass fiber, glass fiber with polyester "scrim", elastomer and Kaowool. As in Figure 2.11, the computation time is 90s.**

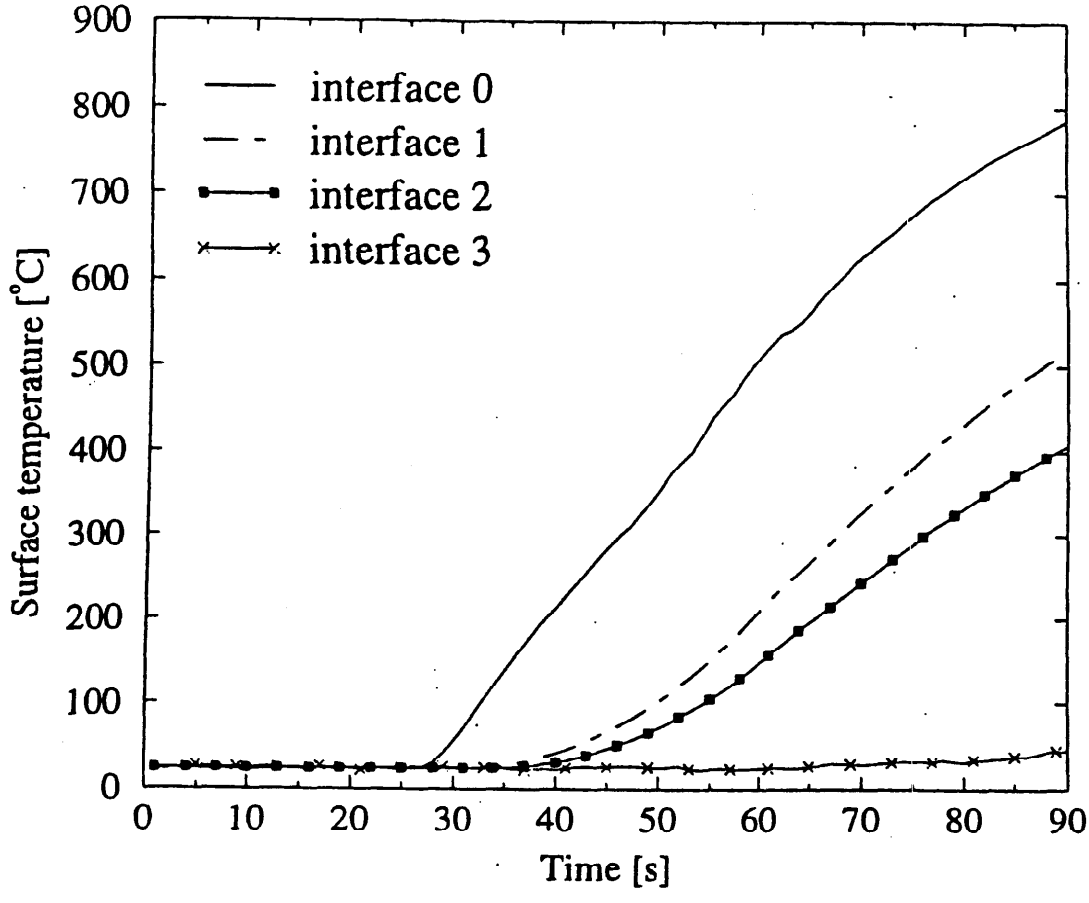

Figure 2.13: **Temperature response of the multi-layered thermal blanket. As in Figures 2.11, 2.12, the computation time is 90s.**

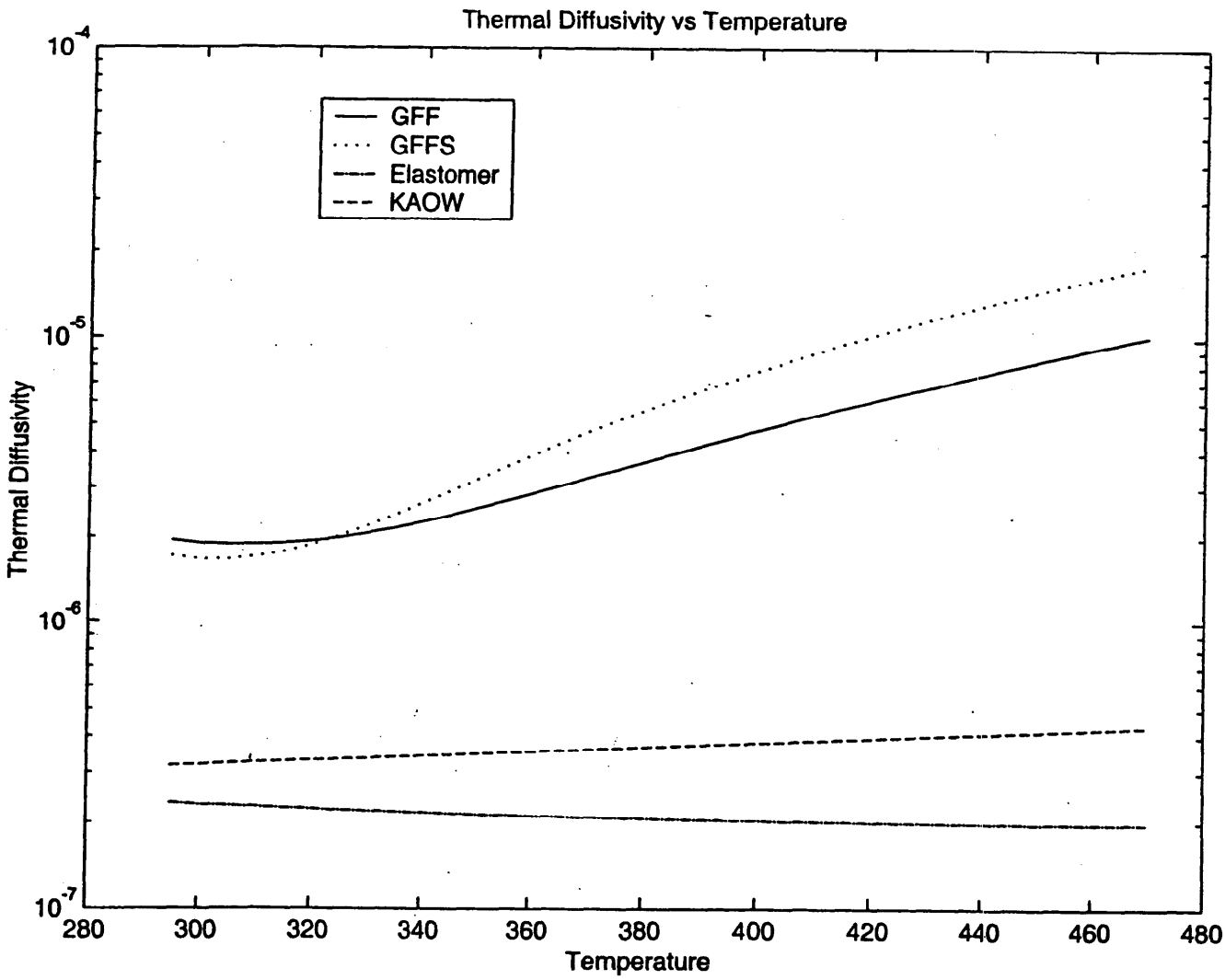

Figure 2.14: Plot of variation of $\alpha=k/\rho c$ versus T for the four tested materials.

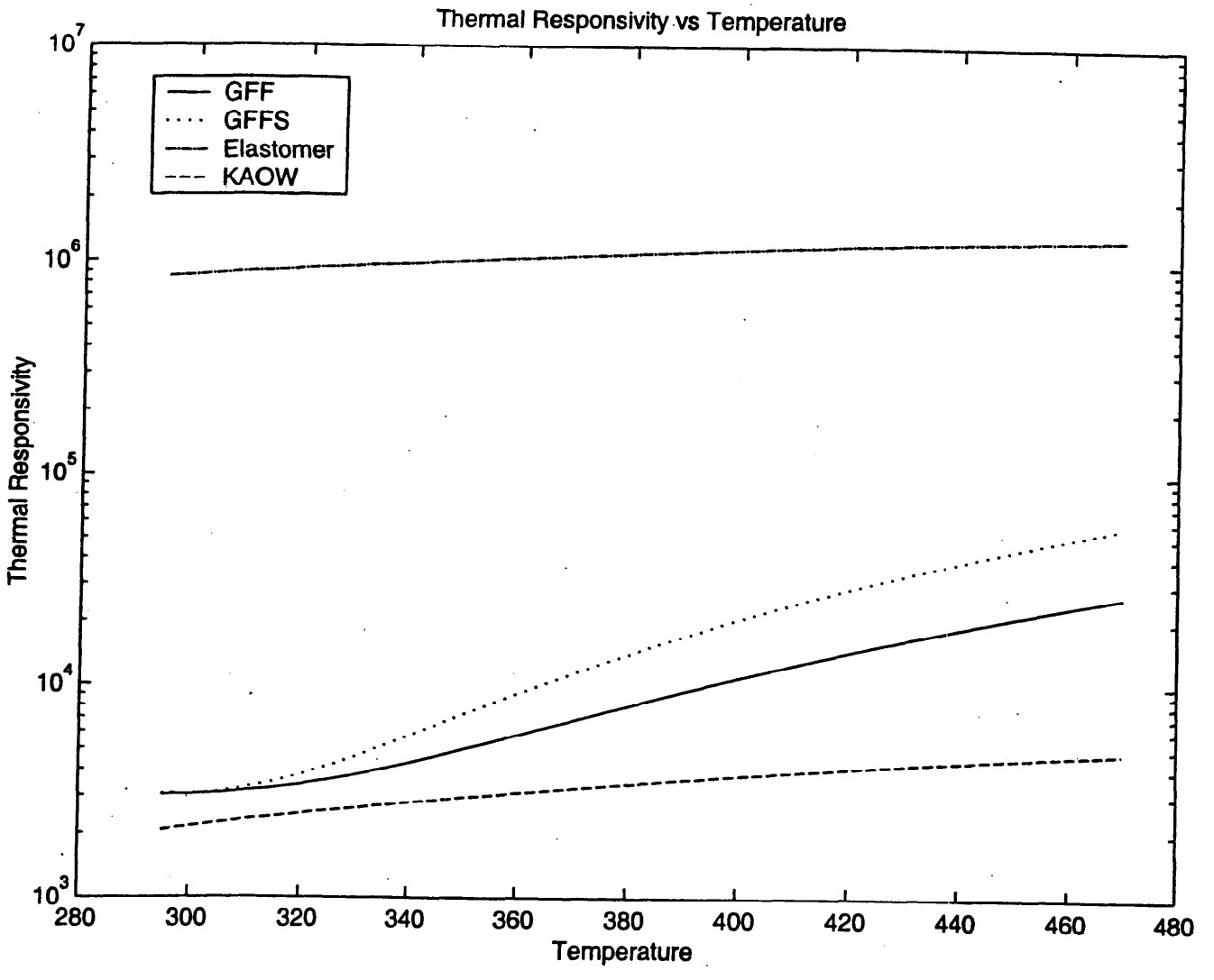

Figure 2.15: Plot of variation of $r^2=k\rho c$ versus T for the four tested materials. The quantity $r=(k\rho c)^{1/2}$ is sometimes referred to as the "thermal responsivity" of the material.

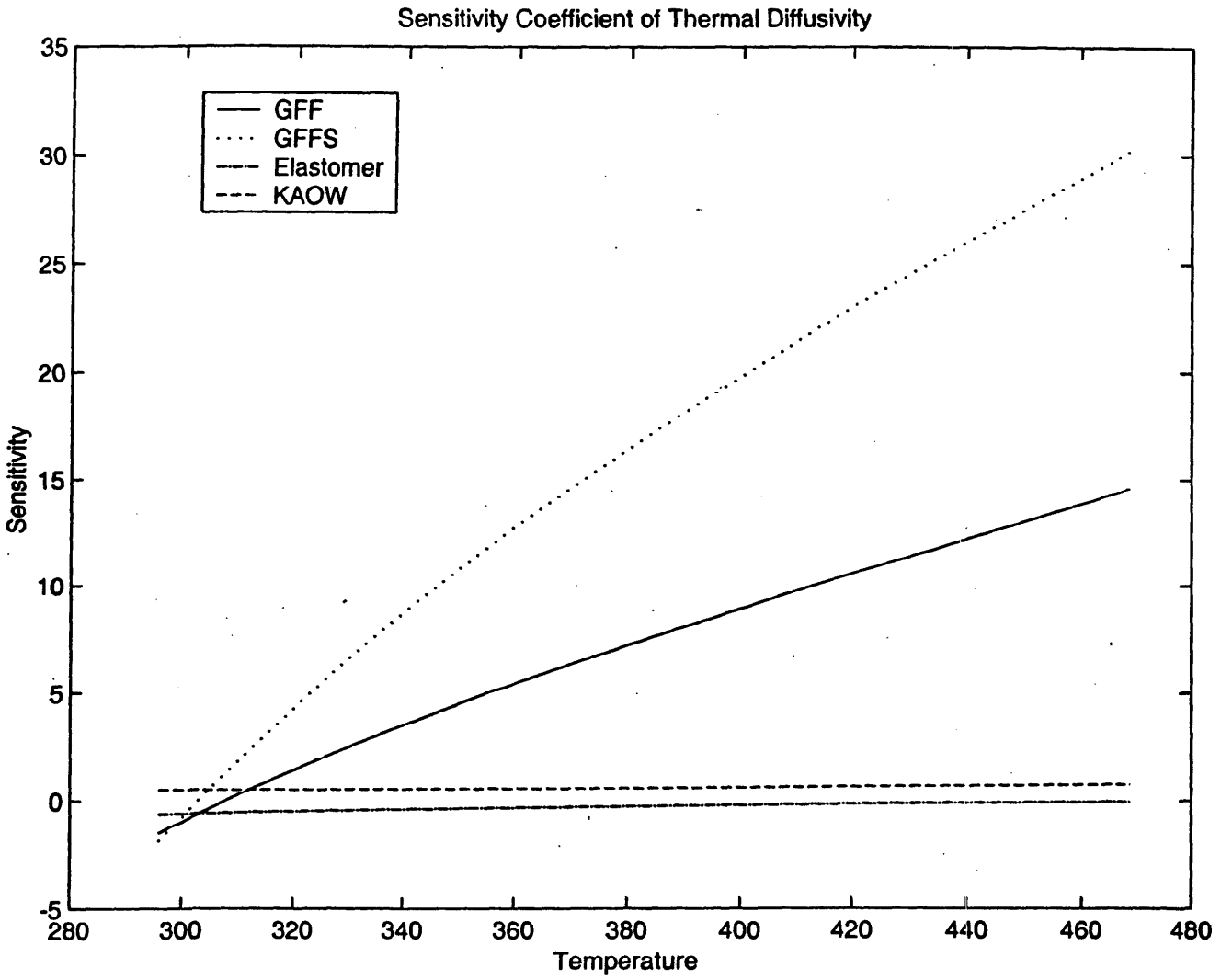

Figure 2.16: Plot of the sensitivity coefficient for the thermal diffusivity, $\alpha^{-1}\partial\alpha/\partial T$, versus T. Note the comparatively weak T-dependence for elastomer and Kaowool.

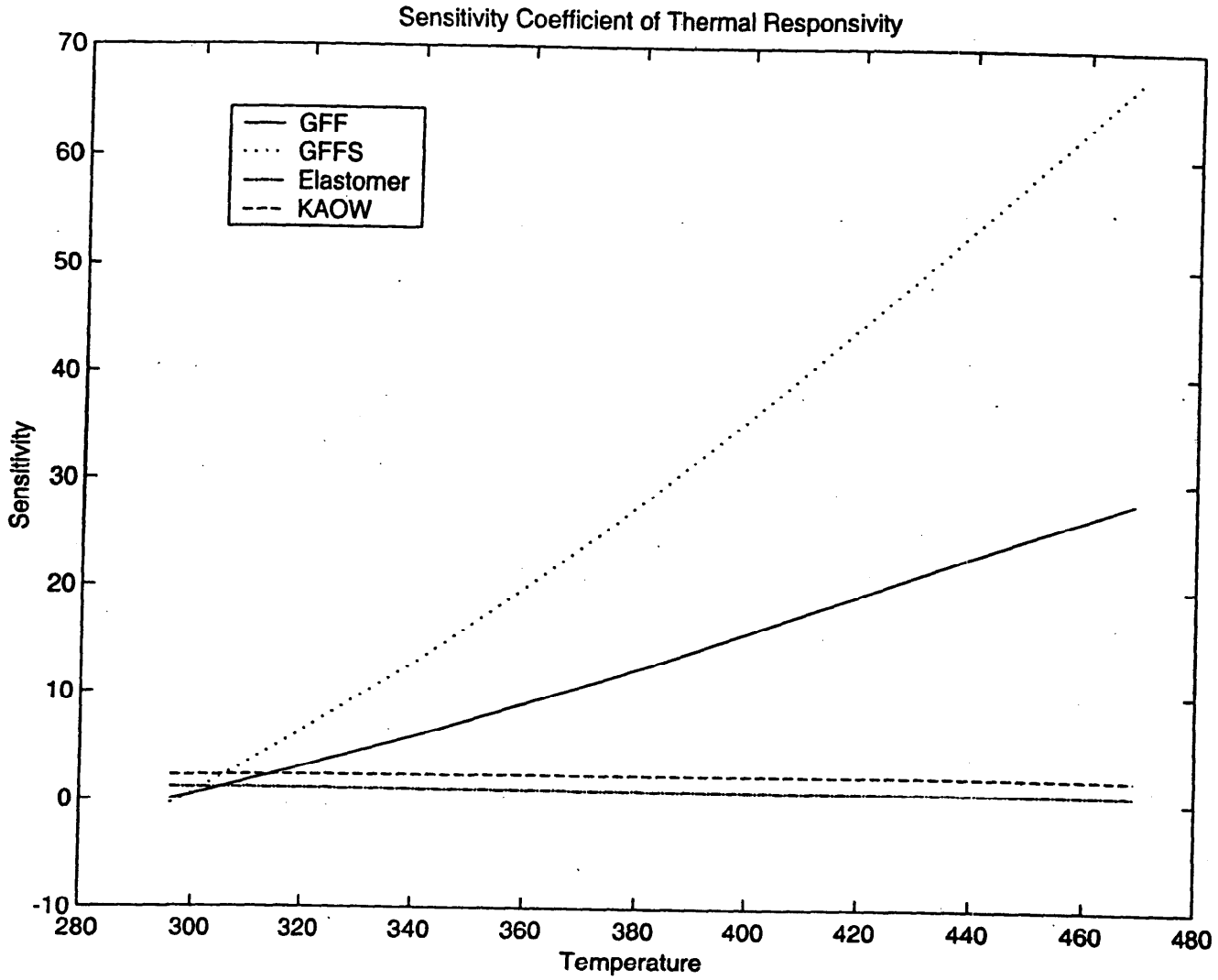

Figure 2.17: Plot of the sensitivity coefficient for the thermal responsivity, $r^{-2}\partial(r^2)\partial T$, versus the temperature, T.

CHAPTER 3

HEAT TRANSFER CALCULATIONS AND PARAMETER ESTIMATION OF THE THERMOPHYSICAL PROPERTIES FOR THERMAL BARRIERS

3.0 INTRODUCTION

The purpose of the work described in this chapter was to develop a mathematical model of heat transfer primarily by conduction through multi-layer materials and, if possible, to determine the thermal diffusivities and other thermal properties of the tested materials and heat transfer coefficients under the conditions of the tests. The material evaluations were performed (1) for the entire assembly, considered as one compound material, and (2) for the separate materials constituting the assembly. In evaluations (2) the properties of one layer (the steel panel) were considered known. The General Motors (GM) Research and Development Center performed measurements using a 32x32 cm heating panel to radiantly heat an insulated flat steel panel of 1/32 in (~0.8mm) thickness. Three thermocouples (TC) were intrinsically welded to each side of the steel panel and three TCs were located within the insulation. The location of the TCs (called K1, K2, K3 in Sec. 2.5, see Figure 2.10) is shown in Figure 3.1. The TCs were unshielded. These data were fitted to heat transfer models by the method of least squares in order to estimate the thermal diffusivity (Özisik (1993)) of the material and the convective heat transfer coefficient (Özisik (1993)) of the non-heated side of the panel. For the compound material, the model produces overall thermal diffusivity and heat transfer coefficient, whereas the models that consider separate material layers produce parameters for the separate materials, such as the insulation layer, for example.

Seven experiments were conducted by GM, designated here as test 1 through test 7. These tests were discussed in Chapter 2, Secs. 2.3.1, 2.5. Test 1 resulted in the detachment of the insulation layer and was therefore discarded from our analysis. Tests 2-4 used a fiberglass insulation of approximately 1.9 cm thickness. Tests 5-7 used a reflective aluminized silica insulation of 0.16 cm thickness. Both insulating materials were fibrous. The degree of contact between the TCs and the insulation was not known and may have varied from test to test and possibly during each test because the material changed during heating. Thus, although a particular TC was located under the incident surface of the insulation layer, the temperature it measured was not necessarily a good measure of the temperature of the insulation (Santrock (1998)). Experiments were conducted at separation distances between heating panel and steel panel ranging from 9 to 12 cm. The heater was utilized at the three intensities 25, 50 and 100 percent of maximum power (15 kW). Table 3.1 shows the power levels and distances from the sample for each experiment. Figure 3.1 shows the configuration of the experiment. Note that "compound material" refers to the combined insulation

layer and steel panel.

The radiant heat flux varied less than 5 percent over an area of approximately 10cm x 10cm on the center of the specimen panel. As shown in Figure 3.1 the specimen panel directly faced the heating panel. Temperature and heat flux measurements were recorded at 1-second intervals during each experiment. The other variables mentioned above were held constant throughout each experiment.

It is necessary to briefly discuss the choice of apparatus used to perform the experiments. In principle, the thermal conductivity and heat capacity of the insulating materials might be measured using standard (e.g., ASTM) testing procedures, and heat transfer coefficients for inclined, heated planes could be estimated without using radiant heating equipment. However, the behavior of a layered material consisting of two or more thermally disparate materials (insulation and steel) is difficult to assess from knowledge, however detailed, of individual material properties. The challenging and unresolved problem of contact resistance between the two disparate materials can produce large differences between predicted and actual behavior (Özisik (1993)). In addition, for these insulations it is very difficult to experimentally estimate thermal properties, as discussed in detail in a companion study (Oladipo (1988), Oladipo and Wichman (1999), see also preceding chapter). Finally, many insulating materials are externally lined with a polymeric material, sometimes referred to as a "scrim" (Santrock (1997)). This "scrim" possesses thermophysical properties generally different from the primary insulating material. The use of DSC (Differential Scanning Calorimeter) (Jodeh (2000)) indicated that the scrim layer consisted of polyester (the black material) and polyethylene (the white material). This was confirmed using FTIR (Jodeh (2000)). As an added complication, the "scrim" can, for sufficiently high radiant fluxes, burn off the face of the insulation, thus exposing the insulation beneath the "scrim" directly to the external radiant flux. An objective of the GM tests was partial fidelity to "actual" conditions. For this reason, the GM experiments employed an experimental apparatus that mimicked conditions that might be encountered during a fire. We qualify this statement by noting that at no time during these GM tests was fire actually present: the radiant fluxes were of "fire level" but they did not originate from a fire.

One of the goals in our examination of the GM data is to provide a means for estimating material parameters that can be used to calculate heat transfer through layered materials. Another goal is to determine the extent to which the layered material can be considered as a single

"compound" material in its thermal properties and heat-transfer rates. The theory ideally should be simple enough to be amenable to engineering analysis. Also, the parameters should provide an accurate description of material behavior in response to heating.

3.1 HEAT TRANSFER MODELS FOR THE COMPOUND MATERIAL OF THE THERMAL BARRIER

In order to estimate thermal parameters from the GM data, a direct solution must first be formulated for heat conduction through the compound insulation and steel plate assembly. As shown in Figure 3.1, the vertically oriented layered material is radiantly heated on the insulation side while the adjacent steel surface is exposed to ambient laboratory air. The difference between this apparatus and that of Chapter 2 (see Figure 2.2), which was designed specifically to evaluate material thermo-physical properties, underscores the different aims of the research described in these two chapters. Some of the incident radiation is absorbed into the material and some is reflected. Heat is lost from the rear of the material by emitted radiation and natural convection. The thermal energy leaving the back surface is a fraction of that absorbed on the front surface.

Table 3.1: Schedule of Power and Distance

Test	Heater Power (%)	Distance from Heater to Sample (cm)	Average Incident Intensity for 0-5 min. (kW/m^2)
2	50	12	43.5
3	100	12	64.3
4	25	9	14.5
5	50	12	38.6
6	25	9	14.1
7	100	12	67.1

The precise mathematical model for a complex, compound material is difficult to formulate rigorously, and is also difficult to solve (Chapter 8 of Özisik (1993), Furmanski and Floryan (1994)). Insulating materials and conductors such as steel are known to have temperature-dependent

thermophysical properties. In addition, fibrous insulating materials may allow radiation to penetrate the irradiated surface before it is fully absorbed. Contact conductance between imperfectly joined materials must be empirically estimated. Certain physical processes such as the internal absorption of surface radiation are too complex to address here. We assume that the "scrim" absorbs the incident radiant flux at the surface although as discussed later this is a moot point because the only measurements we utilize in our models are the actual surface temperature measurements by the attached TCs. The question of contact conductance will be circumvented by mostly examining compound material response, although we also formulate and examine simple models in which the layers of insulation and steel are considered separately. In these latter models the question of contact conductance is not addressed. The question of temperature-dependent properties is also difficult. We shall address this question in our work, even though we shall be forced to assume constant properties during most of our analysis.

We presently formulate the heat transfer model using integral heat transfer analysis. Three related but distinct forms of the model equations will be examined in Secs. 3.1.1-3.1.3.

We first write the integral form of the equation for conservation of thermal energy in the compound material. Over the heated surface A exposed to the uniform incident radiant flux we have

$$\iint_A [q_{in} - q_{out}]dA = \int_V \iiint \dot{E}dV = \int_v \iiint \frac{\partial}{\partial t} \int_{T_o}^{T} \rho c ds dV.$$

Here, we have used $E = \int_{T_o}^{T} \rho c ds$ as the sensible thermal (internal) energy of the material. We write

$$q_{in} - q_{out} = -k\,\partial T/\partial x - [k\,\partial T/\partial x + \Delta x\,\partial(-k\,\partial T/\partial x)/\partial x] + O(\Delta x^2) = \Delta x(\partial(-k\partial T/\partial x)/\partial x,$$

where x is the coordinate normal to the heated surface (see Figure 1) in the material. We write $dV = dAdx$ to find the result

$$\rho c \frac{\partial T}{\partial t} = \frac{\partial}{\partial x}\left(k \frac{\partial T}{\partial x}\right). \tag{3.1}$$

Implicit in our derivation is assumed continuity of $k\partial T/\partial x$ and its first derivative everywhere in the material. Constancy of k and α, is not required in the derivation of Equation (3.1).

3.1.1 Direct Model (Compound Material)

Here we assume constant k and α with respect to t, x and T. In the following computed results for the GM data, it will become apparent that this approximation is not strictly valid. Nevertheless, a reasonable basis for estimating compound properties can be established, and deviations from strict constancy can be approximately accounted for. Equation (3.17) becomes

$$\rho c \frac{\partial T}{\partial t} = k \frac{\partial^2 T}{\partial x^2}. \tag{3.2}$$

The boundary conditions are

$$T(0,t)=T(t), \tag{3.3}$$

$$-k\left[\frac{\partial T}{\partial x}\right]_{x=L} = h(T_{x=L} - T_\infty). \tag{3.4}$$

The initial condition is $T(x,0)=T_\infty$. In these equations, ρ is the density, c is the specific heat, k is the thermal conductivity, h is the convective heat transfer coefficient, and L is the sample thickness. When Equation (3.2) is divided by k, and Equation (4) is divided by k/L, the parameter groups diffusivity and Biot number arise. These are given the symbols α and Bi, respectively, where

$$\alpha = \frac{k}{\rho c} \tag{3.5}$$

and

$$Bi = \frac{hL}{k}. \tag{3.6}$$

Here L is the total thickness of the compound material, $L=L_1+L_2$. The physical meanings of α and Bi are discussed in detail in textbooks on heat transfer (e.g., Özisik (1993)). The former is a measure of the ability of the material to transmit a thermal pulse, the latter a ratio of heat lost from the back surface, $h\Delta T$, to the heat conducted across the layered material, $k\Delta T / L$. Since the parameters contained in these groups do not appear individually in the model equations, the parameter estimates for thermophysical properties k, ρc, h cannot be found individually. If, for example, the conductive heat flux at the surface of the insulation were known, the left boundary condition would become

$$-k\left[\frac{\partial T}{\partial x}\right]_{x=0} = q(0,t).$$

In this case the thermal conductivity k of the compound material could be estimated as a separate

parameter. In the present case, however, the surface heat transfer at the left-hand boundary is complicated and includes incident radiant flux, emitted radiation from front and rear surfaces, convective losses from both faces, and conduction into the solid material. Although the temperature at the surface was measured, the conductive heat transfer rate into the material cannot be isolated. This analysis therefore estimates only the two parameter groups, diffusivity (α) and Biot number (Bi).The boundary condition of prescribed temperature at $x = 0$ is given by the temperature measurements at the insulation surface. This surface is exposed to the incident radiant flux from the heating panel.

The solution to Equations (3.2) - (3.4) is then found via a finite difference method (Forsyth and Wasow (1960)) in the windows-based program GM1.EXE. The parameter estimation computations described in Secs. 3.3.1-3.3.3 are also performed by this program. This program was custom-made for GM as part of this contract research work. The direct solutions were validated with the program **conds.exe**, a conductive heat transfer program developed independently by Prof. A. Haji-Sheikh of the University of Texas at Arlington.

3.1.2 Direct Model (Separate Panel and Insulation)

In this model the thermal properties of the insulation layer are assumed constant, as in Sec. 3.1.1, but Equation (3.2) applies only to the insulation layer We recall that tests 2-4 used fiberglass insulation, tests 5-7 used aluminized silica insulation. The thermal properties of the steel layer, considered known, are (Eshbach (1963)) k_s=49.2 W/mK, $(\rho c)_s$=3.93×10^6 J/kgm^{3}K, so that α_s=0.124 cm^2/s. Subscript "s" denotes steel. The initial condition is the same as in Sec. 3.1.1, $T(x,0)=T_\infty$ everywhere in the material. In addition, the temperature distribution on the heated surface is given by Equation (3.3), while the boundary condition at the back surface of the assembly is given by Equation (3.4).

It is necessary to describe the two boundary conditions at the insulation/steel interface. The first condition is continuity of temperature, for which the temperatures of insulation and steel at this surface are considered identical. The description of the second condition is more complicated. At any location in the material we may write Equation (3.1) as $\rho c\partial T/\partial t=-\partial q/\partial x$ with $q=-k\partial T/\partial x$. This equation is discretized as $\rho c(T(x,t) - T(x,t-\Delta t))/\Delta t = (q(x+\Delta x,t) - q(x,t))/\Delta x$ with $q(x+\Delta x,t) = - k(T(x+\Delta x,t) - T(x,t))/\Delta x$ and $q(x,t) = - k(T(x,t) - T(x-\Delta x,t))/x$. After rearrangement one finds

$$\frac{\rho c \Delta x}{\Delta t} T_i^{j-1} = -\frac{k}{\Delta x} T_{i-1}^j + \left(\frac{k}{\Delta x} + \frac{k}{\Delta x} + \frac{\rho c \Delta x}{\Delta t} \right) T_i^j - \frac{k}{\Delta x} T_{i+1}^j,$$

where $T_i^j = T(x,t)$ and $T_i^{j-1} = T(x,t-\Delta t)$ with similar notation for the other quantities. Individual values of k and ρc are irrelevant in this implicit difference scheme because they appear only in the combination $\alpha = k/\rho c$. At the interface we generalize the above formula by employing the differing property values on each side, viz.,

$$\left(\frac{(\rho c)_1 \Delta x_1 + (\rho c)_2 \Delta x_2}{2\Delta t} \right) T_i^{j-1} = -\frac{k_1}{\Delta x_1} T_{i-1}^j + \left(\frac{k_1}{\Delta x_1} + \frac{k_2}{\Delta x_2} + \frac{(\rho c)_1 \Delta x_1 + (\rho c)_2 \Delta x_2}{2\Delta t} \right) T_i^j - \frac{k_2}{\Delta x_2} T_{i+1}^j,$$

where we have used separate step sizes Δx_1 and Δx_2 on the two sides of the interface. A diagram showing the equations and boundary conditions for this case is shown in Figure 3.2. In the special case $(\rho c)_1 = (\rho c)_2 = \rho c$ and $k_1 = k_2 = k$ and $\Delta x_1 = \Delta x_2 = \Delta x$ the latter equation reduces to the former. In the process of parameter estimation (see Sec. 3.3.2) separate α values are employed in each material. In the case $\Delta x_1 = \Delta x_2 = \Delta x$ it is straightforward to show that if α_1 and α_2 are *fixed* and k_1, k_2 are *specified*, then the resulting ρc values, $(\rho c)_1 = k_1/\alpha_1$, $(\rho c)_2 = k_2/\alpha_2$, are also *fixed*. To illustrate this, we rewrite the preceding equation as

$$\frac{\Delta x^2}{2\alpha_1 \Delta t} \left(1 + \frac{(\rho c)_2}{(\rho c)_1} \right) T_i^{j-1} = -T_{i-1}^j + \left(1 + \frac{\alpha_2}{\alpha_1} \frac{(\rho c)_2}{(\rho c)_1} + \left(1 + \frac{(\rho c)_2}{(\rho c)_1} \right) \frac{\Delta x^2}{2\alpha_1 \Delta t} \right) T_i^j - \frac{\alpha_2}{\alpha_1} \frac{(\rho c)_2}{(\rho c)_1} T_{i+1}^j.$$

In this equation, only the ratios α_2/α_1 and $(\rho c)_2/(\rho c)_1$ appear. Once again, individual values of k and ρc in each material cannot be evaluated separately, even from the interfacial boundary condition. Consequently, the parameter estimation technique described in Sec. 3.3.2 evaluates only the thermal diffusivities α_1, α_2 and the Biot number Bi at the back surface. At the back surface the boundary condition is written in discretized form as

$$\frac{(\rho c)_2 \Delta x}{\Delta t} \left(T_n^j - T_n^{j-1} \right) = \left(T_{n-1}^j - T_n^j \right) \frac{k_2}{\Delta x} + h \left(T_\infty^j - T_n^j \right),$$

which can be rearranged to give

$$-T_{n-1}^j + \left(1 + \frac{\Delta x^2}{\alpha_2 \Delta t} + \frac{h_2 \Delta x}{k_2} \right) T_n^j = \frac{\Delta x^2}{\alpha_2 \Delta t} T_n^{j-1} + \frac{h \Delta x}{k_2} T_\infty,$$

showing that only α_2 and $Bi = h_2 \Delta x / k_2$ can be estimated. In summary, the parameter estimation procedure can be applied only for the estimation of α_1, α_2 and $Bi = h \Delta x / k_2$. The Biot number is

defined with respect to the properties of the steel because k_2 in the preceding formulas is the conductivity of steel.

3.1.3 Direct Model (Separate Panel and Insulation with Panel Acting as a "Calorimeter" to the Insulation)

The discussion of Sec. 3.1.2 has explained why it was possible to estimate only Biot number and diffusivity in Secs. 3.1.1 and 3.1.2. If, however, the heat flux is known at one of the boundaries, *all* thermophysical parameters (k and ρc) can be found independently. In the present analysis, we specify the heat flux at the unheated side of the plate by only utilizing the early measurements of the experiment, before heat loss from the steel plate to the surroundings become appreciable. As part of this approach, the plate is assumed to be "insulated" so the heat flux is *nil*. Thus, the only temperature measurements considered here are for the early part of the experiment, during which time the steel plate temperature rises a few (less than 5K) degrees. The entire steel plate is then considered as a "lumped" mass, or "constant-T calorimeter", whose temperature is assumed to have average value of the six thermocouples attached to it. When the temperature of the steel "calorimeter" is a known function of time, it is necessary to specify initial and boundary conditions only for the insulation layer.

We employ Equations (3.2) and (3.3), along with the initial condition $T(x,0)=T_\infty$ in the insulation. At the insulation/steel boundary we write the expression for the heat flux leaving the insulation and entering the steel plate employing the "lumped" formulation, viz.

$$\left(-k\frac{\partial T}{\partial x}\right)_{insulation} = \rho c L_2 \left(\frac{\partial T}{\partial t}\right)_{steel},$$

where L_2 is the steel layer thickness. Since $(\partial T/\partial t)_{steel}$ is known from the six TC measurements, the flux at the insulation is "known" in terms of ρc, L_2 and $(\partial T/\partial t)_{steel}$. These conditions plus the condition of continuity of temperature at the steel/insulation boundary, enable the estimation of k and ρc for the insulation layer, as demonstrated in Sec. 3.3.3. In this formulation there can be no back-face Bi estimation. A diagram showing the equations and boundary/initial conditions for this case is found in Figure 3.3.

3.2 PARAMETER ESTIMATION METHODS

Using the preceding numerical solution method, the parameters α and Bi can be estimated using the temperature measurements on the back surface $x=L$ of the compound material, where $L=L_1$

+ L_2 in Figure 3.1. These measured temperatures are compared to the calculated temperatures at $x=L$. Parameters α and Bi are found by minimizing the sum of squares of the difference between calculated and measured temperatures, i.e. by the method of ordinary least squares. The parameters α and Bi are adjusted until the experimental temperature profile at $x=L$ matches the theoretical predictions of the direct model as given in Equations (3.2)-(3.6). The expression to be minimized is (Beck and Arnold (1977))

$$S = \sum_{i=1}^{N} (Y_i - T_i)^2,$$

where Y_i designates the measured temperatures at the time step i, T_i designates the calculated theoretical temperature at the time step i, and N designates the number of measurements. This minimization is accomplished through an iterative non-linear regression procedure. In order to refine the parameter estimates between successive iterations, it is necessary to compute the sensitivity coefficients for the two parameters being estimated. These are obtained by differentiating the direct solution for the temperature with respect to the estimated parameters α and Bi. Since the solution is obtained numerically, the derivatives are approximated from the solution. These derivatives were obtained by computing the temperature distribution using the separate sets of α and Bi, and then differentiating the temperature fields with respect to α and Bi. A detailed exposition of all aspects of parameter estimation used in this report is provided in the standard reference on this subject (Beck and Arnold (1977)). The plots shown in Figure 3.2 show what are defined in the literature as "modified" sensitivity coefficients, which are the derivatives mentioned previously multiplied by the applicable parameter. In general,

$$X_n = p_n \frac{\partial T}{\partial p_n},$$

where X_n is the sensitivity coefficient and p_n is the corresponding parameter. The magnitudes of these sensitivity coefficients can be compared directly because they both have units of temperature. Sensitivity coefficients in a well-designed experiment are *large* and *uncorrelated.* (see Beck and Arnold (1977)).

Uncorrelated sensitivity coefficients have shapes which, plotted over time, differ in shape from one another, as a oscillatory sinusoid differs from a monotonically rising exponential, for example. If one coefficient is positive and the other negative, however, they are in fact correlated

if their ratio for the duration of the experiment is approximately constant. In this case, the coefficients are simply multiples of one another.

There are some slight differences in the parameter estimation methods needed for the three models of Sec. 3.1. These differences are described in Sec. 3.3.

3.3 ANALYSIS OF EXPERIMENTAL MEASUREMENTS AND ESTIMATED PARAMETERS

3.3.1 Direct Model (Compound Material)

The estimated parameters are shown in Table 3.2.

Table 3.2: Estimated Parameters

Material	Test	Diffusivity (cm^2/sec)	Biot Number (unitless)	Residual Std. Deviation (°C)	Temperature Rise ΔT (°C)
Fiberglass 1.96 cm Thick	2	0.00939	2.649	2.568	171
	3	0.00894	0.359	8.590	336
	4	0.00521	6.182	2.107	66
Aluminized Silica 0.16cm Thick	5	0.000705	1.307	2.265	68
	6	0.000202	1.527	2.359	26
	7	0.000824	1.331	2.741	156

There is variation of estimated α between experiments of like material. This may be due in part to the variations in heating caused by changes in the insulation in the separates tests under different heat fluxes and, therefore, in the corresponding temperature rises imparted to the materials between separate experiments listed in Table 3.2. Variation in the degree of contact (i.e. contact resistance) between the insulation and plate, however, is also a possible reason for the differing values. Because of the high temperatures encountered, the material can sag, deform and erode during the course of the experiment. These behaviors of the materials under heating can potentially generate significant experimental variations.

We note the variation with temperature rise of property α from the data in Table 3.2,. Between tests 2 and 4, the value of α increases from 5.2×10^{-3} cm^2/sec for a ΔT of 66°C to 9.0×10^{-3} cm^2/sec for a ΔT ranging from 171-336 °C (tests 2 and 3). A similar rise of α with respect to ΔT is found in tests 5-7, with $\alpha = 2 \times 10^{-4}$ cm^2/sec when ΔT=26°C (test 6) up to $\alpha = 8 \times 10^{-4}$ cm^2/sec when ΔT=156°C. In both cases, most of the variation appears in the vicinity of ΔT in the vicinity of 50°C. Beyond ΔT of the order of 100°C, little variation is observed (compare tests 2 and 3 and tests 5 and 7). The value of *Bi*, measuring heat transfer from the back wall, varies throughout each series of tests. For the tests with fiberglass, with approximately 10 times larger α, the variation of *Bi* is more pronounced as a greater quantity of front-surface thermal energy reaches the back surface. For the aluminized silica, whose compound α is approximately 10 times smaller than for the fiberglass compound material, the temperature rise and *Bi* variation are lower. Consequently, these variations of α and *Bi* can be explained in terms of basic heat transfer principles.

A typical example of a simultaneous plot of measured data and calculated temperatures at the rear surface ($x=L$) is shown in Figure 3.5. This plot for the test 2 data has ΔT=171°C. As can be seen, there is good agreement between the final converged solution and the experimental data. This agreement produces the corresponding values of α and *Bi* listed in Table 3.2.

The agreement between theory and experiment is examined quantitatively by plotting the residuals for each experiment. The residuals are defined as the difference between the measured and calculated temperatures for each time step (Beck and Arnold (1977)). They can be positive, negative or zero.

The standard deviation of the residuals is a measure of the absolute variation discrepancy between the model predictions and the experimental data. A more accurate indicator of the agreement between the model predictions and the experimental data, however, is the ratio of the standard deviation of the residuals to the total temperature rise above ambient, ΔT (Beck and Arnold (1977). These values are presented in Table 3.2. For example, the standard deviation of the residuals for test 6 is smaller than for test 3 by a factor of four. When comparing these quantities with respect to the ΔT during each test, however, the theoretical curve for test 3 is understood to be a more accurate model of the measurements than the same theory applied to test 6. This is because the chief comparison is the ratio of the standard deviation of the residuals to the total temperature rise in their respective experiment. In this example the ratio for test 3 is 8.59/336=0.0256, which is smaller than

the same ratio for test 6 given by 2.36/26=0.0908. The latter ratio is bigger than the former by a factor of 3.5.

Figures 3.6 and 3.7 provide graphical plots of the residuals for tests 2-4 and 5-7, respectively. These curves show that there is no systematic pattern in the residuals when comparing the experiments to one another. There appears to be some correlation in the errors in the measurements for test 3 but the pattern is not repeated in any of the other tests. This correlation may have its origins in the burn-off of the "scrim." In this test the thermal damage to the exposed face and underlying glass fiber was the most severe. One of the TCs was also noted to be in open air during part of test 3 (the data from this TC were not used). These facts suggest that numerous difficulties were encountered during this particular test. It is possible that these data manifest themselves in a correlated errors when they are fitted into a theory based on Equations (3.2)-(3.4). For more detailed discussions of these subtle questions which arise in parameter estimation, we refer the reader to Beck and Arnold (1977) and to the literature of parameter estimation and inverse heat conduction.

In an attempt to correlate parameter values with incident radiation, Figures 3.8 and 3.9 show plots of the two estimated parameters versus incident intensity. As a general trend, the estimated α is a monotonically increasing function of the incident intensity, whereas Bi exhibits an inverse relationship. For this plot, the intensity values were obtained by averaging the incident intensity over the first five minutes of the experiment.

Both behaviors can be explained by the appearance of the conductivity k in the numerator of α (which increases) and the denominator Bi (which decreases). This implies that in these tests the compound material conductivity increases with increasing radiant flux. Nevertheless, the product $\alpha Bi=hL/\rho c$ is not constant. This quantity changes as shown in Figure 3.10. If L and ρ are nearly constant during heating, and we assume that c is also nearly constant, then these graphs essentially

represent the variation of the thermal convection coefficient, h, with heating intensity.[1] As seen from Figure 3.10, the functional behavior of $\alpha\, Bi$ is completely opposite for the two materials: monotonically downward for tests 2-4 and monotonically upward for tests 5-7.

An explanation of the behavior of Bi solely in terms of k is not sufficient. The explanation of α in terms of k is sufficient if the variation of ρc with T is much smaller. From definitions in Equation (3.6) it is clear that Bi contains a k part and an h part. The k part represents heat conduction through the compound material whereas the h part represents convective heat transfer to the ambient air behind the material. The latter quantity can be changed independently of the material, for example, by blowing air with a fan across the back of the steel plate. In the GM experiments, no forced variations on h were carried out. An estimate of the dependence of h on temperature is obtained from the laminar free convection Nusselt number correlation (Kanury (1975)) $Nu_x=0.59(GrPr)^{1/4}$ $(10^4<GrPr<10^9)$ where $Gr=gx^3\beta\Delta T/\nu^2$ and $Pr=\nu/\alpha$, β is the coefficient of thermal expansion, and g is the acceleration due to the force of gravity. All properties are for the gas (air) rather than the solid plate. Using $Nu_y=hx/k$, with y the local vertical position on the plate (see Figure 3.1) we see that, for constant k, $Nu_1/Nu_2 = h_1/h_2 =(\Delta T_1/\Delta T_2)^{1/4}$, where ΔT is the temperature difference between the plate and the ambient air. We have assumed negligible variations in Pr and β. If the latter variation is included, we find instead that $h_1/h_2 = (\Delta T_1/\Delta T_2)^{1/4}\cdot(\nu_2/\nu_1)^{1/2}$ or $h_1/h_2 =(\Delta T_1/\Delta T_2)^{1/4}\,(T_2/T_1)^{3/4}$, since $\nu \sim T^{3/2}$ for gases (Vincenti and Kruger (1986)). Between tests 2 and 4, we find $h_2/h_4 =(171/66)^{1/4}\,(339/444)^{3/4}=1.04$, between tests 6 and 5 we find $h_6/h_5=0.87$ and between tests 6 and 7 we find $h_6/h_7=1.19$. Using these relations yields $Bi_i/Bi_j=(h_ik_j/h_jk_i)$, which gives $Bi_2/Bi_4=0.43=1.04k_4/k_2$, $Bi_5/Bi_6=0.86=(1/0.87)k_6/k_5$, and $Bi_7/Bi_5=1.02=(1.04)k_5/k_7$. Our estimates give $k_4/k_2=0.4$, which implies that the compound conductivity between tests 2 and 4 decreases by 60% as the temperature rise diminishes from 171°C to 66°C; $k_6/k_5=0.75$. This indicates that a 25% decrease as the temperature rise diminishes from 68°C to 26°C; $k_5/k_7\approx1.0$ yielding no change in compound conductivity even though the temperature rise of the back face changes from 68°C to

[1] These quantities are likely not constant during heating. See the discussion in Sec. 3.1. The assumption of constancy may be better for tests 5-7 than it is tests 2-4 (Santrock (1998)). It was observed in the GM tests that for tests 2-4 that during heating the insulation became concave in the center as the "scrim" and binder burned off. This was more pronounced at higher incident heat fluxes. Thus, L decreased with time. The density and specific heat c also may have changed with time (as suggested in Chapter 2) because the insulation lost material during burn-off.

156°C. These calculations suggest that the largest part of the *Bi* variation between tests is caused by the variation between tests of the thermal conductivity *k*.

3.3.2 Direct Model (Separate Panel and Insulation)

The parameters estimated are shown in Tables 3.3 and 3.4. For these tests, data from the first five minutes of the experiment were used, which includes the entire transient portion of the experiment. The Biot number estimate uses the conductivity and thickness of steel as its basis, i.e., $L \rightarrow L_2 = 0.08$ cm, $k \rightarrow k_s = 49.2$ W/m-K in $Bi = hL/k$ where subscript "*s*" denotes steel. The heat transfer coefficient h (W/m^2-K) takes the same value in the same experiment. For these reasons, the *Bi* values computed here differ by approximately three orders of magnitude from those in Table 3.2.

Table 3.3 Estimated Parameters: Insulation Only, 300 Seconds

Test	Diffusivity (cm^2/sec)	Biot Number (unitless)	Residual Std. Deviation (°C)	Temperature Rise (°C)
2	.009471	0.0075	2.737	171
3	.00918	0.0011	7.784	336
4	.00516	0.0096	2.145	66
5	.000573	0.0026	2.227	68
6	.000144	0.00075	2.420	26
7	.000698	0.0032	2.702	156

Table 3.4 Estimated Parameters: Insulation Only, 100 Seconds

Test	Diffusivity (cm^2/sec)	Biot Number (unitless)	Residual Std. Deviation (°C)	Temperature Rise (°C)
2	.0116	0.018	1.916	59
3	.0107	0.013	1.683	40
4	.0325	0.45	1.820	7
5	.000467	0.019	2.327*	10
6	.00953	0.15	3.053*	10
7	.000593	0.0028	2.178	33

*Required 180 seconds of data to converge.

The difference between the results in Table 3.3 and Table 3.4 is the duration of the analysis of the experiment. As discussed in the preceding footnote, due to the wide range of temperatures, the assumption of constant parameters throughout the duration of the experiment, which is implicit in this analysis, is not entirely valid. For this reason, it is advantageous to separately analyze the early portion of the experiment, which corresponds to a relatively small temperature rise. The

assumption of constant properties is better over this shorter time interval (Table 3.4).

The advantage of analyzing this early portion of the experiment can be seen by examining the standard deviation of the residuals, which provide a measure of the conformance of model to measured data. The standard deviation of the residuals is given the symbol σ and is defined as

$$\sigma^2 = \frac{1}{N}\sum_{i=1}^{N} (Y_i - T_i)^2 .$$

The first three experiments show appreciable reduction in the residual standard deviation when using only the first 100 seconds of the experimental data. The analysis for tests 5 and 6, however, did not converge with only 100 seconds of data. They required a minimum of 180 seconds to obtain convergence. The advantage of using fewer time steps for the first three experiments can be seen graphically in Figure 3.11. In this figure, the experimental data curve covering the 300 second interval exhibits a distinct pattern, indicating an inadequacy in the conformance of the model to the measured data (Beck and Arnold (1977)). Test 3 produces better results in the shorter interval as the error residuals diverge over the longer interval.

The results for the analysis of the diffusivity of the insulation, for the case when we assumed the diffusivity of the steel was known, are consistent with, and nearly identical to, the results for the diffusivity of the compound material for which both materials were lumped together. Moreover, the low conductivity and greater thickness of the insulating material, in comparison to the steel, appears to dominate the numerical results. This means that there was little difference in the results, whether the insulation was considered separately or both materials were considered as one compound material.

3.3.3 Direct Model (Separate Panel and Insulation with Panel Acting as a "Calorimeter" to the Insulation)

A problem encountered during the actual implementation of the method described in Sec. 3.1.3 was the noise in the measured temperature data. Each measurement was taken one second apart and even when averaging the six TC data together, the measurement noise was too high to implement the parameter estimation method of Sec. 3.3.3. Temperature rises and drops of 3 or 4 degrees were not uncommon in the data, even when the average temperature of the steel had experienced an average overall rise of less than one degree in a 20-second period.

In order to eliminate this noise, the method of mollification described in Murio (1993) was

used. The mollified value of each point in the measured data is determined as follows

$$f(n) = \sum_{i=3\delta}^{i=3\delta} p(i)Y(n+i),$$

where $Y(n)$ is the value of the measured temperature at measurement point n and $p(i)$ is the weighting function for the measurement point n at i measurements away from the point n. The quantity δ is known as the "blurring radius" and is an integer selected by the user based on the kinds of errors encountered. The weighting functions are given as

$$p(i) = \frac{1}{\delta\sqrt{\pi}} e^{-\frac{i^2}{\delta^2}}.$$

Note that the weighting functions sum to unity, i.e.,

$$\sum_{i=3\delta}^{i=3\delta} p(i) \approx 1.$$

For the data in this experiment, a blurring radius of 12 was the minimum required for generating a smooth curve. Note that the first and last points of the data set equal to three times the blurring radius are not mollified. To incorporate these points, a cubic spline was used such that its left end (at time zero) had a value of zero and a slope of zero. Likewise, both the value and slope of the spline at the right side were matched to those of the mollified data. Then the plotted data fell on a continuous, smooth curve.

Table 3.5 shows the results of the analysis, including the number of time steps used in seconds. The number of time steps was chosen for a minimum 1 °C temperature rise for the steel. Also, a minimum number of 50 points were employed in order to accomplish mollification with sufficient data.

Table 3.5 Estimated Parameters: Conductivity and Volumetric Heat Capacity Using the Steel Plate as a Calorimeter

Test	Conductivity (W/m-K)	Vol. Heat Capacity (J/m^3-K)	Diffusivity (cm^2/s)	Residual Std. Deviation (°C)	Temperature Rise (°C)	Time (sec)
2	.074	67,000	1.10×10^{-2}	0.4099	4.71	50
3	.059	87,000	6.78×10^{-3}	0.2044	1.06	60
4	.057	92,000	6.10×10^{-3}	0.1803	1.26	50
5	.0011	33,000	$3.\overline{3}\times10^{-4}$	0.4409	3.44	50
6	.0005	65,000	7.7×10^{-5}	0.6044	1.12	80
7	.0006	54,000	1.1×10^{-4}	0.6283	3.63	50

Another problem encountered as part of the analysis was the correlation between the two parameters, k and ρc, of this model. A regularization procedure was added to the parameter estimation routine in order to provide stability. Without regularization, the parameter estimation equations become nearly singular, making it impossible to distinguish which of the two parameters is responsible for the behavior of the measured temperature changes. The equation for ordinary least squares parameter estimation is

$$X^T X b = X^T (y-\eta)$$

where X is the matrix of sensitivity coefficients, X^T is its transpose (see the Nomenclature for the definition), b is the parameter vector, y is the temperature measurement vector, and η is the calculated temperature vector. Since the calculated temperature is not a linear function of the parameters, this equation must be solved iteratively. This equation minimizes the sum

$$S = \sum_{i=1}^{N} (y_i - \eta_i)^2,$$

which is identical to

$$S=(y-\eta)^T(y-\eta).$$

Using "prior information", as described in Beck and Arnold (1977), the expression to be minimized is

$$S=(y-\eta)^T(y-\eta)+(b-\mu)^T P(b-\mu)$$

where P is a square matrix, the dimension of which is the number of parameters (2) and μ is the prior information vector which contains the anticipated values of the parameters b. The values of P are chosen in accordance with the "residual principle," which prescribes that the standard deviation of the residuals should not be significantly increased by addition of the prior information.

Application of this method to the steel plate calorimeter model showed that stability was added to the parameter estimation calculations. The convergence criteria required that all parameters changed by less than 0.1 percent between iterations. Since convergence was not obtained even with the addition of the regularization procedure, the parameter values listed in Table 3.5 were values beyond which no further reduction in the residuals was achieved. The values of μ chosen for the first three experiments were taken from ASHRAE (1981) for fiberglass building insulation as k=0.04 W/m·K and ρc=10,000 J/m^3·K. The diagonal elements of P were defined as **[25 0.0001]**.

The results from the first three in Table 3.5 indicate that the value for ρc of the material is

greater than that of the fiberglass insulation, presumably due to the compacted state of the material. Although the standard deviation of the residuals is considerably lower than that generated from analysis of the same experiments in Tables 3.3 and 3.4. This is probably due to the mollification of the data rather than improved conformance of the model to the data. The parameter estimation procedure did not converge and, as shown in Figures 3.12 and 3.13, there is a pattern in the residuals for the steel calorimeter model.

For the last three experiments, the same value of ρc=10,000 J/m^3·K was used as prior information, but based on previous estimates of diffusivities in Secs. 3.3.1 and 3.3.2 the conductivity was assumed to be an order of magnitude lower than the fiberglass material. The value k=0.004 W/m·K was used and the diagonal elements of P were defined as **[2 0.000001]** for this analysis. As with the previous three experiments, the calculated value for volumetric heat capacity was larger than anticipated.

3.4 QUASI-STEADY-STATE ANALYSIS OF HEAT TRANSFER THROUGH BARRIER

As another means of extracting information from the GM data, an approximation was made of the steady-state temperature gradient across the insulation in comparison with the gradient across the steel plate. Using this method, the temperatures in the last half of the experiment, *when the temperatures had attained a steady state*, were averaged at each of three locations. Those locations were: the insulation surface, the insulation-steel interface, and the back surface of the steel panel. These averages were used from each experiment to calculate the quasi-steady-state temperature gradient across each material. Using a handbook (Eshbach (1963)) value for the conductivity of steel in the measured temperature range (k = 49.2 W/mK), the conductivity of the insulation was found by the ratio of the measured temperature gradients multiplied by the known conductivity of steel. The validity of this calculation rests on the assumption that the heat flux through the steel and insulation is equal at steady state, so that the ratio of the conductivities of the materials is equal to the reciprocal of the ratios of the thermal gradients, viz.,

$$q = k_1\left(\frac{dT}{dx}\right)_1 = k_2\left(\frac{dT}{dx}\right)_2. \tag{3.10}$$

Therefore, from Equation (3.10), we find the conductivity ratio

$$\frac{k_1}{k_2} = \frac{\left(\frac{dT}{dx}\right)_2}{\left(\frac{dT}{dx}\right)_1}.$$

The results of this analysis are shown in Table 3.6. As with the transient parameter estimation method, there is variability between the estimated thermal conductivity parameter between tests of the same group (2-4 and 5-7). Of the fiberglass insulation tests (2-4), test 3 seems to deviate the most, presumably due to "scrim" burn-off and the other observations discussed in the preceding footnote. As noted in that footnote, degradation of the fiberglass mat of tests 2-4 was observed.

Table 3.6: Thermal Conductivity Approximated by Quasi-Steady State Analysis

Test	Insulation Gradient (°C/cm)	Steel Gradient (°C/m)	Insulation Conductivity (W/m-K)
2	187.7	41.26	12.09
3	86.58	98.24	62.41
4	158.0	16.08	5.596
5	524.9	18.24	1.911
6	148.5	6.937	2.570
7	772.9	19.51	1.391

The results from tests 5-7 for the case of aluminized silica insulation are more uniform. We observe that the conductivities for the fiberglass (tests 2-4) increase with incident heat flux (and consequent overall temperature rise), whereas the conductivities of the aluminized silica decrease with increase of incident heat flux (and consequent overall temperature rise). The former trend is consistent with the results of Chapter 2, as exemplified by Figure 2.8, where it is shown that k_{gffs} increases as the temperature rises.

The large value of the insulation conductivity in comparison with the values listed in the second column of Table 3.5 is noted. This largeness arises from the gradient ratios of Equation (3.10), which are multiplied by the conductivity $k = 49.2$ W/m-K of the steel plate. The statistical variance of the measured temperatures at the front and rear faces of the steel plate was appreciable, which made it difficult to accurately estimate the gradients of temperature across the steel plate. For example, variances of measured TC temperatures were often order unity or greater multiples of the temperature difference across the plate, thus making the plate temperature gradient calculation

suspect. The insulation conductivity calculated in Table 3.6 for test 2 is 12.1 W/m-K whereas Table 3.5 gives 0.074 W/m-K, a factor of 163 smaller. The factors for the remaining tests 3-7 are 1058, 98.2, 1737, 5140 and 2318, respectively. There is some consistency with previous results in that numerical proportionalities for each material seem to agree best for tests 2 and 4 for the fiberglass insulation and tests 5 and 7 for the aluminized silica insulation.

For all but test 3, the temperature rise across the steel plate lies in the approximate range of 0.5 to 3.0°C. The value for test 3 is approximately 8°C. These values, as noted, are often smaller than the variances of the TC readings from one reading to the next.

We note that the insulation conductivity values listed in Table 3.5, which are of the order of 10^{-3} to 10^{-2} W/m-K are of the order of magnitudes commonly listed for materials considered as "insulations" in standard heat transfer texts. Seldom do "insulation" conductivities attain values of the order of 10 W/m-K as in Table 3.6 see, e.g. Arpaci, Kao and Selamet (1999). The quasi-steady calculations appear to produce consistent trends with the other methods, but the absolute numbers are suspect.

3.5 HEAT TRANSFER FROM THE REAR SURFACE

The heat transfer from the rear surface to the region behind it can be calculated from only two of the preceding sets of estimated properties, (1) the estimates of Sec. 3.3.3 for the "calorimeter" and (2) the estimates of Sec. 3.4 for the steady state case. As discussed in Sec. 3.3.3 the "calorimeter" model produces residuals with a distinct pattern and. Moreover, the estimates do not converge hence the thermal properties deduced from this model may not be as reliable as those for the steady-state model. As noted above, however, the conductivity values for the quasi-steady case are suspect, therefore we shall use the "calorimeter" model values. In order to attain a steady state condition of the experiment, however, heat-up thorough the entire transient stage was necessary. Inaccuracies in the steady state model may arise from material degradation during lengthy exposure to high temperatures in the final steady heating stage.

The steady-state results for *Bi*, along with the computed conductivity values of Sec. 3.4, can be used to estimate the heat transfer coefficient on the back surface for each of tests 2-7.

In the steady state analysis *Bi* is based on the conductivity of the compound material. Thus, the compound thermal conductivity must be computed in the same way as in Sec. 2.7. For a layered material of thickness L the solution of the steady, constant-property conduction equation (Equation

(3.2)) gives $L/k_{com} = L_1/k_1 + L_2/k_2$, where subscripts "*1*" and "*2*" represent the insulation and steel plate, respectively. The compound conductivity k_c is given by

$$k_{com} = \frac{L}{L_1/k_1 + L_2/k_2}.$$

This compound conductivity is calculated in the same manner as for the steady-state conduction analysis of Chapter 2. The heat transfer coefficient can be calculated from *Bi*, k_{com}, and the material thickness L as

$$h = \frac{k_{com} Bi}{L}.$$

Plots of dimensionless heat transfer can be constructed from the non-heated side of the plate as

$$q = Bi\left(\frac{T - T_\infty}{T_{max} - T_\infty}\right).$$

Table 3.7 shows k_{com}, *Bi* from the direct model analysis of Sec. 3.3.1, and the corresponding *h* value resulting from the calculations using these parameters.

Table 3.7: Heat Transfer Coefficient from Rear Surface for Steady-State Model

Test	Compound Conductivity W/m-K	Biot Number	Heat Transfer Coefficient h (W/m^2-K)
2	12.4	2.65	16.2
3	61.2	0.36	11.3
4	5.77	6.18	17.5
5	2.81	1.31	10.4
6	3.75	1.53	16.3
7	2.06	1.33	7.71

Note that the *h* for test 3 is of the same order of magnitude ($O(10\ W/m^2K)$) as the *h*'s for tests 2 and 4, even though the *Bi's* for these two cases are separated by an order of magnitude. The coefficient *h* is dependent on the thermal properties of the adjacent air and other quantities such as the temperature difference between the plate and the air, rather than solely on the thermal properties of the compound material. It is perhaps the most reliable parameter of the steady-state analysis.

Figures 3.14 and 3.15 show plots of the heat transfer rate from the unheated side of the

compound material computed using the heat transfer coefficients of Table 3.7. The heat transfer coefficients for tests 2-4 are similar hence the heat flux magnitude in these cases is controlled by the temperature attained by the plate. Test 3 attained the highest plate temperature and therefore exhibits the largest heat flux. The same statements hold for tests 5-7 in Figure 3.15. We calculate from these figures the ratios of the heat flux from the rear surface to the heat flux incident on the front surface. From Figure 3.14 we find for tests 2-4 the values 2.5, 3.4 and 0.75 kW/m^2 at t = 300 sec. Comparison of the incident values 43.5, 64.3 and 14.5 listed in Table 3.1 yields the following ratios: test 2, 6%; test 3, 5%; test 4, 5%. From Figure 3.15 we find for tests 5-7 the values 0.4, 0.3 and 0.6 kW/m^2 at t = 300 sec. Comparison of the incident values 38.6, 14.1 and 67.1 listed in Table 3.1 yields the following ratios: test 5, 1%; test 6, 2%; test 7, 1%. Thus, the convective fluxes from the rear surfaces calculated by this method are of the order of one to five hundredths of the incident fluxes. This suggests that most of the losses are by radiation not convection. Some support for this statement is provided in Table A.2 of the Appendix and the calculations leading to Table A.2.

Figures 3.16 and 3.17 show the dimensionless heat flux from the rear or non-heated surface versus time. In contrast with the previous two plots, these are governed primarily by the magnitude of *Bi*. The reason for this is the scaling of the temperature in such a manner that the maximum temperature is always unity. Consequently, the heat fluxes rise and fall with the magnitude of *Bi*. The heating curves vary in magnitude from zero to *Bi*. There is a fairly wide variation in *Bi* for tests 2-4 as seen in Table 3.7. In the second group, tests 5-7, however, the values of *Bi* are reasonably similar, so that the three curves are nearly identical.

3.6 DISCUSSION OF RESULTS

We employ our estimated α values in order to calculate the approximate times at which the back surface is heating up fastest, and when the back surface temperature has risen to a significant fraction (50%, 90%) of its final value. This is achieved by solving the heat transfer model given as Example 9-5 in Özisik (1993), viz., $\partial T/\partial t=\alpha\partial^2 T/\partial x^2$ with $T(x,0)=T_i$, $T(0,t)=T_o$, $\partial T(L,t)/\partial x=0$. In this model the heated face (x=0) has constant temperature T_o while the back face at $x=L$ is insulated (i.e., no heat is lost from the rear surface). The material initial temperature is designated as T_i. This problem is an idealization of the one we have studied in Secs. 3.1-3.4: in our case heat is lost from the back face. Therefore, these theoretically estimated heat-up times for zero heat loss should be considered as *lower bounds* to the actual heat-up times. In other words, we expect that our heat-up

times will be larger because heat losses from the rear surface depress its temperature.

The initial boundary-value problem described above has a solution, which can be calculated numerically or analytically. The former is exact to within a specified convergence error, whereas the latter (though exact) is unusable unless expressed in approximate form (Özisik (1993)). We find from the numerical solution that the time at which the back face temperature rate of increase is a maximum is $t_{max\ rate}=0.167L^2/\alpha$. From the approximate analytical solution (Özisik (1993)) the times at which the back face attains 50% and 90% of T_o-T_i are $0.42L^2/\alpha$ and $1.1L^2/\alpha$, respectively. For the fiberglass insulation (see Table 3.2), we employ L=1.96cm+0.08cm (insulation layer plus steel plate)=2.04cm. For the aluminized silica we use L=0.16cm+0.08cm=0.24cm. The α-values for GM tests 2-74 and 5-7 (see Table 3.2) yield Table 3.8.

Table 3.8: Estimated Characteristic Heat Transfer Times for the Compound Model of Sec. 3.3.1

Test	Diffusivity (cm^2/sec)	Material Thickness (cm)	$t^*=L^2/\alpha$ (sec)	$t_{max\ rate}=0.167t^*$ (sec)	$t_{50\%}=0.42t^*$ (sec)	$t_{90\%}=1.1t^*$ (sec)
2	0.0094	2.04	442.7	73.9	185.9	487.0
3	0.0089	2.04	467.6	78.1	196.4	514.4
4	0.0052	2.04	800.3	133.7	336.1	880.3
5	0.00071	0.24	81.1	13.5	34.1	89.2
6	0.00020	0.24	288.0	48.1	121.0	316.8
7	0.00082	0.24	70.2	11.9	29.5	77.2

We observe that the average $t^*=L^2/\alpha$ value for the compound fiberglass/steel material is 570 sec, while for the compound aluminized silica/steel it is 146.4 sec. Therefore the characteristic times $t_{max\ rate}$, $t_{50\%}$, $t_{90\%}$, etc. always have the average ratio 570/146.4=3.9. If from each set (fiberglass and aluminized-silica) we discount the single "anomalous" reading (800.3 sec for the former, 288 for the latter) the average ratio is 455/75.7=6. We therefore anticipate that characteristic heat-up times for the back face are at least 4-6 times longer for the fiberglass than the aluminized-silica compound material. Since the α-value for the aluminized-silica compound material was generally at least 10 times smaller than the α-value for the fiberglass compound material, the reason for the faster heat-up of the latter is the smaller thickness of 0.24 cm compared with 2.04 cm for the fiberglass. Discounting the "anomalous" readings, we see that when $L_{Al\text{-}silica}$=2.04 cm the average t^* value becomes 5440 sec, so that instead of decreasing, heat-up times are increased for the aluminized-silica

layer by the factor 5440/455 =11.9. The insulation layer thickness is an important part of its resistance to transient heat flux, and thicker materials with smaller α and larger L can provide improved insulation. The relevant quantity for heat transfer rate is $t^*=L^2/\alpha$.

An attempt was made during the course of this research project to estimate *three parameters* simultaneously by solving the coupled energy equations in both insulation and steel panel. These three parameters were *Bi*, α_i and α_s ("*i*" = insulation, "*s*" = steel). When the sensitivity coefficients were plotted, however, a strong correlation was formed between *Bi* and α_s. For this reason, no subsequent parameter estimates were made using this model. We were thus unable, using our combination of model equations and experimental data, to estimate simultaneously four separate material properties for the insulation/steel plate assembly. Figure 3.19 shows the sensitivity coefficients for the three-parameter model. The correlation between *Bi* and α_s is obvious.

3.7 CONCLUSIONS

The least squares method was used to estimate thermal parameters from data measured in radiant heating experiments using flat panels of various compositions exposed to different radiant heating intensities. The thermal parameters estimated from these measurements were thermal diffusivity (α) and rear surface heat transfer coefficient (*Bi*). In addition to transient measurements that enabled estimation of thermal diffusivity, quasi-steady-state measurements were used to estimate thermal conductivity (k).

The results of the parameter estimation were produced by enforcing agreement between the *measured back surface temperatures* and the numerically *computed back surface temperatures*. The estimated thermal parameter values varied between experiments because of the variation in measured temperatures. Other phenomena such as material breakdown and loss of contact between layers of the compound material may also have produced disagreement. Overall, the results **for the models of Sec. 3.1** provide the best thermal parameter estimates obtainable under conditions of radiant heating. Other models can be developed in which temperature variation of the thermal properties is accounted for, but these models are much more complicated.

From Figures 3.8 and 3.9 it is clear that the reflected aluminized silica of tests 5-7 produced a smaller value of α, by approximately a factor of 10, than does the fiberglass insulation of tests 2-4. Although thermal energy propagates by diffusion through the material in such a way that the penetration distance is proportional to the square root of αt, the compound material of tests 5-7

shows an approximately 10 times shorter time to heat the back surface than the compound material of tests 2-4. As discussed, this was caused principally by the large difference in compound layer thickness L. Even though the α of the aluminized silica insulation was of the order of ten times that of the glass fiber mat, its L-value was approximately ten times smaller. The L effect enters in a square power, the α effect in a linear power. The result, shown here, is an approximately ten times faster rear surface heating rate for the compound aluminized silica panel.

A detailed discussion of the *Biot* number *Bi* was presented. The dependence of *Bi* on the combined insulation and steel thermal conductivity was described. In the section describing experimental results, the detailed *Bi* temperature dependence was examined. The behavior of *Bi* was in all cases consistent with physical predictions, except for test 3, as discussed.

The results of the three models of Sec. 3.1.1-3.1.3 show identical trends, since the thermal diffusivity of the fiberglass insulation is approximately an order of magnitude larger than that of the aluminized silica. The fact that the parameters did not converge in Sec. 3.3.3, and the distinct pattern in the residuals, makes these results somewhat unreliable. As a result, in the calculation of the heat transfer from the rear surface, thermal parameters from the steady state model were used. We observer that the heat transfer from the rear face did not include radiation, although the radiant flux can be calculated from measured rear surface temperature and the known radiant properties of the steel panel. The main difficulty in the model of Sec. 3.1.3 is that the rear surface of the material is not actually insulated. The rear surface, in fact, is exposed to the ambient atmosphere and the assumption of an insulated condition, though accurate in principle for the initial part of the experiment, becomes progressively worse with time. Not coincidentally, the correlation of the parameters by this model also worsens with time, as seen in Figures 3.12 and 3.13.

The apparatus employed in the GM experiments was not designed for the purpose of thermal property parameter estimation. The estimation of parameters for the insulation materials is discussed in Chapter 2, where the MSU property measurement apparatus of Figure 2.2 is employed. Nevertheless, in order to compute the heat transfer to and from such assemblies as shown in Figure 3.1, estimates of compound material thermal properties are needed. This chapter has demonstrated that estimates of such parameters can be made when the experiment is appropriately matched with the computation. The limitations of this modeling have been discussed.

A major question in this method of solution of the problem (Santrock (1998) arises when one

considers that the material layer is subjected to radiant fluxes at the front surface. If the radiant fluxes for the two materials (fiberglass, aluminized-silica) are exactly identical, it is likely that the net heat flux passed into the materials differs because the material absorptivities and reflectivities differ. The glass fiber mat, which is black, absorbs more of the incident radiant flux than the reflecting aluminized silica cloth. We have avoided this potentially difficult issue by using only the *temperature data* at the front surface in our computations. That is, although the GM tests also measured the incident radiant flux, these data were not used because we could not account for the reflected and absorbed portions. If in-depth absorption of the radiant flux is not accurately known the temperature of the front surface, as measured in the GM experiments, represents an accurate boundary condition for the heat conduction computation. Consequently, in principle (and subject only to the hypothesis that in-depth absorption of the radiant flux was negligible) the TC temperature measurements produce data that can be reliably used in the numerical simulations. Nevertheless, as indicated by Dr. Santrock (1998), attaching and fixing the location of the TCs in the GM experiments was difficult: in response to the high incident fluxes, in one case (test 3) the "scrim" on the glass fiber mat burned off, thus rendering these data slightly suspect. Given these qualifiers, the general order-of-magnitude agreement between test groups 2-4 and 5-7 is encouraging.

ACKNOWLEDGEMENT

The research described in this chapter was funded by General Motors pursuant to an agreement between GM and the U.S. Department of Transportation.

3.8 REFERENCES

American Society of Heating, Refrigerating and Air-Conditioning Engineers (ASHRAE) Fundamentals, Atlanta, GA (1981).

[3.1] V. S. Arpaci, S.-H. Kao and A. Selamet, Introduction to Heat Transfer, Prentice-Hall (1999).

[3.2] J. Beck and K. Arnold, Parameter Estimation, Wiley, New York, (1987).

[3.3] O. Eshbach, Handbook of Engineering Fundamentals, Wiley and Sons, New York, (1963).

[3.4] G. Forsyth and W. Wasow, Finite Difference Methods for Partial Differential Equations, Wiley, New York, (1960).

[3.5] P. Furmanski and J. M. Floryan, "Wall Effects in Heat Conduction Through a Heterogeneous Material," *International Journal of Heat and Mass Transfer*, 37 (No. 13), pp. 1945-1955

(1994).

[3.6] S. Jodeh, Personal communication, 2000.

[3.7] A. M. Kanury, Introduction to Convection Phenomenon, Gordon and Breach, New York, (1975).

[3.8] D. Murio, The Mollification Method and the Numerical Solution of Ill-Posed Problems, Wiley-Interscience, NY (1993).

[3.9] A. B. Oladipo and I. S. Wichman, "Study of Thermal Barrier Materials Separating Automobile Engine and Passenger Compartments," Proceedings of the 33rd ASME National Heat Transfer Conference, Albuquerque, NM, August 15-17, 1999.

[3.10] M. N. Ozisik, Heat Conduction, 2nd Edition, Wiley and Sons, New York, (1993).

[3.11] J. G. Quintiere, Principles of Fire Behavior, Delmar Publishers, Albany N.Y., 1998.

[3.12] J. Santrock, Personal communication, 1997-1998.

[3.13] W.G. Vincenti and C.H. Kruger, Introduction to Physical Gas Dynamics, Krieger Publishing, Maladar, Fla., (1986).

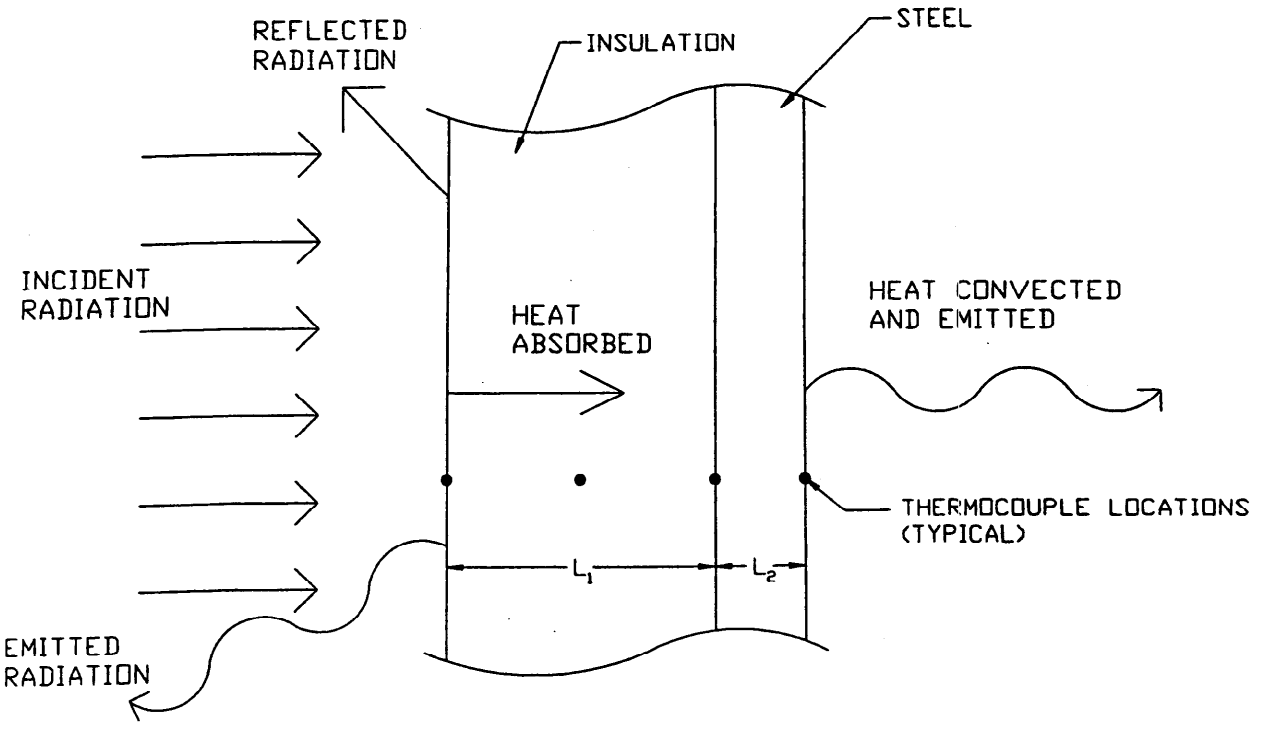

Figure 3.1: **Schematic diagram of the one-dimensional two-layer material. Note the position of the thermocouples (TC). Also note that $L=L_1+L_2$ is the thickness of the compound (insulation plus metal) material. Location $x = 0$ is the heated face while location $x = L$ is the rear surface.**

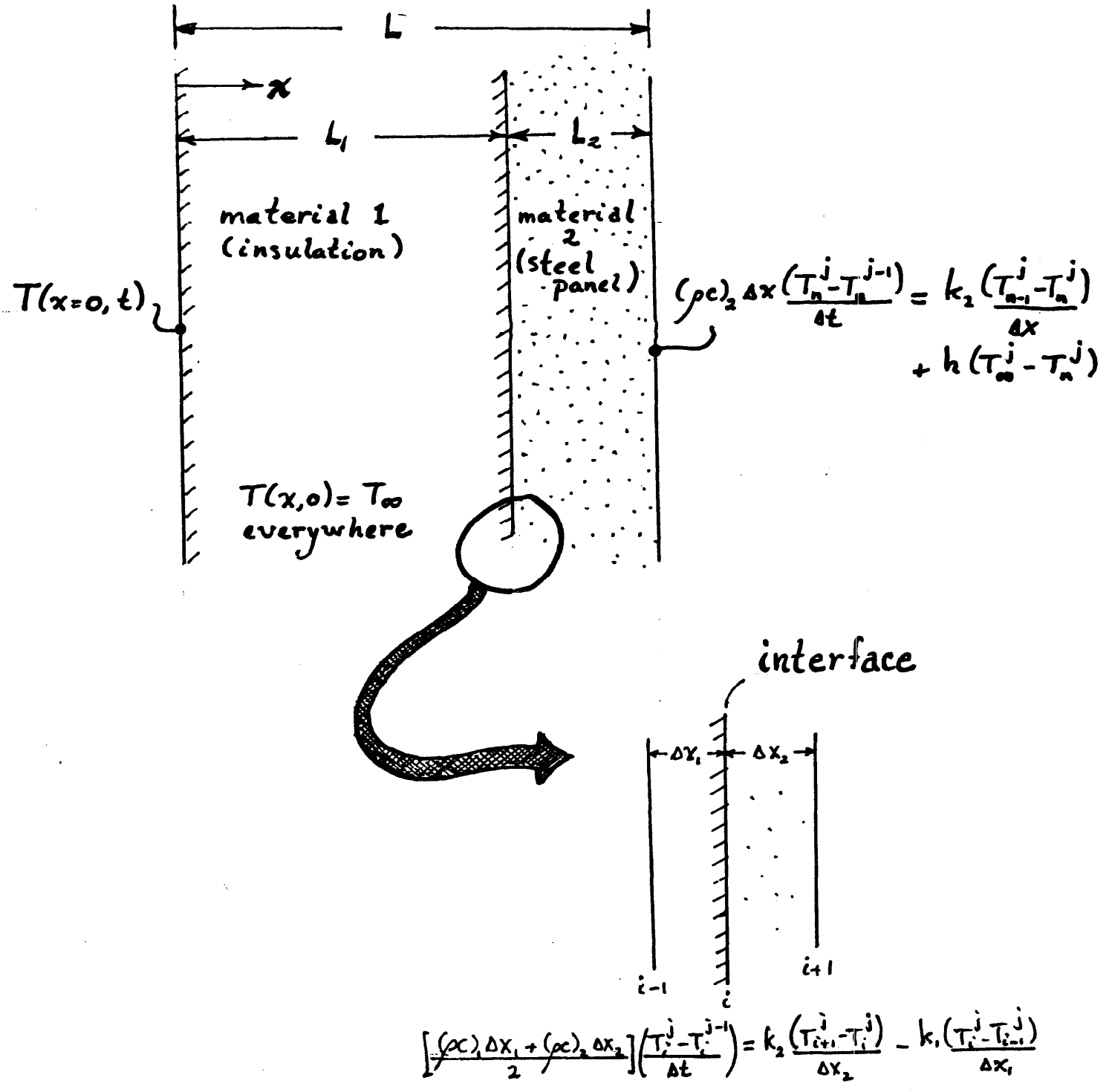

Figure 3.2: Equations and boundary conditions for the insulation plus steel backing. The initial condition is $T=T_\infty$ everywhere. Here the two layers are considered separately, with properties of the steel layer considered known. The insert shows the boundary conditions applied across the insulation/steel interface.

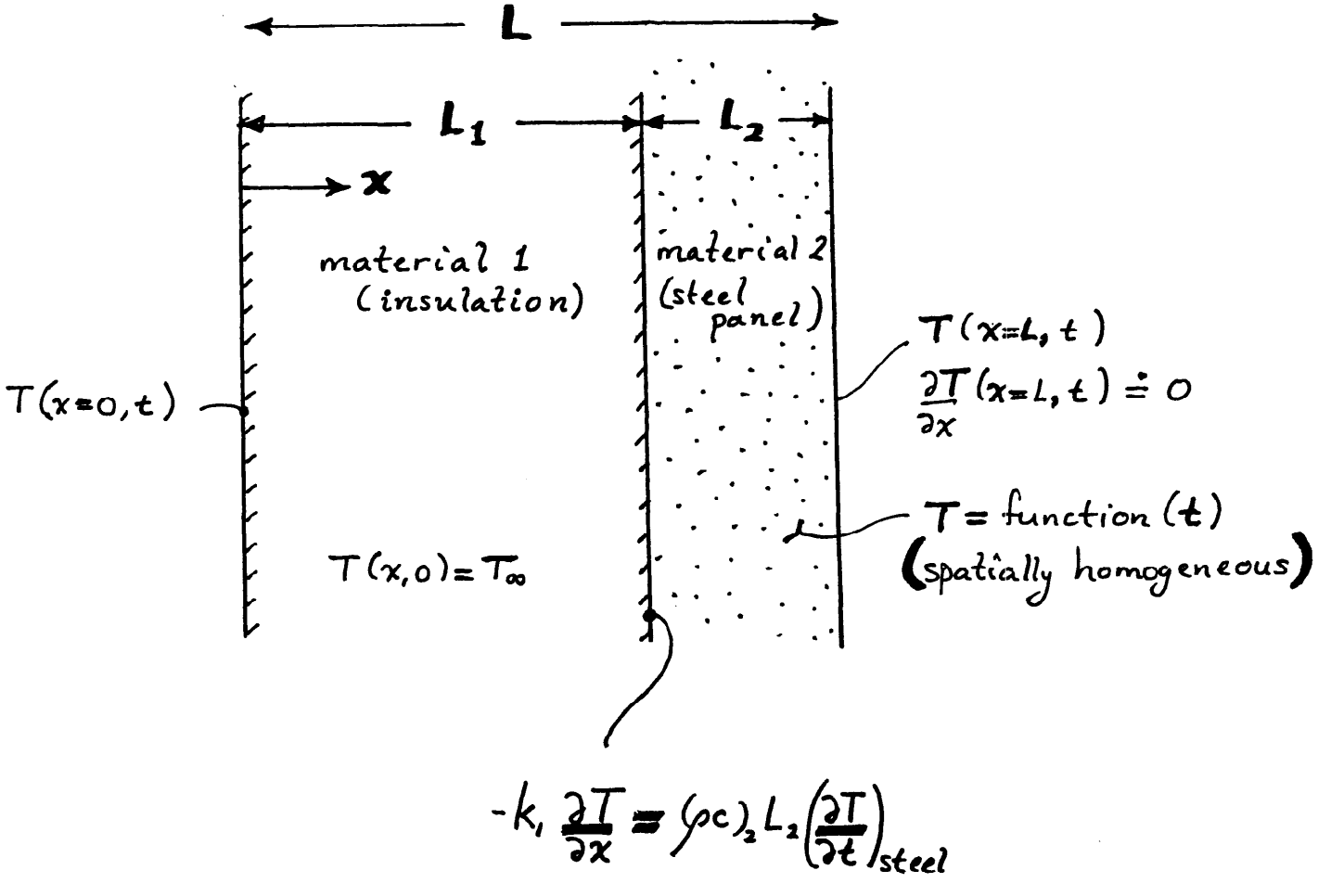

Figure 3.3: **Equations and boundary conditions for the insulation plus steel backing with the latter considered as a "calorimeter" whose temperature varies only with time. For the duration of the parametric analysis, the heat flux from the steel backing to the ambient is considered negligibly small, i.e., zero. The initial condition is $T = T_\infty$ everywhere, as in the previous models.**

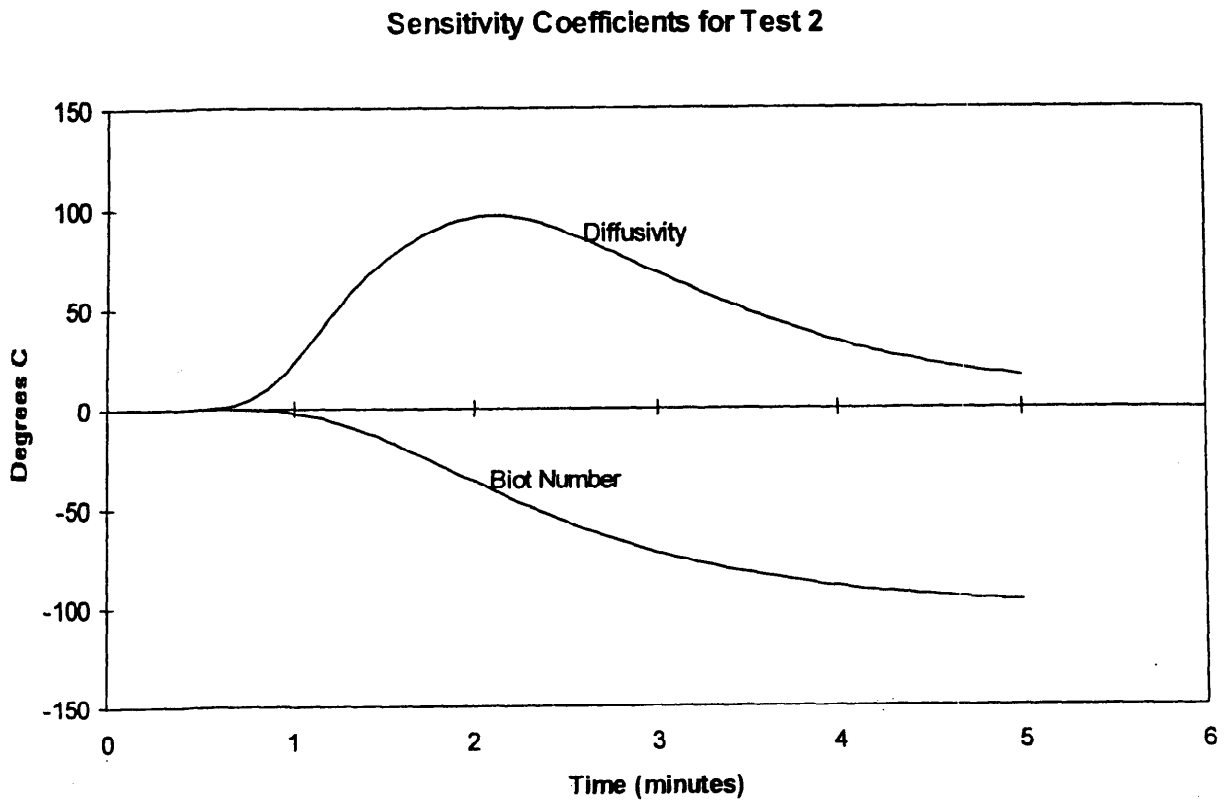

Figure 3.4: **Sensitivity coefficients for the compound panel. Note that the functions are *linearly independent.* That is, a constant, whether positive or negative, multiplied by one function does not reproduce the other.**

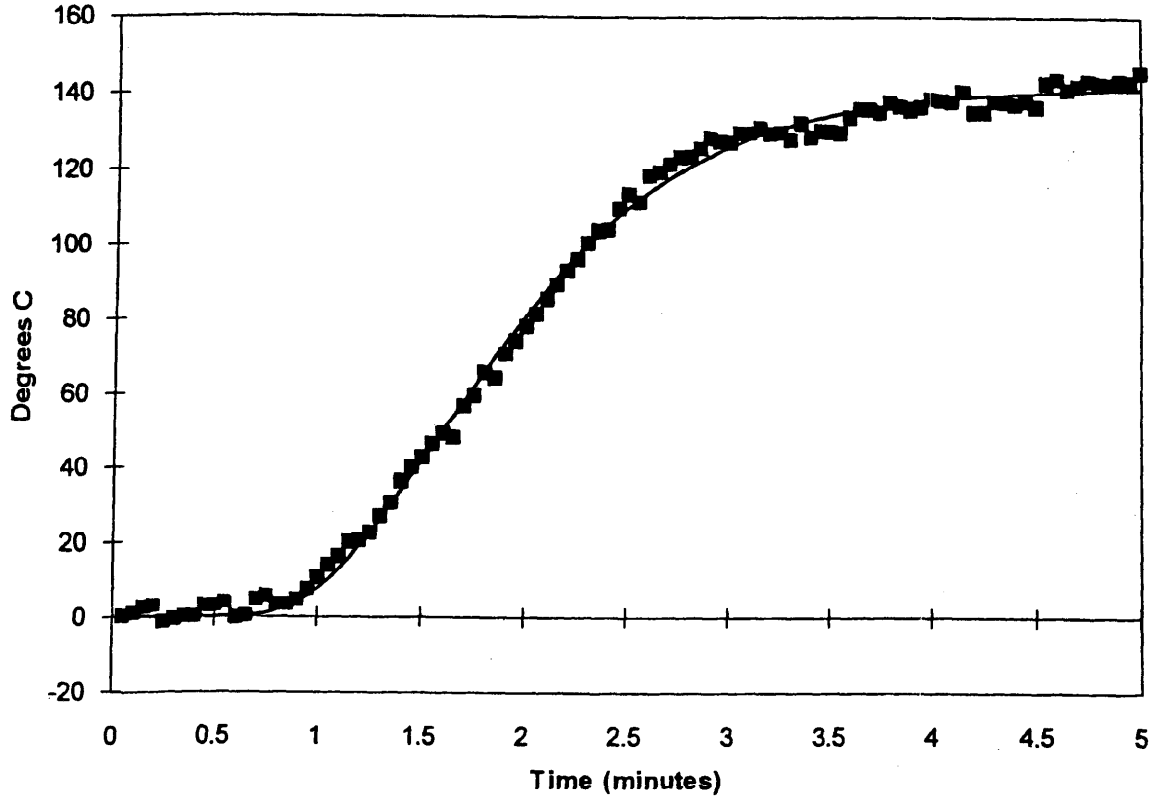

Figure 3.5: **Simultaneous plot of calculated and measured temperatures for the data gathered for test 2 at the rear surface of the heated assembly, i.e. at $x = L$.**

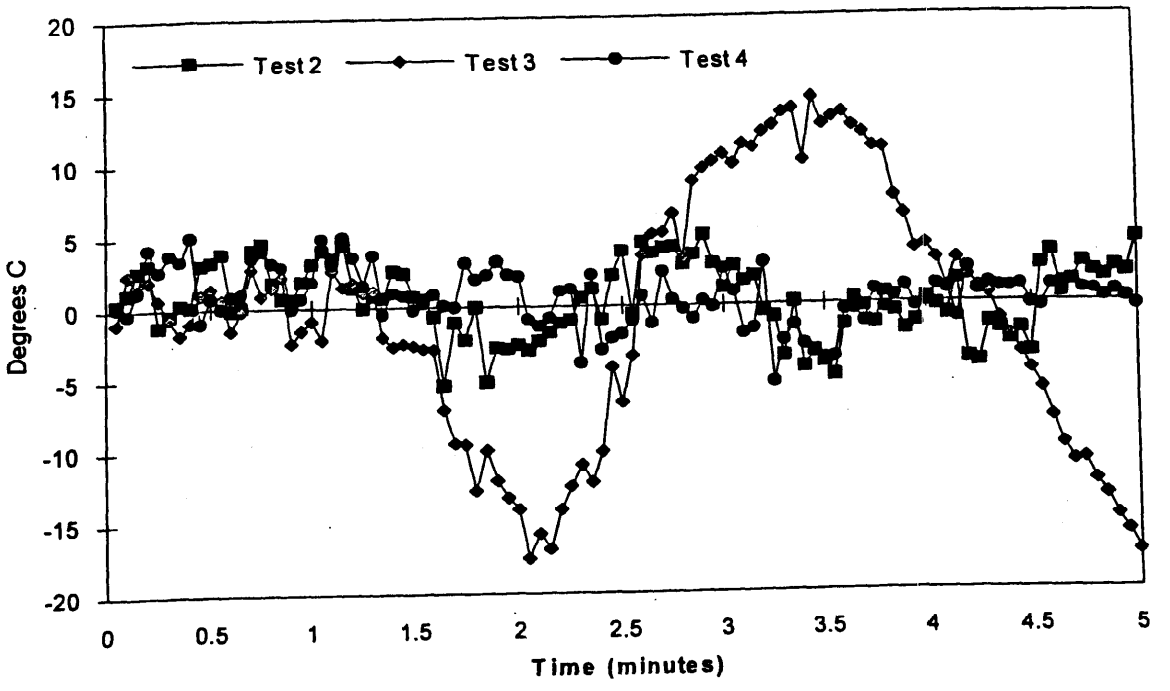

Figure 3.6: **Residuals for tests 2 through 4. The lack of a systematic pattern between experiments indicates random errors rather than a misapplication of the model (Beck and Arnold (1977). This suggests that the parameters derived are applicable to these tests in the manner that they were derived in Equations (3.2)-(3.4).**

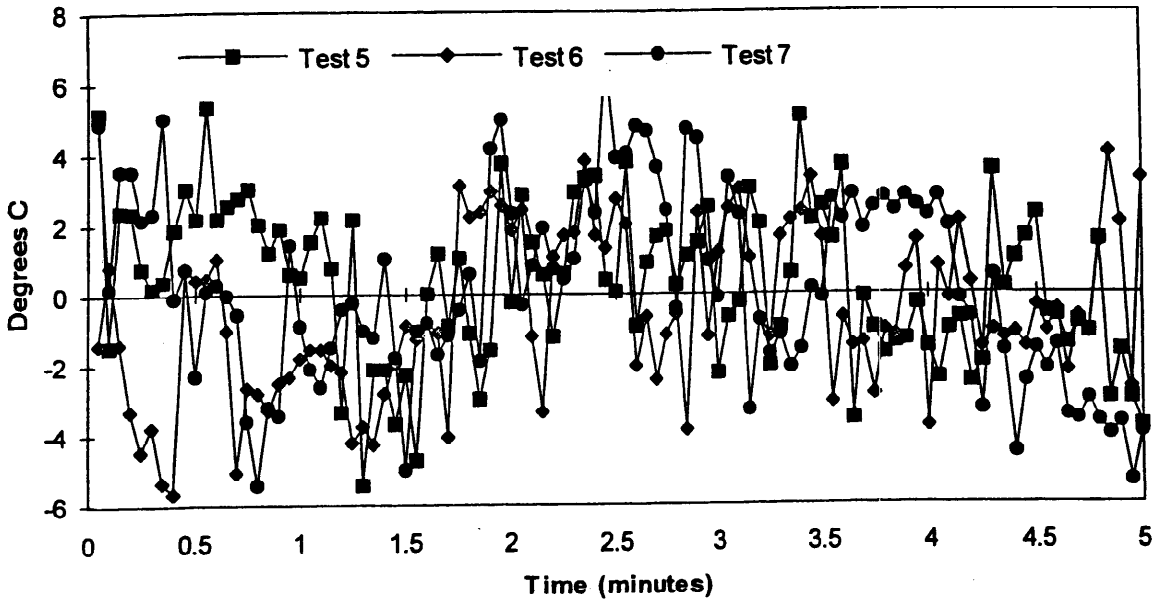

Figure 3.7: Residuals for tests 5 through 7. As with tests 2 through 4, there is no observable systematic error between experiments, indicating a reasonable fit (Beck and Arnold (1977)) between the mathematical model and the experimental measurements.

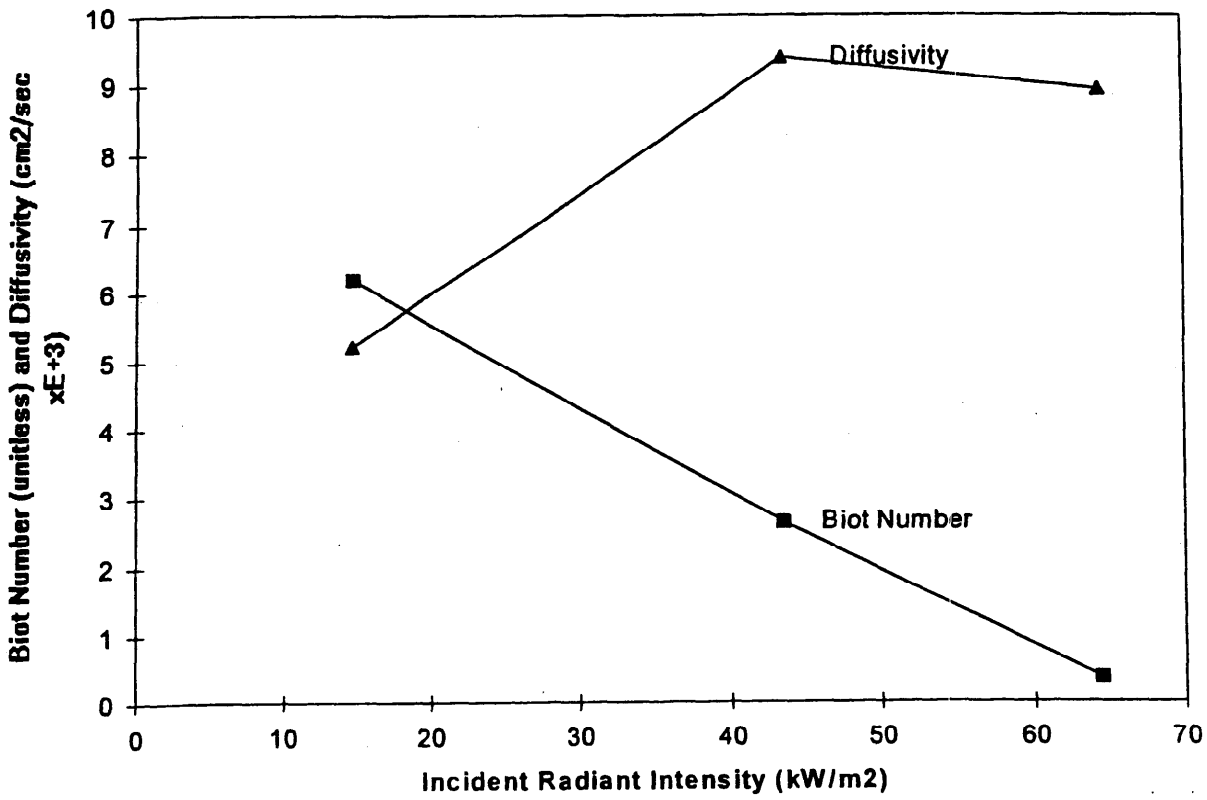

Figure 3.8: **Plot of parameters vs. intensity for tests 2 through 4. The diffusivity is generally monotonically increasing as a function of intensity whereas Biot number monotonically decreases. These changes suggest that the parameters are in fact functions of temperature because the temperature rise in the material is related to the incident radiant intensity, see, e.g., the final columns of Tables 3.1 and 3.2.**

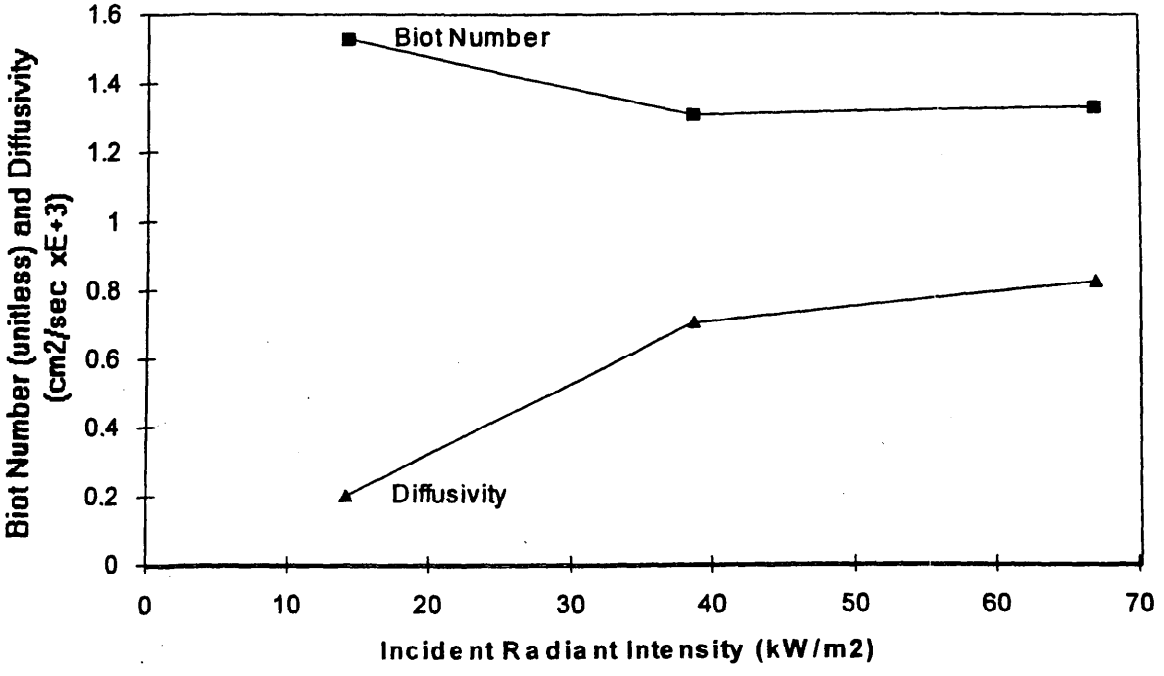

Figure 3.9: **Plot of parameters vs. intensity for tests 5 through 7. Although the material used in these tests has a much lower diffusivity, the trend for both parameters as functions of time is the same as in tests 2 through 4.**

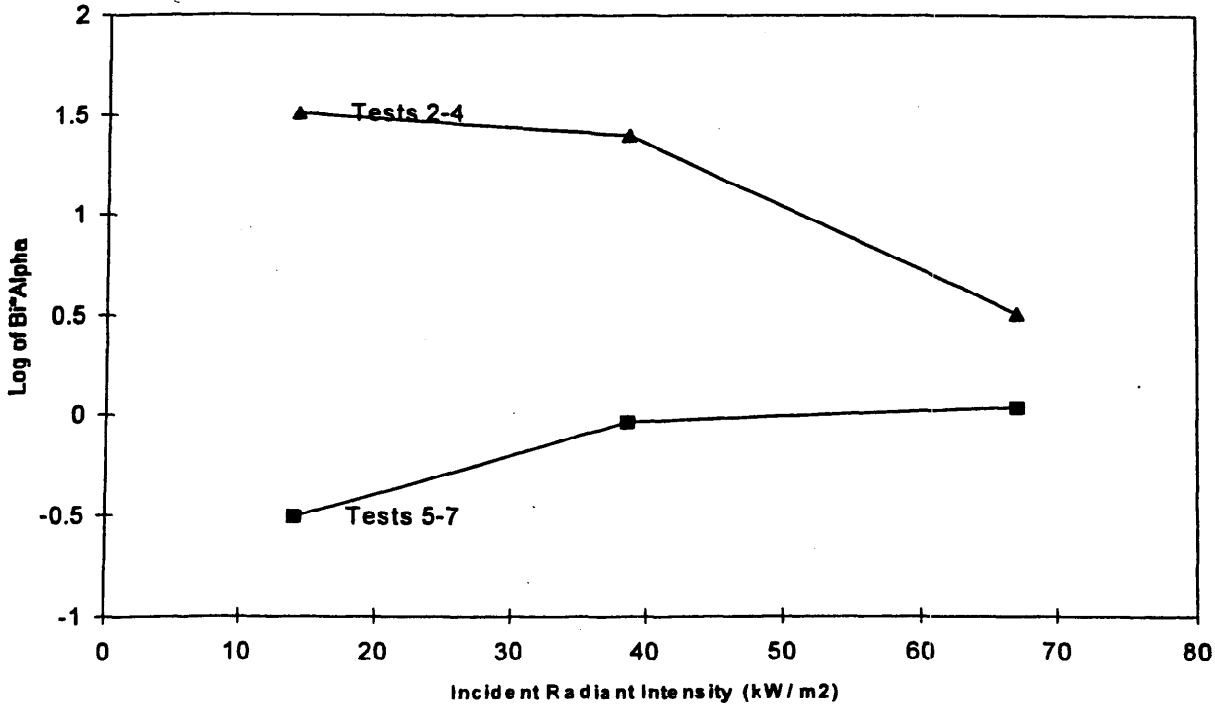

Figure 3.10: Plot of the logarithm of the product of αBi as a function of incident intensity. This product essentially represents the heat transfer coefficient, assuming constant L, c and ρ.

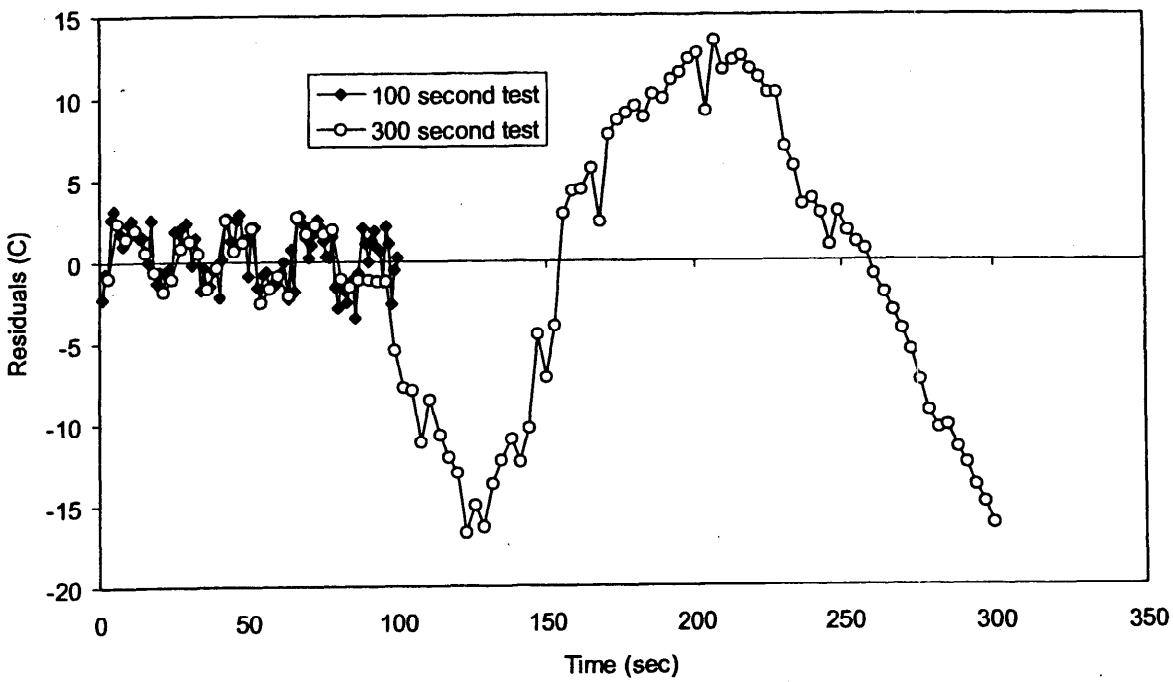

Figure 3.11: **Residuals comparing 300 sec interval to 100 sec interval for test 2. Note that when the experimental data covering 300 seconds is analyzed, a distinct pattern becomes evident, indicating an inadequacy in the conformance of the model to the measured data (Beck and Arnold (1977)). This is possibly caused by the variation of the material thermal properties during the course of the experiment.**

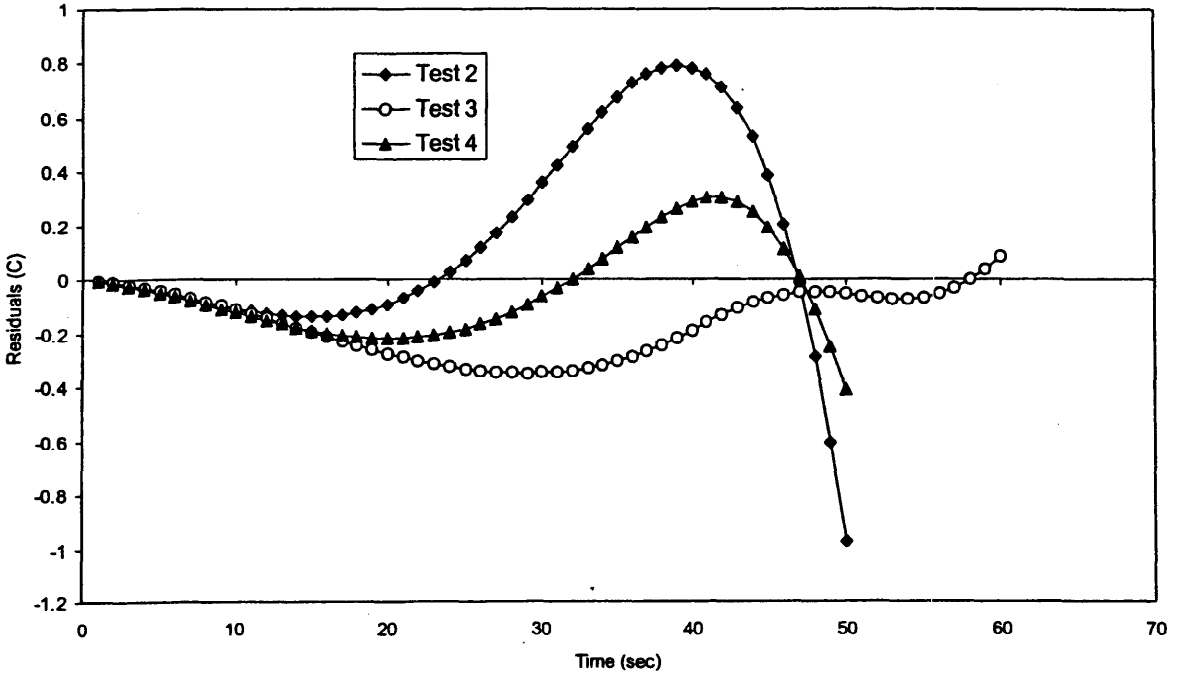

Figure 3.12: **Residuals comparing tests 2, 3 and 4 using the steel as a calorimeter. Although the plots of the residuals exhibit a very smooth appearance due to mollification, a distinct signature or pattern is evident, giving indication of a poor match between the mathematical model and the measured data. This progressive degeneration of the match with the model is possibly caused by the assumed zero-flux condition at the rear surface of the steel panel, an assumption that worsens with time**

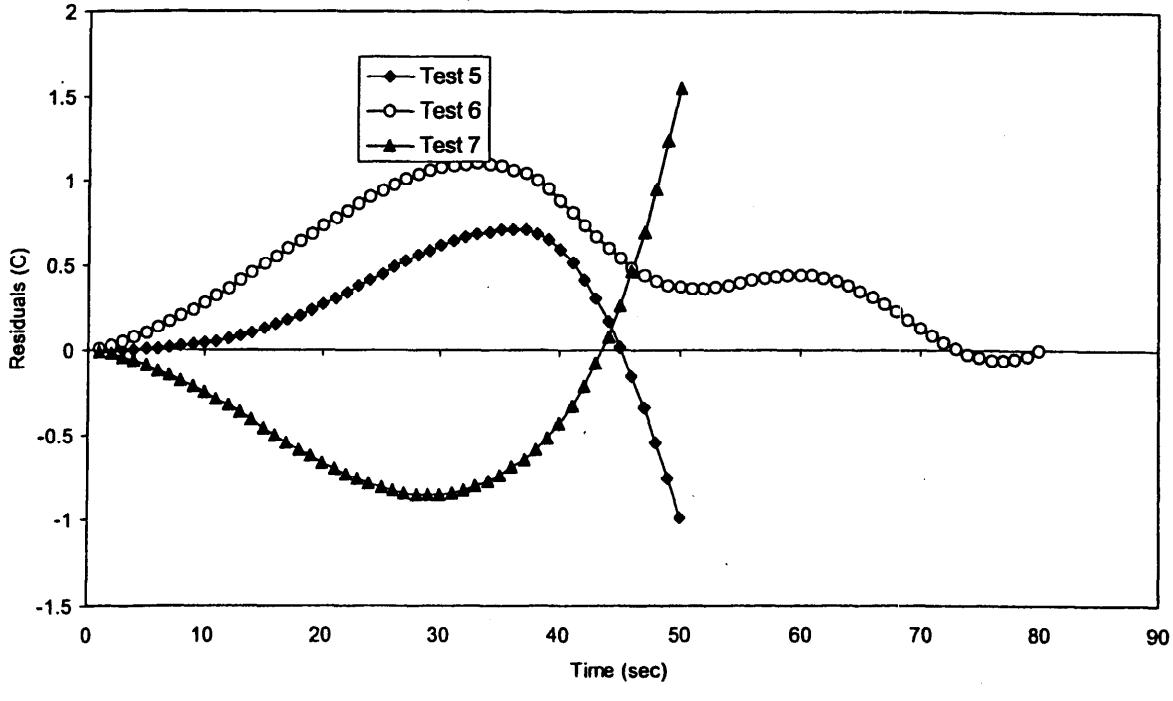

Figure 3.13: Residuals comparing tests 5, 6 and 7 using the steel as a calorimeter. Although the plots of the residuals exhibit a very smooth appearance due to mollification, a distinct signature or pattern is again evident (compare previous figure), giving indication of a poor match between the mathematical model and the measured data.

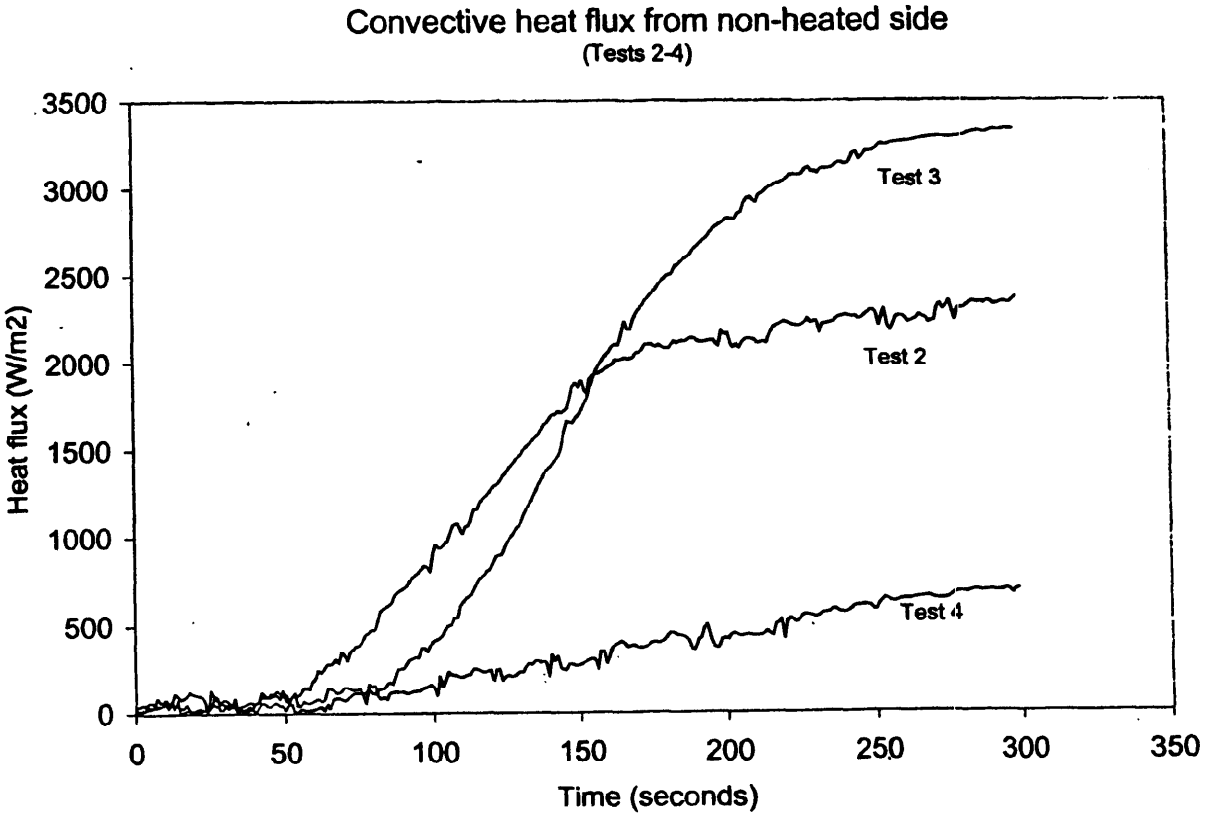

Figure 3.14: Convective heat flux from the rear surface of the heated thermal barrier for tests 2-4. The abscissa has units W/m^2. The measurement interval is 300 sec.

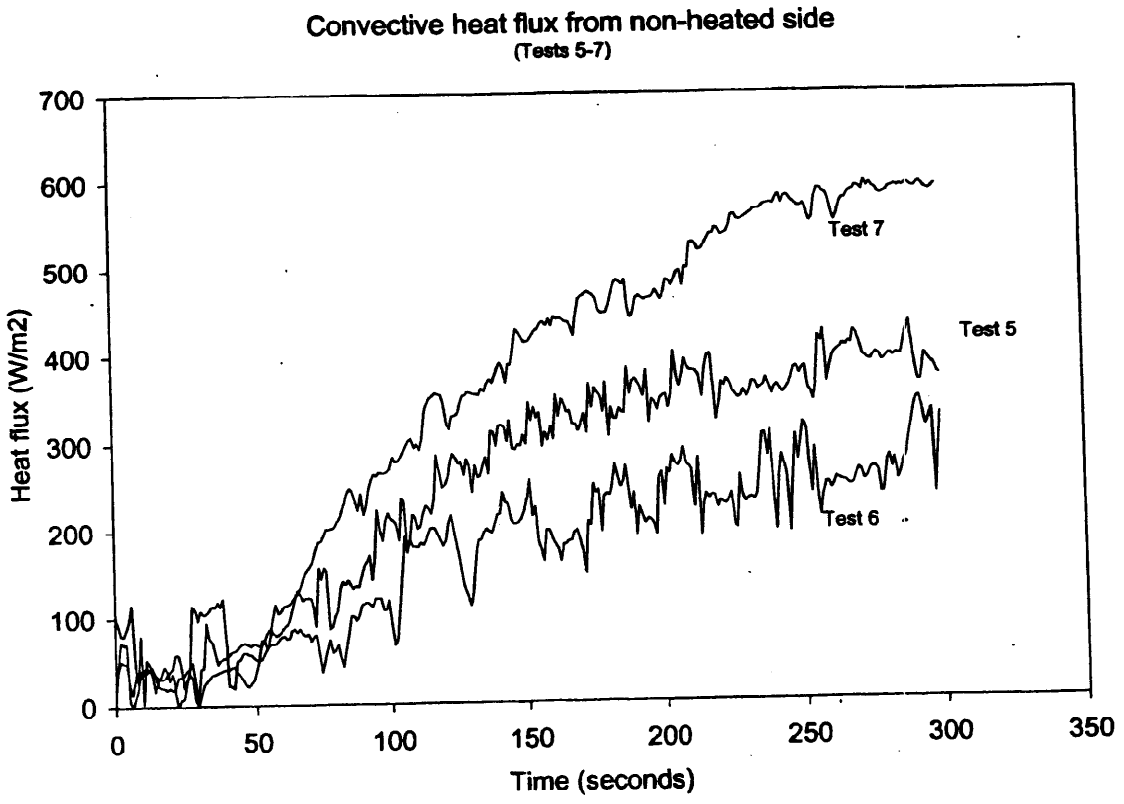

Figure 3.15: **Convective heat flux from the rear surface of the heated thermal barrier for tests 5-7 The abscissa has units W/m^2. The measurement interval is 300 sec.**

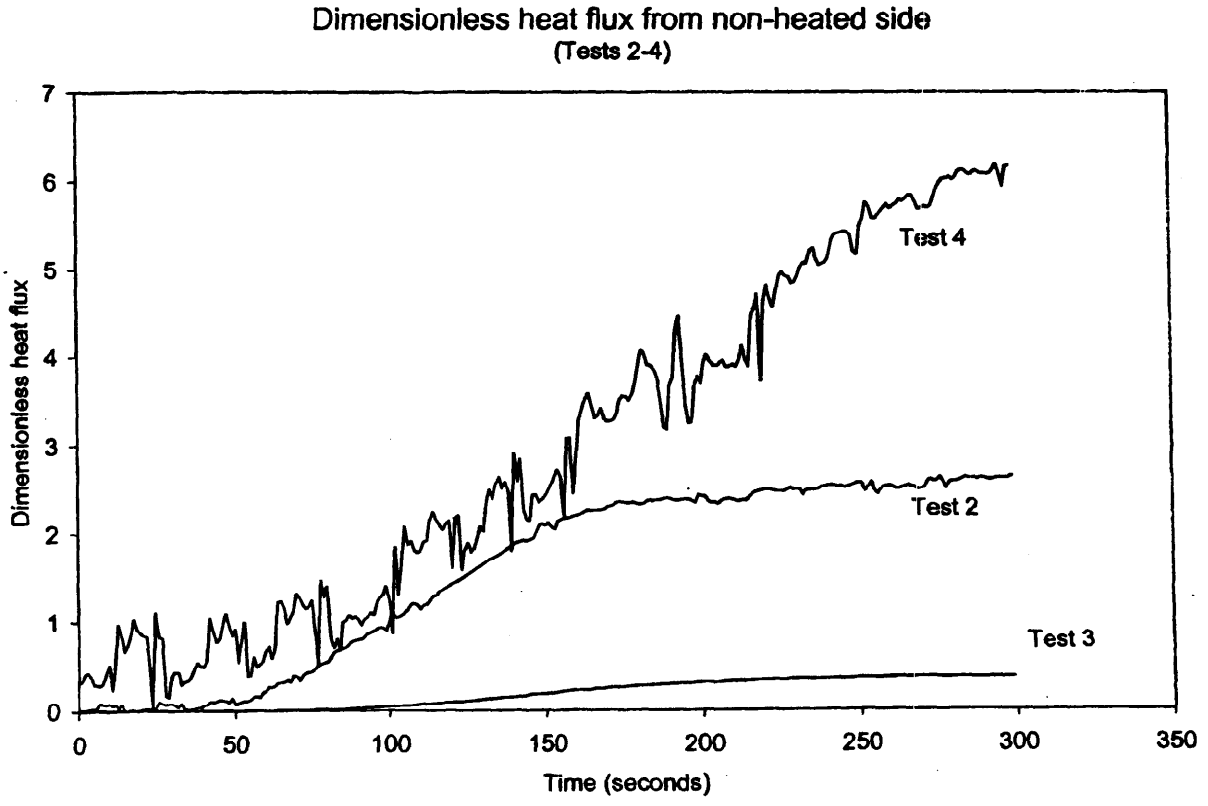

Figure 3.16: **Dimensionless heat flux from the rear surface of the heated thermal barrier, the difference to the dimensionless heat flux magnitudes is attributed to the different *Bi*. The dimensionless flux for test 4 is approximately ten times as large as that of test 3 although the dimensional flux for test 3 is between six and seven times as large as for test 4 (see Figure 3.14).**

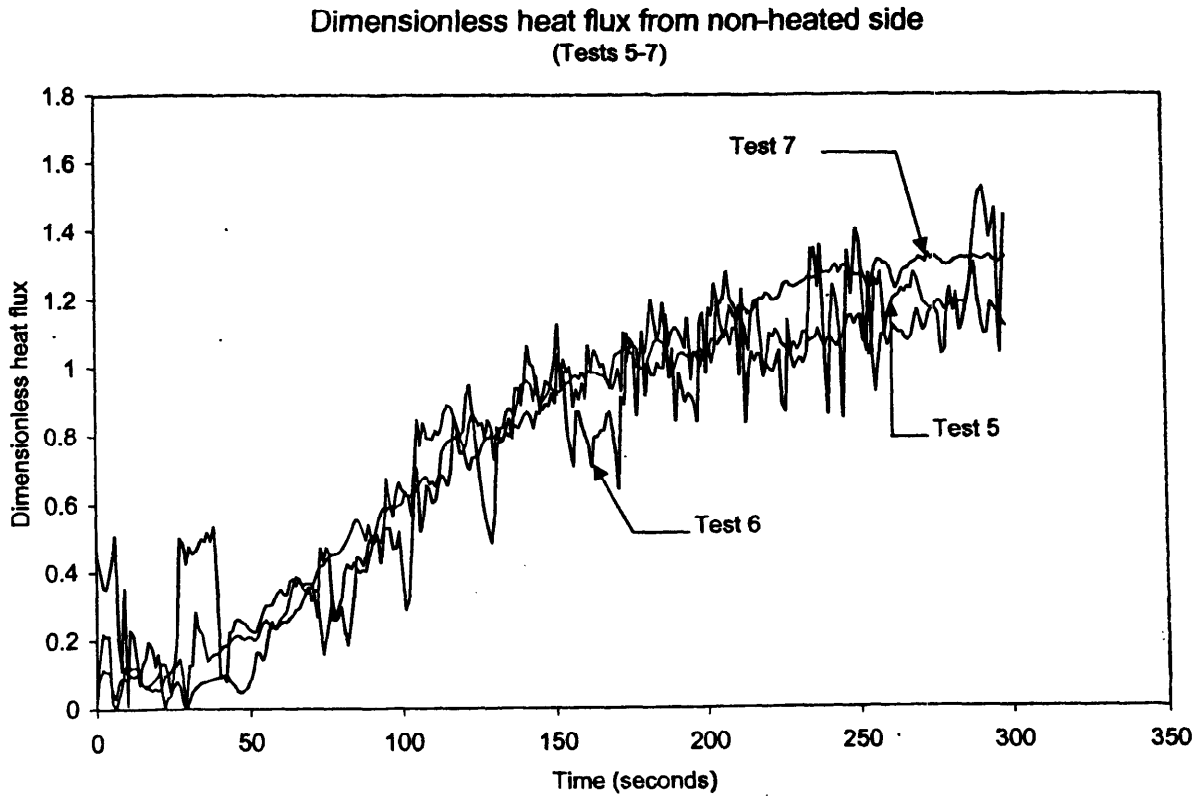

Figure 3.17: **Same as Figure 3.16 for tests 5-7. Since the Bi are nearly identical, so are the dimensionless fluxes. The dimensional fluxes of Figure 3.15 do not collapse to a single curve.**

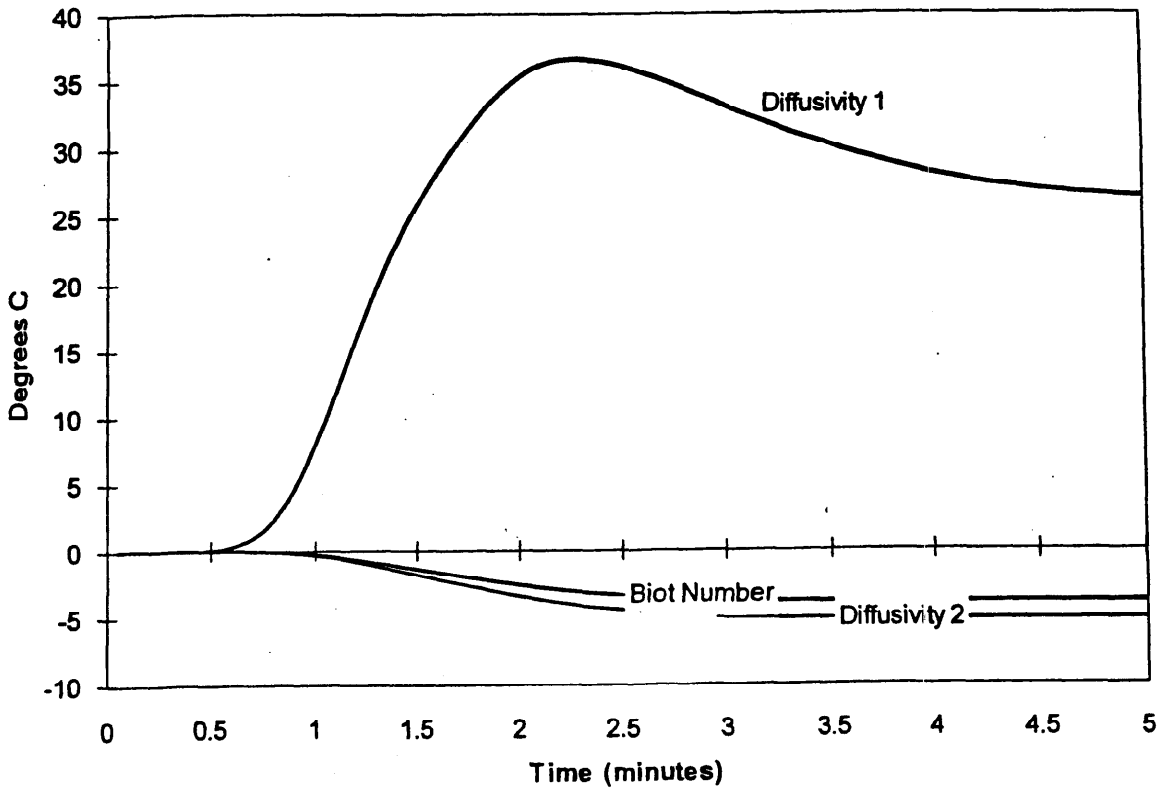

Figure 3.18: **Sensitivity coefficients for the three-parameter case. The property labeled *"Diffusivity 1"* pertains to the insulating material whereas *"Diffusivity 2"* is for the steel plate.**

CHAPTER 4

COMPARISIONS, DISCUSSION, CONCLUSIONS

4.0 INTRODUCTION

In this chapter we compare some of the results of Chapters 2 and 3. In addition a brief summary of the research project is given. Finally, a restatement of the deliverables set forth in Sec. 1.3 of the Introduction is provided for comparison of results with stated initial objectives.

4.1 COMPARISONS

Because the work of Chapter 3 primarily estimated the thermal diffusivity, we compare this quantity between Chapters 2 and 3. The material with which comparisons can be made is the glass fiber mat with polyester scrim (gffs). This material is evaluated as one of four materials in the property measurements of Chapter 2 and it is employed as one of the insulating materials in the GM tests of Chapter 3. The temperature rise in the Chapter 2 experiments is from 295K to approximately 345K, which is 50K. The temperature rises in Chapter 3 (see Table 3.2) are 66K, 171K and 336K. Comparison with the latter case seems inappropriate. For the former two temperature rises the average value of the thermal diffusivity (Table 3.2) is (0.00939 + 0.00521)/2 = 0.0073 cm^2/s. At the highest allowable temperature of Chapter 2 (i.e., 345 K) we have a thermal diffusivity value of 0.02cm^2/s, whereas at the average temperature rise of Chapter 3 ((66 + 171)/2 = 119K) we have a value of 0.1 cm^2/s. The ratio of these diffusivity values ranges from 0.02/0.0073 = 2.7 to 0.1/0.073 = 13.7. The diffusivity values of Chapter 2 are therefore higher than for Chapter 3 by a factor from approximately 3 to approximately 14. A case can be made that the former estimate of 2.7 is by far the more reasonable estimate because the only means for calculating the diffusivity of Chapter 2 at an average temperature rise of 119K is to use the *extrapolated graph* of Figure 2.14 far beyond the region of applicability of actual measurements. For a strict comparison in (or very near) the measured temperature range of Chapter 2, we find $\alpha = 0.025$ cm^2/s at 360K (i.e., for a temperature rise of about 65K), whereas from Chapter 3 we have $\alpha = 0.00521$ cm^2/s. The diffusivity ratio is now 4.8, which is between order unity and order ten.

Comparisons of the thermal conductivity can also be made for the same material. Here we use the results given in Figure 2.8 for the Chapter 2 results and those given in Tables 3.5 and 3.6 in Chapter 3. The conductivity values in Chapter 2 are larger by about a factor of 2-4 than those of Chapter 3. This estimation appears to be the principal source of the discrepancy in the preceding thermal diffusivity comparison.

4.2 DISCUSSION

The property estimations of Chapter 2 are consistent with those of Chapter 3. The emphasis of Chapter 3, however, was heat transfer calculation not property evaluation. The latter is necessary to accurately conduct the former. Property estimation in Chapter 2 was made difficult by placement of TCs, which could not easily be affixed to insulation surfaces.

4.3 CONCLUSIONS

The summary and deliverables specified in Sec. 1.3 have been satisfied:

1) An analytical/numerical model for property evaluation was described in Chapter 3. The thermal diffusivity was seen to be very important.

2) Separate results for each layer of the "bulkhead" were derived in Chapter 2. Variations of these parameters were described.

3) Residual databases of the experimental results are given in our experimental results in graphs and tables in this report.

APPENDIX

RADIANT PANEL SURFACE TEMPERATURE CALCULATION AND DISCUSSION OF HEAT LOSSES FROM RADIANT PANEL

INTRODUCTION

General Motors Research performed measurements using a 32×32 cm heating panel to radiatively heat a flat steel panel. These tests were performed for calibration purposes in preparation for experiments to be performed on composite panels of fiberglass insulation and steel, which are described in Chapters 2 and 3 of this report. Three thermocouples (TCs) were located on each side of the steel panel. Additionally, there were heat flux sensors in various locations.

Experiments were conducted at various distances, l, from the heating panel to the steel panel, ranging from 3 to 15 cm. The heater was utilized at four intensities. These were 25, 50, 75 and 100 percent of maximum power, which was 15 kW. The radiant heat flux was found to be relatively uniform over the heated area of the steel panel, which directly faced the heating panel. Temperature and heat flux measurements were made at 1-sec intervals over the course of each experiment with the other variables held constant throughout each experiment.

BLACK BODY CALCULATIONS OF RADIANT HEAT TRANSFER

Although temperature measurements were made on the surface of the steel panel, it was desired to compare the measured temperature to the theoretical black body temperature under the experimental conditions. A comparison of measured temperatures to black body temperatures can aid in the evaluation of the extent to which heat losses influence the experiment. This can facilitate assessment of the accuracy expected from heat transfer models. In addition, a comparison will be made of measured and calculated temperatures when heat losses are included in the analysis.

In general, the calculation of surface temperatures of interacting black body surfaces in radiant equilibrium requires information on the temperature and absorptivity of each surface. An equilibrium temperature must be calculated for each surface because the temperature of each surface influences the heat flow balance between each surface and hence, overall equilibrium. These inter-related temperatures are normally calculated through a set of simultaneous algebraic equations, one for each surface (Siegel and Howell (1981)). If the heat addition rate is known for the non-adiabatic surface, or surfaces, all the surface temperatures of the separate surface elements can be calculated with this information.

In the present case, more information is available than simply the heat input rate to the system. Specifically, the actual incident radiant intensity on the surface of interest has been measured. With this information, the effective black body surface temperature of the steel panel can

be calculated directly through the heat balance for the panel. If the *radiant heater* is designated as *Surface 1* and the *steel panel* is designated as *Surface 2*, we can write the equation of heat transfer as follows:

$$q_2 A_2 = F_{2\text{-}1} A_2 \sigma T_2^4 + (1 - F_{2\text{-}1}) A_2 \sigma (T_2^4 - T_\infty^4) \qquad \text{(A.1)}$$

The left side of Equation (A.1) represents the incident radiant heat flux on Surface 2, the steel panel, from Surface 1, the heater. The right side of the equation represents the heat loss by emission from Surface 2 only by radiation. Not included are convective and conductive losses from the front surface and radiant, convective and conductive losses from the rear surface. Since the heat generated in Surface 2 is nil, the incident radiant heat is equal to the heat lost by emission. The terms in Equation (A.1) are the following:

q_2 is the measured incident radiation on Surface 2 (W/m^2)

A_2 is the surface area of Surface 2 (m^2)

$F_{2\text{-}1}$ is the view factor from Surface 2 to Surface 1. It is dimensionless

σ is the Stefan-Boltzman constant, 5.729×10^{-8} W/m^2K

T_2 is the temperature of Surface 2 (K)

T_∞ is the temperature of the surroundings (K).

The preceding equation was derived by first writing the equation for thermal equilibrium (Siegel and Howell (1981)) at Surface 2, viz. $0 = A_2[F_{21}\sigma(T_2^4 - T_1^4) + (1 - F_{21})\sigma(T_2^4 - T_\infty^4)]$. This equation can be rearranged so that the term $A_2 F_{21} \sigma T_1^4$ is shifted to the left-hand side. Then the right sides of this rearranged equation and Equation (A.1) are identical leading us to identify $q_2 = F_{21}\sigma T_1^4$. Equation (A.1) can be solved for T_2, viz.,

$$T_2 = \left[\frac{q_2}{\sigma} + (1 - F_{2\text{-}1}) T_\infty^4 \right]^{1/4} \qquad \text{(A.2)}$$

We observe that in this calculation of T_2 no heat losses were considered in the analysis.

The view factor $F_{2\text{-}1}$ must be calculated. By modeling the experiment as the two-dimensional problem shown in Figure A.1, the view factor is evaluated by using the Hottel crossed-string method (Siegel and Howell (1981)). The view factor equals the sum of the diagonal distances between surface endpoints, minus the sum of the direct distances between endpoints, divided by twice the one-dimensional area of the incident object. The geometry of this problem is shown in Figure A.1.

Using the lettered indices shown in this figure, the equation for the view factor becomes

$$F_{21} = \frac{AD + CB - AC - BD}{2CD}.$$

In this symmetric case, we have $AD=CB$ and $AC=BD$, so that $F_{21}=(AD-AC)/CD$. For the particular dimensions shown in Figure A.1, assuming the area of uniform radiation is approximately equal to the heater area, this can also be written as

$$F_{2-1} = \frac{\sqrt{1024 + l^2} - l}{32},$$

where $1024 + l^2 = 32^2 + l^2$, see Figure A.1. Table A.1 lists the view factors for each distance l used in the experiments.

The black body temperatures calculated using this method are shown along with the measured temperatures from the experiment. The black body temperatures are close to the measured values and display exactly the same trends with respect to incident flux. We note in addition that the ratio of the black body temperatures to the measured temperatures is quite uniform over the various distances, l. Nevertheless, the calculated temperatures always exceed the measured temperatures by approximately 25%. For this reason, it is evident that heat losses from both front and back of the metal surface play a role in the temperature calculation. Our calculations in the following section are an attempt to describe the heat losses in a straightforward way.

TABLE A.1

Comparison of Measured and Calculated Black Body Temperatures

Power Level	Distance (cm)	Incident Flux (KW/m^2)	View Factor	BB Temp (K)	Measured Temp (K)	Ratio
25%	3	21.2	0.91064	742	619.05	0.83
	6	16.9	0.82993	687	573.75	0.84
	9	13.8	0.75755	639	538.75	0.84
	12	10.3	0.69300	583	497.45	0.85
	15	8.3	0.63566	542	466.75	0.86
	3	100.7	0.91064	1095	989.25	0.90

50%	6	76.0	0.82993	998	897.25	0.90
	9	59.2	0.75755	917	822.05	0.90
	12	44.6	0.69300	837	755.85	0.90
	15	34.4	0.63566	769	696.35	0.91
75%	6	120.7	0.82993	1120	1017.95	0.91
	9	92.0	0.75755	1024	935.45	0.91
	12	69.1	0.69300	933	858.45	0.92
	15	54.2	0.63566	861	797.15	0.93
100%	9	98.8	0.75755	1042	955.05	0.92
	12	72.1	0.69300	943	868.25	0.92
	15	57.6	0.63566	874	810.25	0.93

We observe from Table A.1 that the experiments performed at higher incident flux produce measured temperatures which are closer to the new black body temperatures than those performed at lower incident fluxes. This is expected since the higher temperatures cause the heat transfer to be more radiative than convective due to the T^4 dependence of radiative emission on temperature.

We note that if to the RHS of Equation (A.1) we add the heat loss term $\sigma(T_2^4 - T_\infty^4)$, which arises from the hypothesis that the rear surface temperature is nearly T_2 and that the entire rear surface exchanges heat radiantly with the ambient, we obtain for T_2 the result

$$T_2 = \left[\frac{q_2}{\sigma} + T_\infty^4(1 - F_{2-1}) + T_\infty^4\right]^{1/2} \frac{1}{2^{1/4}} = \frac{1}{2^{1/4}} T_{2BB}\left(1 + \frac{T_\infty^4}{T_{2BB}^4}\right)^{1/4},$$

where T_{2BB} is given by Equation (A.2). Since T_∞^4 / T_{2BB}^4 is very small we obtain the approximate result $T_2 \approx 0.84 T_{2BB}$, which is a reasonable order-of-magnitude estimate for the temperature T_2 in light of the ratios listed in the final column of Table A.1. It is clear from the ratios for power levels greater than or equal to 50% that this estimate for T_2 is too low, since the ratios are much closer to 0.9. Therefore, radiant losses from the rear surface at $T_{rear\ surface} = T_2$ are too high.

CALCULATIONS OF HEAT LOSSES

We begin our simplified calculation of cumulative heat losses by rewriting Equation (A.1) as

$$q_2 = F_{2\text{-}1}\sigma T_2^4 + F_{2\text{-}\infty}\sigma(T_2^4 - T_\infty^4) + h_2(T_2 - T_\infty), \tag{A.3}$$

where we have written $F_{2\text{-}\infty}$=1-$F_{2\text{-}1}$, we have divided out the surface area A_2, and we have included a "convective" heat loss term, $h_2(T_2\text{-}T_\infty)$ on the RHS. We now write this heat loss term as $h_2(T_2 - T_\infty) = \eta\sigma(T_2^4 - T_\infty^4)$, where η is a factor to be determined by comparison of zero-heat-loss black body temperatures (column 4 in Table A.1 defined here as T_{2BB}) with actual measured surface temperatures (column 5 in Table A.1 defined here as $T_{2\text{exp}}$). We recall from Equation (A.2) that $T_{2BB}^4 = q_2/\sigma + F_{2\text{-}\infty}T_\infty^4$. Substitution of this result into Equation (A.3) along with $h_2(T_2 - T_\infty) = \eta\sigma(T_2^4 - T_\infty^4)$ and then identifying the T_2 on the RHS of Equation (A.3) as $T_{2\text{exp}}$ gives the following equation for η:

$$\eta = \left[(T_{2BB}/T_{2\text{exp}})^4 - 1\right] / \left[1 - (T_\infty/T_{2\text{exp}})^4\right] \tag{A.4}$$

This fraction enables us to calculate the ratio between lost heat unaccounted for in the prior analysis and incident heat. This ratio is

$$\frac{loss}{incident} = \eta\frac{(T_{2\text{exp}}^4 - T_\infty^4)}{q/\sigma} = \eta\sigma\frac{(T_{2\text{exp}}^4 - T_\infty^4)}{q}. \tag{A.5}$$

The heat losses are convection and conduction from the front (heated) surface, and radiation, convection and conduction from the rear (unheated) surface.

Based on these estimates, we construct Table A.2. All of the "lumped" heat losses described above amount to a fraction that is between 15-41% of the incident flux. As the overall power level increases, the overall percentage of such losses decreases, presumably because surface temperatures are higher and more of the heat losses are already accounted for as radiation from the sample front surface.

Table A.2

Power	Incident Flux (kW/m^2)	$F_{1\text{-}2}$	T_{2BB} (K)	T_{2exp} (K)	η (-)	$\frac{loss}{incident}$	Percent Loss Range
25	21.2	0.91064	741.6	620	1.11	0.41	27-41%
	16.9	0.82993	686.5	574	1.13	0.38	
	13.8	0.75755	638.5	539	1.07	0.34	
	10.3	0.69300	582.4	497	1.02	0.30	
	8.3	0.63566	542.3	467	0.986	0.27	
50	100.7	0.91064	1094.8	989	0.506	0.27	19-27%
	76.0	0.82993	997.8	897	0.538	0.26	
	59.2	0.75755	916.8	822	0.557	0.24	
	44.6	0.69300	836.8	756	0.514	0.21	
	34.3	0.63566	768.8	696	0.506	0.19	
75	120.7	0.82993	1119.9	1018	0.468	0.23	15-23%
	92.0	0.75755	1023.9	935	0.443	0.21	
	69.1	0.69300	932.8	858	0.403	0.18	
	54.2	0.63566	860.8	797	0.368	0.15	
100	98.8	0.75755	1041.8	955	0.418	0.20	15-20%
	72.1	0.69300	942.9	868	0.398	0.18	
	57.6	0.63566	837.8	810	0.361	0.15	

REFERENCES

[A.1] R. Siegel and J. Howell, Thermal Radiation Heat Transfer, Hemisphere Publishing Corp., New York (1981).

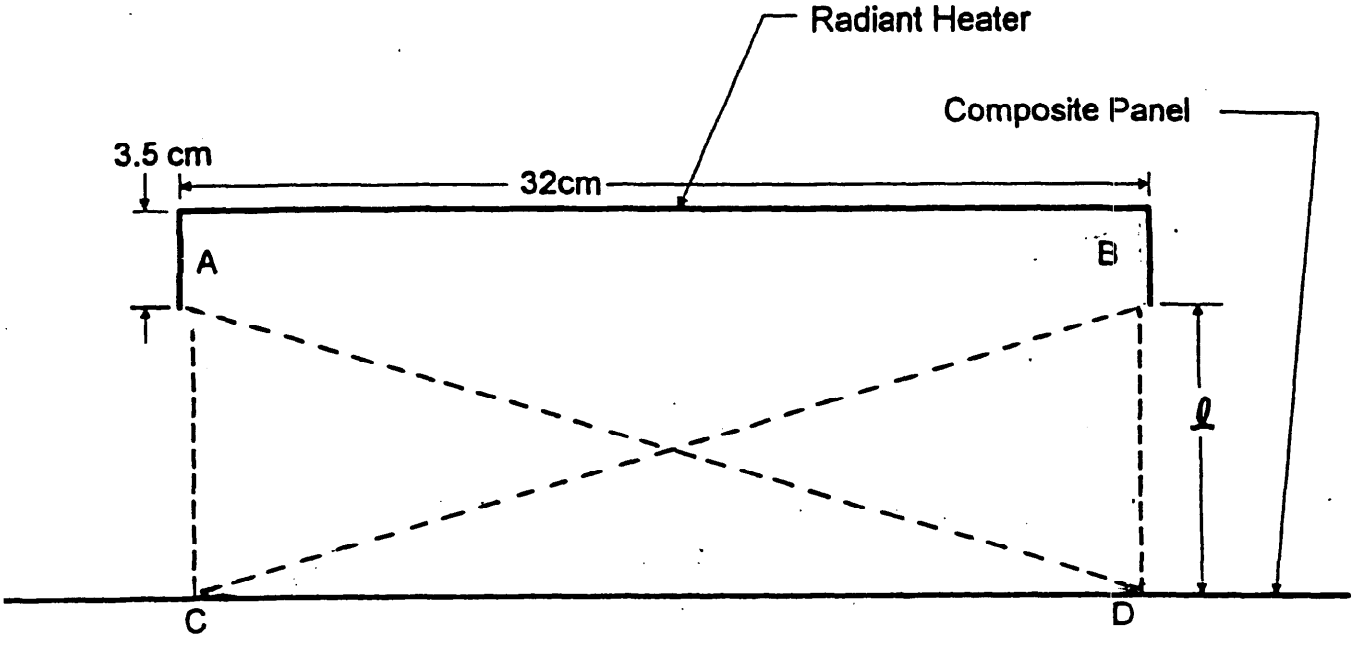

Figure A.1: **Two-dimensional diagram of experiment showing radiant heater and heated surface.**